SSRv manuscript No.
(will be inserted by the editor)

Dust in Supernovae and Supernova Remnants II: Processing and Survival

E. R. Micelotta · M. Matsuura · A. Sarangi

Received: date / Accepted: date

Observations have recently shown that supernovae are efficient dust factories, as predicted for a long time by theoretical models. The rapid evolution of their stellar progenitors combined with their efficiency in precipitating refractory elements from the gas phase into dust grains make supernovae the major potential suppliers of dust in the early Universe, where more conventional sources like Asymptotic Giant Branch (AGB) stars did not have time to evolve. However, dust yields inferred from observations of young supernovae or derived from models do not reflect the net amount of supernova-condensed dust able to be expelled from the remnants and reach the interstellar medium. The cavity where the dust is formed and initially resides is crossed by the high velocity reverse shock which is generated by the pressure of the circumstellar material shocked by the expanding supernova blast wave. Depending on grain composition and initial size, processing by the reverse shock may lead to substantial dust erosion and even complete destruction. The goal of this review is to present the state of the art about processing and survival of dust *inside* supernova remnants, in terms of theoretical modelling and comparison to observations.

1 Introduction

The solid state component of the Interstellar Medium (ISM) is identified with the generic term of "interstellar dust". It is composed by large molecules, mainly Poly-

E. R. Micelotta
Department of Physics, PO Box 64, 00014 University of Helsinki, Finland
E-mail: elisabetta.micelotta@helsinki.fi

M. Matsuura
School of Physics & Astronomy, Cardiff University, The Parade, Cardiff , CF24 3AA, UK
E-mail: MatsuuraM@cardiff.ac.uk

A. Sarangi
NASA Goddard Space Flight Center, Greenbelt, MD, 20771, USA; Physics Department, The Catholic University of America, Washington, DC, 20064, USA
E-mail: arkaprabha.sarangi@nasa.gov

cyclic Aromatic Hydrocarbons (PAHs) and fullerenes C_{60} and C_{70}, nanoparticles (Very Small Grains – VSGs) and larger carbonaceous/silicate grains. Although very scarce (1-2 % of the total mass of the ISM), dust is the key agent that drives and regulates the core physical and chemical processes responsible for star formation and galaxy evolution. Dust absorbs visual and ultraviolet radiation from stars, and re-emits it in the infrared (IR) and sub-millimetre (sub-mm) part of the electromagnetic spectrum, dominating the emission from all types of galaxies, from local to distant, from regular to starburst and active. Dust contributes to the thermal balance of the ISM via photo-electric heating while the thermal (far-infrared) emission from dust strips away a relevant fraction of the gravitational energy of a collapsing cloud, providing the necessary conditions for star formation to occur. Many fundamental chemical reactions, including the formation of molecular hydrogen H_2, occur on the surface of dust grains acting as catalyst. These grains shield at the same time these fragile molecules against strong stellar radiation fields allowing them to survive. Dust grains lock up the majority of the refractory elements (e.g. C, Si, Mg, Fe, Al, Ti, Ca) removing important ISM coolants from the gas phase. In addition, they represent the seeds for the formation of planetesimals in protoplanetary disks, which will eventually lead to planets.

Star formation shapes the formation history of galaxies and their evolution. The way dust traces star formation is ultimately determined by its interaction with the other components of the ISM: radiation fields (excitation, ionisation, dissociation), gas (through surface chemical reactions and larger scale phenomena like shocks, winds, turbulence), cosmic rays and magnetic fields. These processes modify the optical properties and the dust size distribution (through coagulation/accretion, erosion, fragmentation), which in turn leave distinct signatures in the shape of the spectral energy distribution. The comprehension of all the astronomical phenomena connected/regulated by dust thus requires the precise determination of the origin and physical properties of dust particles, and a deeper understanding of the response of dust to the different processes occurring in space at all redshifts.

It is widely accepted that dust is mainly formed at high densities and temperatures in the ejecta of evolved stars such as those populating the Red Giant Branch and the Asymptotic Giant Branch (RGB and AGB stars). However, the detection of a large amount of dust ($\gtrsim 10^7 M_\odot$) at very high redshift ($z > 6$ Bertoldi et al 2003, Watson et al 2015) when RGB and AGB stars did not have time to evolve, raises questions about the origin of cosmic dust in the distant Universe. From an evolutionary point of view, young supernovae (SNe) could represent a viable source of dust in high-redshift galaxies, although their role is still controversial.

Dust condensed in supernovae has been detected in meteorites (Clayton and Nittler 2004, Zinner 2008) and there is observational evidence of dust emission in young unmixed supernova remnants (SNRs) such as Cassiopeia A (Cas A; Lagage et al 1996, Rho et al 2008, Dunne et al 2009, Barlow et al 2010, Arendt et al 2014) or the Crab Nebula (Hester 2008, Gomez et al 2012, Temim and Dwek 2013). Dust emission has been also observed in other remnants: N132D (Rho et al 2009c), G292.0+1.8 (Ghavamian et al 2009), 1E 0102.2-7219 (E0102 – Sandstrom et al 2009, Rho et al 2009b) and G54.1+0.3 (Temim et al 2010, 2017). This latter is a Crab-like SNR with a dust mass comparable to SN 1987A (see below), but no evidence of a reverse shock.

Observations of the young supernova SN 1987A have revealed the presence of an increasingly large amount of dust (Danziger et al 1989, Moseley et al 1989, Dwek et al 1992, Wooden 1997, Bouchet et al 2004, Matsuura et al 2011, Indebetouw et al 2014, Matsuura et al 2015, and references therein). Observations with Herschel (Matsuura et al 2011, Matsuura et al 2015) and ALMA (Indebetouw et al 2014) in particular have shown that a large amount of freshly formed dust resides in the inner (cold) ejecta of SN 1987A (0.4 – 0.7 $M_\odot$ and > 0.2 $M_\odot$ respectively). These detections are in agreement with theoretical predictions (0.1 – 1 $M_\odot$, Todini and Ferrara 2001, Nozawa et al 2003) and seem to confirm that SNe are indeed efficient dust factories. At the same time, this discovery raises a fundamental question about the fate of dust: how much is injected into the ISM and can therefore be detected in galaxies at all redshifts?

The dust resides in the supernova cavity and is heavily processed by the reverse shock, generated from the impact of the SN blast wave with the circumstellar medium (CSM) and propagating towards the centre of the remnant. The gas particles accelerated and heated by the reverse shock collide with the dust grains, progressively eroding them through a process called sputtering. It might be expected therefore that only a fraction of the dust mass originally synthesised by SNe will be able to reach the ISM, with composition and size distribution different from those expected shortly after formation. The goal of this review, which is the second paper of a series of two, is to provide the state of the art about the processing and survival of dust *inside* supernova remnants, in terms of theoretical modelling and comparison with observations. The theoretical and observational aspects related to the formation and detection of dust in supernovae are discussed in our companion Paper I (Sarangi et al 2018).

This review is organised as follows. Sec. 2 introduces some basic concepts about the evolution of SNRs and the formation of the forward and reverse shocks. In Sec. 3 we present the observational evidence of dust processing and destruction in supernova remnants and in Sec. 4 we review some of the methods used to estimate dust destruction from observational data. Sec. 5 discusses the theoretical modelling of dust processing by the reverse shock in SNRs, examining some of the key ingredients required by this task and comparing how different works include such ingredients in their implementations. The theoretical results are then contrasted with observations. In Sec. 6 we discuss briefly the global role of SNRs as dust source and sink and in Sec. 7 we present our summary and conclusions.

2 The evolution of SNRs and the development of shockwaves

2.1 The evolutionary stages of SNRs

The evolution of SNRs originating from core collapse SNe (CCSNe) is characterised by four different phases (Fig 1; e.g. Weiler and Sramek 1988, Padmanabhan 2001, Gaensler and Slane 2006).

1. **Free expansion** or **ejecta-dominated (ED)** phase, which lasts for a few hundred years after explosion.
2. **Adiabatic** or **Sedov-Taylor (ST)** phase for the next ~20,000 years.
3. **Radiative** or **snow-plow** phase up to 500,000 years.

4. **Merging** phase.

The explosion of the supernova progenitor star accelerates the envelope, causing turbulence (e.g. Wongwathanarat et al 2015). The turbulence settles after a few months after the explosion (McCray 1993). After that, the ejecta material expands freely with a nearly constant velocity. The mass of the expelled ejecta dominates over the swept-up circumstellar material. The ejecta travel at supersonic speed, which implies the formation of the so-called blast-wave (or forward) shock ahead of them. The ambient medium shocked by the blast-wave reacts pushing back on the ejecta, with the consequent formation of the reverse shock. This latter decelerates, compresses and heats the ejecta. During the free-expansion phase, the expanding blast wave sweeps up the ambient ISM material, and eventually, the total mass of the swept-up material exceeds the original SN ejecta mass. The remnant enters then the adiabatic phase, and its radius, r, is generally described by the expression $r \propto t^{2/5}$, where t is the age of the SNR. This phase is also called Sedov-Taylor because it can be shown that the blast-wave of the remnant will tend to evolve towards the so-called Sedov-Taylor solution for the expanding blast-wave generated by a "point explosion", i.e. the sudden release of a large amount of energy into a background fluid. Such a solution was found independently by Taylor (1950) and Sedov (1959).

When the radiative losses of the hot shocked gas become important, the remnant enters the radiative phase. Emission lines from neutrals and ions cool down the gas, and the temperature drops sharply. The cool gas accumulates into a dense shell enclosing a central volume of hot gas where radiative losses are negligible. This phase is also called snow-plow because the sweeping-up of the ambient medium progressively increases the mass of the dense shell. The velocity of the shock front decreases gradually until it reaches the sound speed of the gas which it is propagating through. The shock wave fades away into a sound wave and the SNR finally merges into the ISM.

Starting from the Sedov-Taylor phase, the velocity of the expanding shell decreases with time from a few thousands km s^{-1} to a few hundred km s^{-1}, and finally integrates into the ISM gas which has velocities of a few km s^{-1}, as illustrated in Figure 1.

2.2 Forward and reverse shocks in SNRs

In SNRs, the blast-wave or forward shock is generated by the ejecta moving supersonically into the circumstellar and interstellar medium. The reaction of the shocked ambient medium results in the formation of a reverse shock, which propagates inwards in the frame of the ejected gas. Fig. 2 shows the density structure of a SNR as a function of radius, where the location of these two shocks is highlighted. The radius of the forward shock increases continuously with time, while the reverse shock is initially carried outwards before accelerating towards the centre (Fig. 3).

The forward shock is responsible for the processing and destruction of the dust grains already present in the CSM/ISM, while the reverse shock processes the dust freshly formed in the SN ejecta. This review focuses on this latter phenomenon.

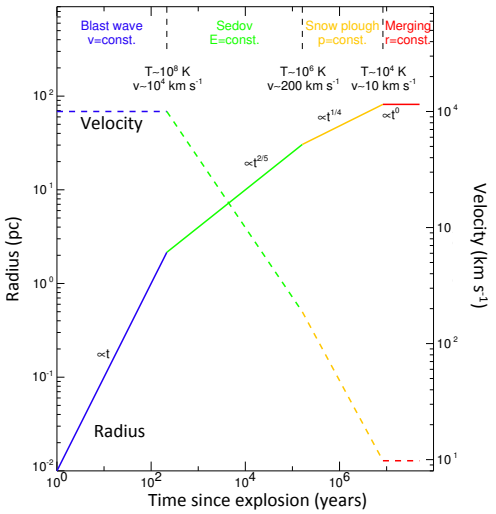

Fig. 1 Phases of supernova remnants resulting from core collapse SNe. While the radius (left axis) of a SNR increases with time, the blast-wave velocity (right axis) decreases. The evolution of the remnant radius was originally published by Padmanabhan (2001), while that of the velocity has been added by Wilms (2012).

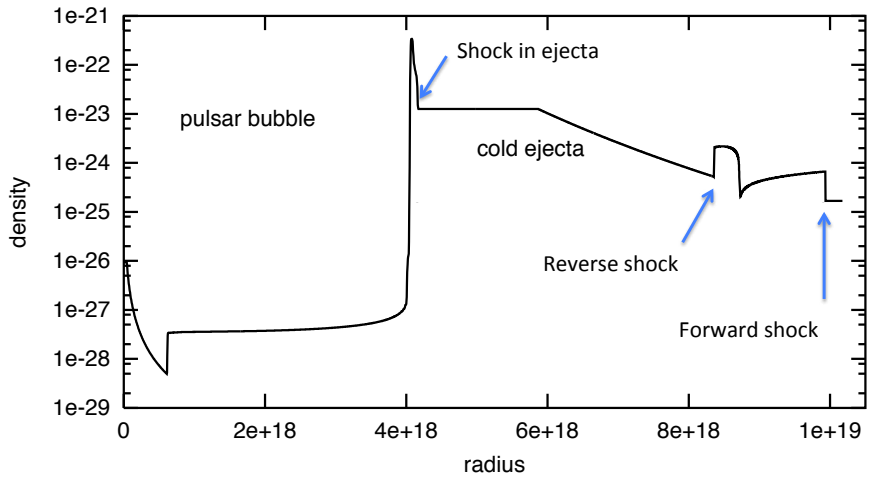

Fig. 2 Density structure of a SNR as a function of radius (Blondin et al 2001). The forward and reverse shocks are indicated by the arrows. The model includes a pulsar wind nebula in the inner region, responsible for the formation of an additional shock in the ejecta. This shock has not always been detected in SNRs originating from core collapse SNe.

3 Observational evidence of dust processing and destruction in SNRs

While there is increasing observational evidence that SNe form dust in their ejecta, as summarised in our companion paper (Sarangi et al 2018), quantifying dust processing and destruction in SNRs is challenging. We present here observational examples of dust processing and destruction in the two young supernova remnants SN 1987A and Cas A, followed by a few more examples of older SNRs.

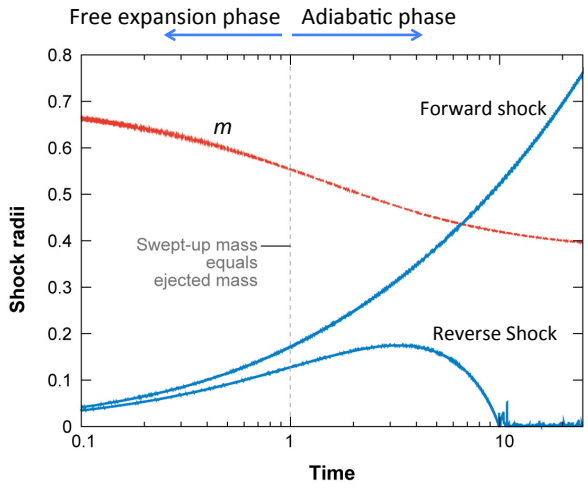

Fig. 3 Radii of the forward and reverse shocks (blue lines), together with the parameter $m = vt/R$ (red line) as a function of time. Figure from Reynolds (2008).

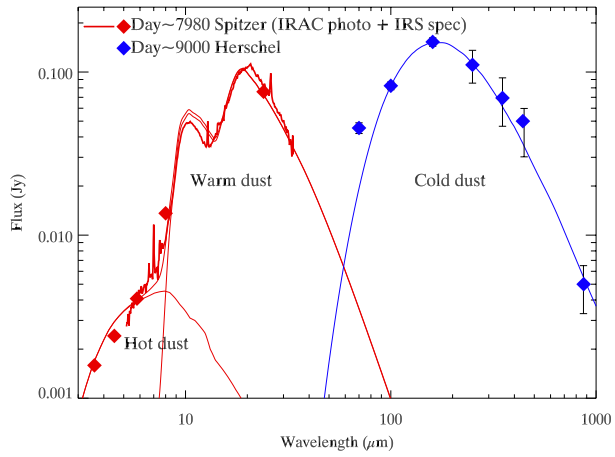

Fig. 4 Spectral energy distribution (SED) of SN 1987A, fitted with three discrete dust components: cold (~20 K), warm (~180 K) and hot (~400 K). The observational data are taken from Dwek et al (2010) for day~7980, and Matsuura et al (2015) for day~9000.

3.1 SN 1987A

3.1.1 Ejecta dust in SN 1987A — newly formed dust and possible grain growth?

SN 1987A is the first SN where dust formation was detected. The thermal emission of newly formed dust was detected starting from 615 days after the explosion (Danziger et al 1989, Moseley et al 1989, Wooden et al 1993), with the optical light curve being extinguished by dust (Whitelock et al 1989). Additionally, the detection of blue-shifted lines in the optical was suggested to be due to dust condensation within the ejecta (Lucy et al 1989). The inferred dust mass was 10^{-4} $M_\odot$ at day 775, with a dust temperature of 300–400 K (Wooden et al 1993).

About twenty years later, the Herschel Space Observatory detected SN 1987A at far-infrared and submillimetre wavelengths (Fig. 4; Matsuura et al 2011). The inferred dust mass was ~0.5 $M_\odot$ at days 8500–9090 (ignoring the current limit of

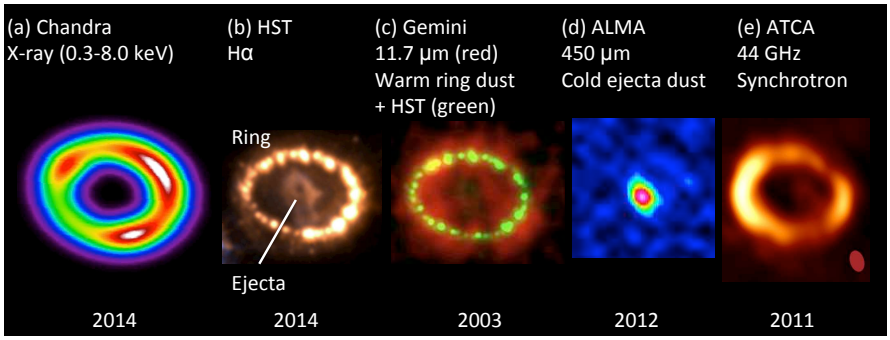

Fig. 5 Images of SN 1987A at different wavelengths. X-rays (a) and synchrotron radiation (e) trace the shocked gas in the ring. The HST image (b) shows the bright ring with faint ejecta in the center. Warm dust has been identified in the ring (c), while the emission from the cold dust originates from the ejecta in the centre. Images from (a) to (e) are taken from Frank et al (2016), Fransson et al (2015), Bouchet et al (2006), Indebetouw et al (2014) and Zanardo et al (2013), respectively.

~0.25 $M_\odot$ of carbon predicted by nucleosynthesis models, Matsuura et al 2015). This thermal dust emission was confirmed to be associated with the ejecta by spatially resolving the emission at submillimetre wavelengths (Fig.5; Indebetouw et al 2014, Zanardo et al 2014). Radioactive decay of ^{44}Ti was suggested as the heating source of the ejecta dust (Matsuura et al 2011).

After the detection of such a large amount of dust in the ejecta, the historical dust masses of SN 1987A have been revisited. There are currently two hypotheses about the time scale to acquire ~0.5 $M_\odot$ of dust. The first hypothesis is that such a large dust mass was already present in early days, but the emission was optically thick and the inferred dust mass was underestimated (Dwek and Arendt 2015). The second hypothesis is that the initial dust mass was indeed small (~10^{-3} $M_\odot$) and increased over 20 years via grain growth (Wesson et al 2014, Bevan and Barlow 2016). In the future, far-infrared observations of newly exploded SNe performed in the first couple of years after explosion would help to disentangle these two hypotheses, because at these wavelengths dust emission tends to be optically thin, therefore possibly reflecting the actual mass of dust.

Although the reverse shock has been detected in SN 1987A, it is still just inside of the equatorial ring (France et al 2010). The ejecta dust in SN 1987A is located much further inside, and has not yet encountered the reverse shock. Future monitoring will make possible to follow the propagation of the reverse shock inside the remnant and evaluate its efficiency at destroying dust.

3.1.2 Dust in the ring of SN 1987A — collisional heating by the blast wind

From the early days after explosion, the detection of asymmetries in polarisation observations has suggested the presence of a circumstellar nebula (e.g. Cropper et al 1988). The Hubble Space Telescope has revealed that the circumstellar material is arranged in rings (Fig. 5; Jakobsen et al 1991, Panagia et al 1991). These rings are thought to be composed of the material lost from the progenitor, when

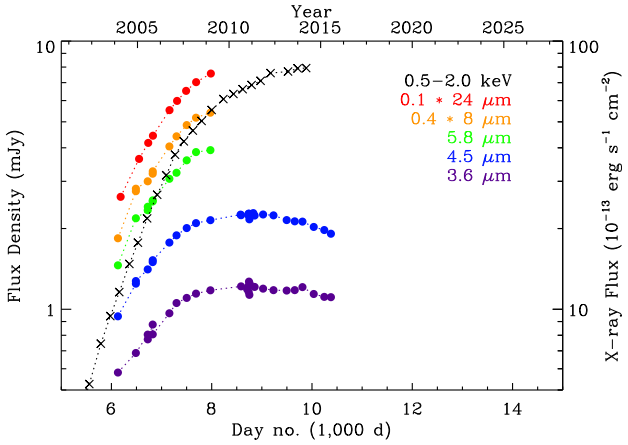

Fig. 6 Evolution of the infrared and X-ray fluxes of SN 1987A (Arendt et al 2016). Both the infrared and X-ray fluxes have continuously increased until 2012. The infrared flux at 3.6 and 4.5 μm shows a peak followed by decline, while the X-ray radiation continues to increase.

the star was in the red-supergiant phase ~40,000 years ago (Arnett et al 1989, McCray 1993).

The bright equatorial ring is another location within SN 1987A where dust emission has been detected. Using the mid-infrared instrument T-ReCS on the Gemini Telescope, Bouchet et al (2004) found that dust emission at 10 μm is dominated by ring dust (Fig. 5). While the blast winds from the explosion collide with the ring, the collisional energy generates X-ray radiation (Fig. 5) and heats up the dust grains which had formed during the supergiant phase (Bouchet et al 2006).

Since its launch in 2003, the Spitzer Space Telescope has been intensively used to investigate dust emission in SN 1987A. Spitzer data have allowed to identify two components. The first one is the warm (~180 K) dust, emitting in the range 8–35 μm and associated with the ring. In particular, from the data of the spectrometer on board Spitzer it has been possible to identify silicate dust features at 10 and 18 μm (Fig. 4; Bouchet et al 2006). The second component is the excess emission detected from 3.5 μm up to 8 μm (Fig. 4). It has been suggested that this component is associated with hot dust in the ring, where small (radii<0.03 μm) dust grains radiate at temperatures of ~400 K (Dwek et al 2010).

Spitzer has been used to monitor the evolution of the warm and hot dust on a half-a-year basis. The infrared flux from 3.6 to 24 μm has continuously increased until Spitzer's helium ran out in 2009 (Dwek et al 2010). Although the overall flux has increased, the shape of the silicate feature has remained the same. During that same period, the X-ray luminosity has also increased (Fig.6; Dwek et al 2010, Frank et al 2016), as well as the optical brightness of the ring and the synchrotron radiation (Larsson et al 2011, Zanardo et al 2010, McCray and Fransson 2016). The interaction between the ejecta blast-wave and the ring generates energy, heating up the ring material and brightening it up at all wavelengths. More material from the ejecta has been plunging into the ring, increasing its brightness.

Dwek et al (2008) have modelled the infrared emission of dust assuming that the grains are collisionally heated in the X-ray emitting plasma. Dust sputtering due to the fast moving ions in the plasma results in the erosion and possible destruction of the grains. The infrared luminosity increases slower than the X-ray

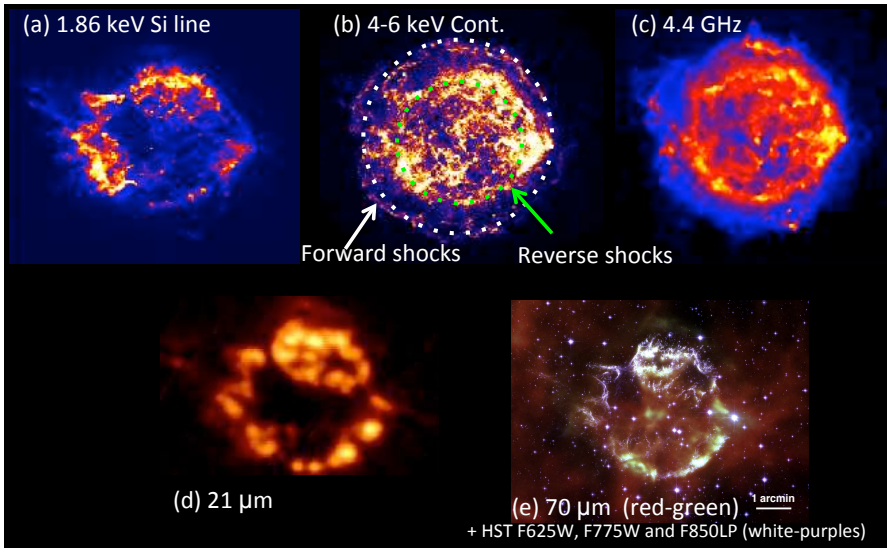

Fig. 7 Images of Cas A at various wavelengths. Panels (a) to (c) are taken from Gotthelf et al (2001) and show the Chandra X-ray Kα silicon emission, the Chandra X-ray continuum with the location of the forward and reverse shocks highlighted, and a radio map at 4.4 GHz from the VLA, epoch 1997, respectively. The warm dust is traced by the Spitzer 21 μm emission (panel (d) - Rho et al 2008), while colder dust is traced by the Herschel 70 μm emission (panel (e) - De Looze et al 2017).

luminosity, therefore Dwek et al conclude that the dust grains are destroyed in the ring.

Spitzer continued to be used to monitor the infrared brightness employing the two bands still in operation after its helium ran out in 2009 (3.6 and 4.5 μm, Arendt et al 2016). The infrared brightness kept increasing until 2010 (about day ~8500 after the explosion) and remained constant for two years, then started fading. The beginning of the decline was more or less coincident with the time when the Hubble Space Telescope captured indications that the outermost part of the blast wave had passed the bright ring (Fransson et al 2015). In contrast to the infrared brightness, the X-ray luminosity continued to increase. Arendt et al (2016) suggest that the time scale for the destruction of dust grains is shorter than the cooling time of the shocked gas: the bulk mass of dust has been reduced by shock destruction, decreasing the infrared brightness, while the X-ray flux reflects the temperature (but also the density and volume) of the shocked gas.

Dust grains in the ring will continue to interact with the blast wave, but at a lower rate than in the 2000s decade. While Spitzer will continue being used to monitor the flux of the ring, the launch of the JWST will allow us to study spatially resolved shock interaction during its mission.

3.2 Cassiopeia A – forward shock, dust processing by the reverse shock and dust emission from the unshocked centre

Cassiopeia A (Cas A) is the remnant of a Type IIb SN explosion which occurred approximately 335 years ago (Fesen et al 2006, Krause et al 2008). Estimates from X-ray observations indicate a rather high ejecta mass of $4\,M_{\odot}$ (Vink et al 1996). Chandra observations of the SNR have revealed the location of the forward and reverse shocks (Fig.7; Gotthelf et al 2001, Hwang et al 2004). The remnant has a filamentary structure with asymmetric shells. Maps of ionised lines show that elements from different nucleosynthesis processes are distributed in slightly different locations within the remnant (e.g. Isensee et al 2012, Grefenstette et al 2014, Milisavljevic and Fesen 2015).

Dust in Cas A has been found both in the reverse-shocked gas and in regions still unshocked. Spitzer observations of 19–23 μm have shown that mid-infrared dust emission is mainly coincident with the [Ar II] emitting region (Ennis et al 2006, Rho et al 2008), and that this also corresponds to the reverse-shocked region (Fig.7 - d). Dust emission at 70 μm has been also detected. The temperature of the dust has been estimated between 50–500 K, with an estimated mass of 0.020–$0.054\,M_{\odot}$.

Hines et al (2004) reported about Spitzer MIPS imaging of Cas A at 24 and 70 μm. From the total MIPS fluxes combined with IRAS, ISO and MSX observations, they estimated in Cas A a total dust mass up to $3 \times 10^{-3}\,M_{\odot}$.

Barlow et al (2010) analysed Herschel images of Cas A taken in five bands between 70 and 500 μm. They found that while warm (~80 K) dust grains indeed reside in the reverse-shocked region, there is a cold (~25 K) dust component located in the unshocked region in the centre of the system (green dots in the centre of Cas A in Fig.7 - e). Their estimated dust mass is $0.075\,M_{\odot}$.

To determine the dust mass in Cas A, Bevan et al (2017) adopted the method proposed by Lucy et al (1989), which is based on photons scattering and absorption by dust in the expanding ejecta. Using the Monte Carlo line transfer code damocles (Bevan and Barlow 2016), Bevan et al (2017) found that the most likely dust mass given by their modelling of the integrated optical spectrum of Cas A (Milisavljevic and Fesen 2013) is $\sim 1.1\,M_{\odot}$.

De Looze et al (2017) revisited the analysis of dust mass and temperature in Cas A, using Spitzer and Herschel images, together with Planck and Herschel spectra. Their analysis using spatially resolved maps involves careful removal of ISM lines and ISM dust emission from the far-infrared images. The ISM dust model from Jones et al (2013, 2017) was used to remove the contribution from the ISM dust. They concluded that the data are best-fitted by $0.3 - 0.5\,M_{\odot}$ of silicate grains (with a temperature of ~30 K) or $0.4 - 0.6\,M_{\odot}$ of an equal mixture of silicates and carbonaceous grains. Their dust map shows a larger dust mass in the unshocked region than in the reverse-shocked region, suggesting that 70 % of the dust formed in the SN could have been destroyed by the reverse shock. Different dust temperatures in the reverse-shocked region and in the unshocked region clearly indicate that dust grains are experiencing collisional heating in the reverse-shocked region, with potential dust destruction via sputtering and shattering.

In the case of Cas A, the evaluation and subtraction of the ISM dust along the line of sight affects the final estimate of the SN dust mass. That remains challeng-

ing in many Galactic SNRs with heavy contamination from ISM dust along the line of sight.

3.3 Sagittarius A East — a 10,000 year old SNR with surviving dust?

Sagittarius A East is a SNR remnant close to the Galactic centre, with an estimated age of ∼10,000 years. Such an old age implies that the reverse shock should have reached the centre of the remnant. Lau et al (2015) have detected infrared dust emission from the centre of the SNR at 5.8–70 μm. The location of the dust emission is coincident with that of the iron Kα line, which traces shocked gas. While the fraction of small grains appears to be low, Lau et al (2015) suggest that the excess far-infrared emission requires the presence of large dust grains (∼0.04 μm) which could have survived the passage of the reverse shock.

4 Estimating dust destruction from observations

4.1 Dust depletion of elements and dust destruction

Lines from ionised and neutral species detected in the UV, optical and X-ray domains are commonly used to measure elemental abundances. The discrepancies between the measured atomic abundances in the ISM and the solar abundances of refractory elements are generally attributed to the depletion of such refractory elements into dust grains in the ISM (e.g. Savage and Sembach 1996). Elemental abundances and dust depletion can be estimated in SNRs, and any spatial variation of the dust depletion rates across shocks can be due to dust destruction.

Vancura et al (1994) showed that the X-ray spectra of shock waves are substantially modified when the effects of grain destruction are taken into account. Their theoretical results were reasonably in agreement with observations of the Cygnus Loop. Seab and Shull (1983) presented theoretical and observational evidence that both the depletion of heavy elements and the UV extinction curves are modified by the processing of interstellar dust grains due to SN blast waves propagating into the ISM. Raymond et al (2013) measured the carbon abundance within the Cygnus Loop SNR, using UV spectra obtained by the Hubble Space Telescope. They found that the C IV to He II ratio changes from the shock front to the post shock region. They argue that carbon atoms are sputtered from dust grains, enhancing the carbon abundance in the post shocked region.

4.2 Modelling the infrared dust emission

4.2.1 The modified blackbody analysis – advantages and limitations

The modified blackbody analysis – This technique is widely used to estimate dust mass and temperature from the infrared emission of dust grains in stars and in the ISM. It can be also used to estimate the dust mass present in SNe and SNRs.

Table 1 Input and output parameters of the modified blackbodies used in Fig. 8.

	Warm		Cold		Fitted results	
	$T_{\rm warm}$ K	$M_{\rm warm}$ $M_\odot$	$T_{\rm cold}$ K	$M_{\rm cold}$ $M_\odot$	$T_{\rm fit}$ K	$M_{\rm fit}$ $M_\odot$
Example (a)	30	1	15	1	29.9	1.1
Example (b)	20	1	15	2	19.7	1.5

In the optically thin case, the flux density F_λ at the wavelength λ can be represented by a modified blackbody:

$$F_\lambda = 4\pi M_d \frac{\kappa_\lambda B_\lambda(T_d)}{4\pi D^2}, \tag{1}$$

where M_d is the dust mass, D is the distance to the object, $B_\lambda(T_d)$ is the Planck function and T_d is the dust temperature (Hildebrand 1983). The dust mass absorption coefficient κ_λ is expressed as

$$\kappa_{\lambda,a} = 3Q_\lambda/4\rho a, \tag{2}$$

where ρ is the mass density of the dust grains, Q_λ is the dust emissivity at the wavelength λ and a is the grain size. In the Rayleigh limit, i.e. grain size a much smaller than the emitting wavelength λ, the coefficient κ_λ for spherical grains can be simply expressed as a power-law

$$\kappa \propto \lambda^{-\beta}. \tag{3}$$

Thus, the flux F_λ at a given dust temperature, T_d, becomes independent from the grain size. These simple equations can provide dust masses from a few measured flux data points at infrared wavelengths.

Advantages and limitations – The modified blackbody analysis has both advantages and limitations. The advantage is that this method is very simple and easy to use. As far as all the grains have the same temperature, the equation does not depend on the grain size in the wavelength range where $a \ll \lambda$. One limitation is that the assumption of all grains having the same temperature might not be applicable in some cases. The dust absorption coefficients at UV and optical wavelengths depend on the size of the grains, and small grains can reach higher temperatures. In case of radiatively heated dust, if the incoming radiation has the spectrum of the interstellar radiation field, the dependence is approximately $T_d \propto a^{-0.06}$ for β=1 (Tielens 2010, Draine 2011). The majority of dust in SNRs is collisionally heated in the shocked gas. This case is discussed in Sect. 4.3.

Can the modified blackbody analysis be used to estimate dust destruction? – The answer to this question depends on the degree of dust destruction and on the temperature and mass of both the SNR and ISM dust. In fact the definite answer is that this method should be cautiously used to estimate dust destruction, because the emission from the hot SNR dust can hide the emission from the cold ISM dust.

Often, SNRs are surrounded by interstellar clouds, therefore the infrared emission coming from a SNR is contaminated by interstellar dust emission along the

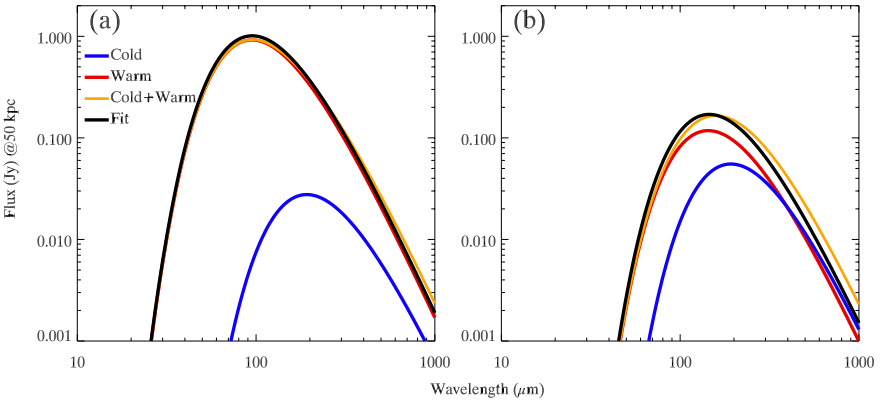

Fig. 8 Example of modified blackbody fits of two dust components: warm dust from a SNR (red curve) and cold interstellar dust along the line of sight of the remnant (blue curve). The two components are added together (yellow curve) and the summed emission is fitted with a modified blackbody (black curve) to recover the input dust masses and temperatures. In panel (a) the two components have an equal mass (1 $M_\odot$) and temperatures of 15 and 30 K respectively. The total emission is dominated by the warm dust, which hides the cold dust. The fitting yields a dust mass of 1.1 $M_\odot$ and a dust temperature of 29.9 K, almost reflecting the warm component only. In panel (b) the temperatures of the warm and cold dust are 20 and 15 K, and their masses are 1 and 2 $M_\odot$ respectively. Fitting of the total emission with a modified blackbody yields 1.5 $M_\odot$, which is only half of the total input dust mass (3 $M_\odot$). The input and output parameters are summarised in Table 1.

line of sight. The proper estimate of the amount of interstellar dust is crucial to correctly measure the amount of SNR dust (Sect. 3.2). The evaluation of the emission coming from the ISM is not a simple task. The modified blackbody analysis is often used for this purpose, but it requires particular attention because the results can be misleading, as demonstrated by the example below.

Dust in SNRs often has a slightly higher temperature than interstellar dust. The interstellar dust temperature has been found to be typically 15–25 K (Gordon et al 2014), while the supernova dust located in shocked regions tends to have a higher temperature of 20–120 K (e.g. Sandstrom et al 2009, Lakicevic et al 2015, De Looze et al 2017). Let's consider two dust components: warm dust from a SNR and cold interstellar dust along the line of sight of the remnant (Fig. 8 and Table 8). We add these two components as if they were both optically thin in the infrared, fit the summed emission using a modified blackbody and test whether we can recover the input dust masses and temperatures.

Panel (a) in Figure 8 illustrates a case where the cold and warm dust components have an equal mass (1 $M_\odot$) and temperatures of 15 and 30 K, respectively (Table 8). We adopt for the grains the emissivity of silicates (Ossenkopf et al 1992). As shown in Fig. 8 - (a), the total emission is dominated by the warm dust component, which hides the cold dust. The χ-square fitting of the sum of the two emission components yields a dust mass of 1.1 $M_\odot$ and a dust temperature of 29.9 K (Table 1), almost reflecting the warm component only. In the direction of the SNR, the mass of interstellar dust appears reduced with respect to its actual value.

Panel (b) in Figure 8 shows what happens if the two components have similar luminosities. The temperatures of the warm and cold dust are 20 and 15 K, and their masses are 1 and 2 $M_\odot$ respectively (Table 1). Fitting the sum of these two components with a modified blackbody yields 1.5 $M_\odot$, which is only half of the total input dust mass (3 $M_\odot$).

The above analysis shows that, when trying to find cold ISM dust behind hot SNRs, depending on the temperatures and column densities of both components, the inferred dust masses, particularly the cold ISM dust mass, can be distorted. The use of modified blackbody fitting to ISM and SNRs dust emission needs to be very cautious, and does not provide conclusive evidence of SNRs destroying ISM dust.

4.3 Modelling the infrared emission of collisionally heated dust

As mentioned in Sect. 4.2.1, dust grains of different sizes have different temperatures. The calculation of the dust temperature gradient requires balancing the heating and cooling rates of the grains. This review article focuses on dust processing and destruction in SNRs, where dust grains are mainly heated via collisions with fast moving particles, predominantly electrons. Infrared emission is the main cooling channel for the hot dust. In this section, we briefly discuss the modelling of the infrared emission from collisionally heated dust, which has been studied intensively by Draine (1981), Dwek (1986, 1987), Dwek et al (2008) and summarised by Draine (2011).

The collisional heating rate of a dust grain of radius a is given by

$$H = \pi a^2 \sum_j n_j \, v_j \, E^j_{\rm dep}, \tag{4}$$

where the index j runs over the different constituents of the plasma (ions and electrons) embedding the dust, n_j is the number density of the jth plasma component, v_j is its thermal velocity and E_j is its thermally-averaged energy deposition in the grains (Dwek et al 2008). It is assumed that ions and electrons have the same temperature, which implies $v_e \gg v_{\rm ions}$. Therefore, the dust heating rate is dominated by collisions with electrons. For simplicity, we set $E^e_{\rm dep} \equiv E_{\rm dep}$. Dwek et al (2008) consider two cases: if most of the electrons are stopped by the grains, on average $E_{\rm dep}$ is equal to the thermal energy of the electrons, i.e. $E_{\rm dep} \propto T_e$, where T_e is the electron temperature. The electron velocity is given by $\sqrt{8kT_e/\pi m_e}$, where m_e is the electron mass, therefore

$$H \sim a^2 n_e T_e^{3/2}. \tag{5}$$

If most of the electrons traverse entirely the grains, $E_{\rm dep}$ is proportional to the electron stopping power in the solid, $\rho^{-1}({\rm d}E/{\rm d}x)$, where ρ is the mass density of the material. In the energy regime considered here, ${\rm d}E/{\rm d}x \propto E^{-1/2}$, so that $E \propto T_e^{-1/2} a$ and

$$H \sim a^3 n_e. \tag{6}$$

The cooling of the dust is dominated by its own emission. The radiative cooling rate is given by:

$$L = 4\pi\sigma_{\rm d} \int_0^\infty Q(\lambda) B(T_{\rm d}, \lambda) d\lambda, \tag{7}$$

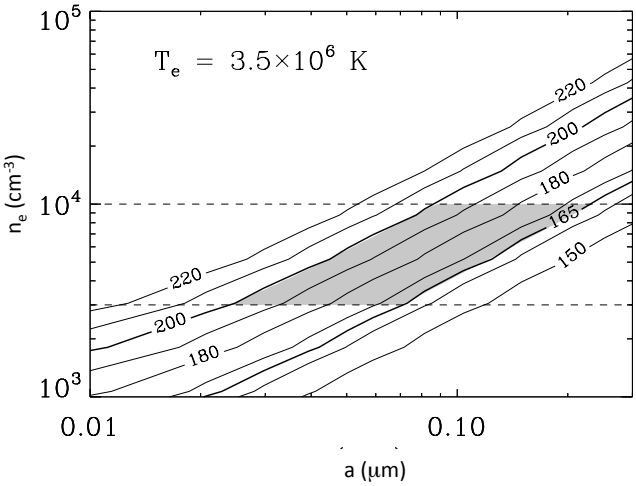

Fig. 9 Contour plot showing the dust temperature dependence on grain size (a) and electron density (n_e) for the given electron temperature, T_e (Dwek et al 2008). The dashed horizontal lines indicate the range of electron densities in the ring of SN 1987A, estimated from the analysis of ionised emission. Within these values of n_e, the range of observed temperatures (between 165 and 200 K) limits the viable grain sizes between 0.023 and 0.22 μm (gray area).

where σ_d is the geometrical cross section of the grains, $Q(\lambda)$ is the dust absorption efficiency at wavelength λ, B is the Planck function and $T_{\rm d}$ is the dust temperature. The average of $Q(\lambda)$ over the Planck function is given by the following expression:

$$< Q(T_d) >= \frac{\pi}{\sigma T_d^4} \int_0^\infty Q(\lambda) B(T_d, \lambda) d\lambda, \tag{8}$$

where σ is the Stefan-Boltzmann constant. For $a \ll \lambda$, $Q(\lambda) \propto \lambda^{-\beta}$, thus $< Q > \propto aT_d^\beta$ for spherical grains. The cooling rate becomes

$$L = \pi a^2 T_d^4 < Q > \approx \pi a^3 \sigma T_d^{4+\beta}. \tag{9}$$

In case of thermal equilibrium, $H = L$ and the dust temperature can be written as

$$T_d \propto (\frac{n_e}{a})^\gamma T_e^{\gamma/2} \tag{10}$$

for electrons stopped in a grain, and

$$T_d \propto n_e \gamma \tag{11}$$

for electrons which traverse the grain, where $\gamma = 1/(4 + \beta)$ (Dwek et al 2008). The values of β are typically between 1 and 2 (~2 for silicates and ~1 for amorphous carbon; Mennella et al 1998). Eq. 11 shows that, when the electrons are not stopped inside the grain, the dust temperature becomes independent from the grain size a. In the optically thin case, the flux density F_λ at wavelength λ is then given by Eq. 1.

Figure 9 shows the modelled dust temperature as a function of the electron density and grain size. For the same electron temperature, smaller grains can reach higher temperatures than the larger ones. The figure also shows that a combined estimate of the dust temperature (from infrared emission) and of the electron density (from X-ray or optical measurements) can potentially constrain the range of dust grain sizes. For the dust in the circumstellar ring of SN 1987A, Fig. 9 suggests grain sizes in the range 0.023–0.22 μm.

X-rays come from the hot shock-heated plasma, while the infrared luminosity reflects the energy emitted by dust grains collisionally heated in the shocked gas. Dwek et al (2008) introduced the infrared-to-X-ray luminosity ratio as a tracer of the heating and cooling balance of dust grains. This will be discussed in Sect. 4.6. As already mentioned, dust heating is dominated by collisions with electrons. Dwek et al (2008) suggested that the infrared-to-X-ray ratio, which shows some dependence on grain size, is also a good indicator of the electron temperature of the plasma.

4.4 Modelling the infrared emission from dust with a modified size distribution

Dust grains embedded in a shocked gas are affected by different destructive processes (Sec. 5.6). Two of the most important are erosion due to collisions with gas particles (sputtering) and fragmentation due to collisions with other grains (shattering). Grain-grain collisions are less frequent than gas-grain collisions because of the low dust density, but each collision can be more efficient in destroying the collision partners. Sputtering and shattering modify the initial size distribution of the dust, completely destroying the smallest grains and reducing the size of the bigger ones via progressive erosion or fragmentation. The result is a size distribution shifted towards smaller dust sizes with respect to the initial one (see e.g. Williams and Temim 2016, for a review).

Infrared emission from grains with a modified size distribution can be calculated assuming collisional heating of the dust (e.g. Dwek and Arendt 1992, Sec 4.3). Using the method from Borkowski et al (2006), the required input parameters are the electron and proton temperatures, the proton density, n_p, and the shock sputtering age. The optical spectra of non-radiative supernova remnants are dominated by Balmer lines, which are used to determine the shock parameters, in particular the electron/proton temperature ratio and the shock velocity (Ghavamian et al 2007). The sputtering age is equivalent to the ionisation timescale, and for Sedov dynamics reaches a maximum at around $1/3\, n_p\, t$, where t is the true age of the SNR (Borkowski et al 2001). Knowing the dust sputtering rates (e.g. Tielens et al 1994) and the sputtering age, it is possible to calculate the size distributions of the grains which are progressively modified by processing in the hot gas, and compute the corresponding emission spectra using the equations in Sec. 4.3.

4.5 Estimates of dust destruction rates in specific SNRs

The approach described in Sec. 4.4 can be used to model the infrared emission from dust whose size distribution has been modified by shocks. The results have

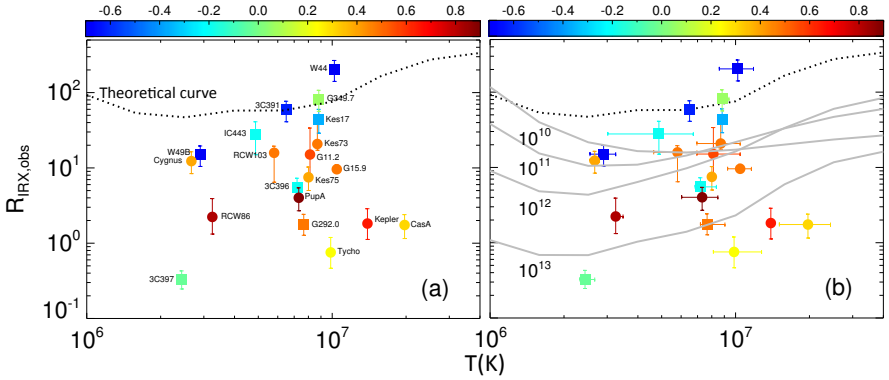

Fig. 10 Infrared-over-X-ray luminosity ratio, $R_{\rm IRX}$, as a function of the electron temperature of the X-ray plasma (Koo et al 2016). The dotted line on panel (a) shows the theoretically predicted ratio for a plasma in thermal and collisional equilibrium with dust having the MRN interstellar grain size distribution. Panel (b) includes the ratios resulting from an out-of-equilibrium gas where the grain size distribution is modified by sputtering (grey lines). The curves show $R_{\rm IRX}$ at different times, given by the ionisation timescale $\tau_{\rm ion}$, after the gas has been shocked, with $\tau_{\rm ion}$ = 10^{10}, 10^{11}, 10^{12} and 10^{13} s cm^{-3}. The colour of the SNRs symbols indicates the value of the coefficient of correlation between the morphology of the infrared and X-ray emissions. The coefficient ranges from -0.7 to 0.9 as in the colour bar.

been compared with the Spitzer 24 over 70 μm flux ratio in various SNRs. Borkowski et al (2006) estimated that 35–40 % of dust has been destroyed in two LMC SNRs, DEM L71 and 0548−70.4, Sankrit et al (2010) applied the same method to the Cygnus Loop, suggesting that 35 % of the dust has been destroyed by shocks over 1350 years. Blair et al (2007) analysed the same infrared ratio in the type Ia SNR Kepler, finding a dust destruction rate of 85 %, though later Williams et al (2012) determined that only 10 % of dust could have been destroyed in some parts of this SNR. The same method applied to LMC core-collapse SNRs, suggests that 27–50 % of the dust has been destroyed Williams et al (2006). Using Spitzer 24, 70 and 160 μm images of the Pup A SNR, Arendt et al (2010) estimated that 25 % of dust grains could have been destroyed. It should be noted that all these works do not specify which kind of shocks are responsible for dust destruction.

4.6 Is the infrared-over-X-ray luminosity ratio universal?

Dust grains residing in a hot, X-ray emitting gas are mainly heated by collisions with electrons and cool down through infrared emission (Sec. 4.3). A correlation between X-ray and infrared emission could therefore be expected. Dwek (1987) tested this hypothesis first on Cas A and the Cygnus loop and later on seven more Galatic SNRs (Dwek et al 1987). Koo et al (2016) expanded this kind of study to 20 Galactic SNRs, and Seok et al (2013), Seok et al (2015) to SNRs in the Large Magellanic Cloud.

Koo et al (2016) find that the measured infrared and X-ray luminosities of the 20 Galactic SNRs under examination do not follow the theoretical trend. The adopted infrared and X-ray luminosities are similar to those of Dwek (1987), but the more recent model of Weingartner and Draine (2001) for interstellar dust is

used instead. Some SNRs are much more brighter than predicted in the X-ray with respect to the infrared, with discrepancies larger than a factor of 100. Their initial model considers a hot, dusty plasma in thermal and collisional equilibrium, with dust having the MRN interstellar grain size distribution (Mathis et al 1977). The calculations are extended to consider a plasma where dust grains are continuously injected and sputtered in the hot gas. The theoretical IR-to-X-ray ratio curves corresponding to this out-of-equilibrium gas with modified grain size distributions cover a wider range of values and are able to reproduce the majority of the measurements (Fig. 10).

Koo et al (2016) have carefully examined the properties of individual SNRs. Low infrared luminosity SNRs tend to have a known additional X-ray emission component, such as the ejecta, on top of the X-ray radiation due to the expanding remnant ploughing the surrounding ISM. On the other hand, SNRs with high infrared luminosities tend to have radiative shocks, and the infrared luminosity is largely due to dust heated by the shock radiation. The study of LMC SNRs by Seok et al (2013), Seok et al (2015) suggests that the lower dust-to-gas ratio in this galaxy may affect the infrared and X-ray luminosities. These studies show that modelling dust emission and dust destruction requires a careful examination of the SNRs properties.

5 Dust processing by the reverse shock: one problem, different approaches

Studying the survival of freshly formed dust in SNRs requires some key ingredients. It is necessary to have a physically motivated picture of the remnants: morphology, composition, temperature, density structure of the ejecta (e.g. clumpiness), ongoing radiative processes, in short everything that can affect the properties of the ejecta. These properties impact directly the processing of the dust. For instance, the composition of the ejecta determines which species will bombard and erode the dust, while the temperature determines which mechanisms will be more effective in processing the grains. The physical description of the SNRs must be included into reliable model(s) for the dynamical evolution of the remnants, i.e. the evolution of radius and velocity of the forward and reverse shocks. Well founded models capable of reproducing observations are necessary not only to properly evaluate current dust processing but also to make realistic predictions. The dynamical models will have to be coupled with the description of the dust (size, composition, physical and chemical properties) and of the different processes capable of eroding, fragmenting or even destroying dust grains while they reside inside the supernova remnants.

It has been our choice to focus this section on the works which actually treat the processing of dust by the reverse shock, presenting them at a level of detail sufficient to appreciate the different approaches used by the authors. We do not include therefore the many papers only mentioning the possible effect of the reverse shock in modifying the dust. The studies that we have considered are briefly introduced below. In Sects. 5.1 to 5.6 we discuss how the different authors include in their models the key ingredients listed at the beginning of this section. In Sec. 5.7 we summarise the results in terms of the amount of dust mass surviving the processing by the reverse shock, and show how these findings compare with observations. It is interesting to note that, to our best knowledge, after the study

of Itoh (1985) it has been necessary to wait twenty years to have dust survival in SNRs investigated again, with a renewed and this time persistent interest.

Itoh (1985) estimates the amount of dust erosion in both the blast-shocked circumstellar medium and the reverse-shocked ejecta, adopting self-similar solutions for the expansion of the SNR. The results are applied to the remnants of SN 1979c and SN 1980k.

Dwek (2005) discusses the destruction of SN-condensed dust by the reverse shock assuming homogenous ejecta expanding into a uniform medium, but emphasises that in reality, observations show that the ejecta are clumpy and that the dust resides primarily in these clumps. This is the case for instance for the remnant of Cas A, where dust has been detected in fast moving knots (Lagage et al 1996, Arendt et al 1999). When the reverse shock propagates inside the clumps, its velocity is reduced with respect to the value in the more tenuous medium. The presence of clumpy ejecta has therefore important consequences on the survival of the dust.

Bianchi and Schneider (2007) revise the dust formation model of Todini and Ferrara (2001) based on classical nucleation theory (CNT) and assess the role of the reverse shock in modifying the size and mass of the newly synthesised grains, making predictions on dust properties from formation up to few hundreds of years later, i.e., only considering the non-radiative phase of supernova remnants.

Nozawa et al (2007) study the evolution of dust formed inside primordial type II supernovae (SNe II) and pair-instability supernovae (PI SNe). They follow the dynamics and destruction of the dust, together with the time evolution of gas temperature and density, until 10^5 – 10^6 years after explosion, well extending into the radiative phase. This provides a better idea of how much dust is actually injected into the ISM. An important point addressed by this work is how the thickness of the H envelope of the progenitor star affects the survival of the dust.

Nozawa et al (2010) adapt the dust evolution model developed by Nozawa et al (2007) to study the formation and processing of dust in hydrogen/helium poor CCSNe such as Type Ib/Ic and Type IIb.

Nath et al (2008) adopt an analytical approach which treats directly the effect of reverse shocks traveling through ejecta with a power-law mass distribution, instead of a uniform distribution as in previous works. While various important processes such as dust dynamics are not included, this formalism allows to make a clear separation between destruction occurring within the reverse shock itself, and the processing taking place in the region between the reverse and forward shock.

Silvia et al (2010, 2012) tackle a different aspect of the problem of dust destruction inside supernova remnants considering the processing of dust when this is located inside overdense clumps, instead of being dispersed into a homogeneous medium. This aspect is particularly important because, as previously mentioned, SN ejecta are indeed clumpy (e.g. Fesen et al 2006, Hammell and Fesen 2008) and observations have shown that the dust resides in such dense clumps. This is typically the case of Cas A. To study this problem, Silvia et al. perform numerical simulations on an individual ejecta clump containing dust and encountering a planar reverse shock.

Bocchio et al (2016) study the survival of freshly formed dust inside four well-known core-collapse SNRs: Cas A and the Crab Nebula (in the Milky Way) and

SN 1987A and N49 (in the Large Magellanic Cloud). The formation of dust and the evolution of SNRs are described as in Bianchi and Schneider (2007), with an upgraded molecular network and an updated sputtering treatment.

Biscaro and Cherchneff (2014, 2016) approach the problem of the formation and survival of molecules and dust in Cas A via a rigorous study of the chemistry of the ejecta of type IIb supernovae, which led to the Cas A supernova remnant, including in particular the chemistry of the reverse shock. Biscaro and Cherchneff (2014) focuses on the formation and processing of molecules and dust clusters synthesised in the gas-phase, and it discussed in our companion paper. Biscaro and Cherchneff (2016) deals with the condensation of dust clusters, the grain size distributions expected from the type IIb SN and the processing of dust in the ejecta clumps and in the inter-clump medium.

Micelotta et al (2016) tackle the question of dust survival in SNRs after the passage of the reverse shock, with special application to the clumpy ejecta of Cas A. They adopt a global approach which combines a realistic description of the remnant and its evolution with a robust treatment of dust sputtering, first in the clumps and later on into the smooth inter-clump medium. In particular, a combination of analytical methods and Monte Carlo simulations allows to follow dust sputtering "on-the-fly", taking into account simultaneously the deceleration and erosion of the grains as a function of their size and position inside the clumps.

Depending on their initial size, the newly synthesised grains will be progressively eroded and possibly completely destroyed due to collisions with the shocked gas. As previously mentioned, this phenomenon is known as sputtering (e.g. Tielens et al 1994, and references therein) and consists on the progressive removal of atoms or molecules from the surface of the grains, induced by impacts with the particles populating the gas. According to the velocity distribution of the incoming projectiles, sputtering is classified as kinetic (or inertial) when the collision velocity is given by the relative motion of the grains through the gas, and thermal when the velocity of the projectiles is due to their thermal motion and is determined by the temperature of the shocked gas. Dust destruction via sputtering is discussed in Sec. 5.6.

5.1 Modelling the dynamical evolution of supernova remnants

The velocity of the reverse shock determines the velocity distributions of the gas particles which will impinge on dust grains, progressively eroding them. The velocity of the reverse shock is related to the velocity of the forward shock, and they can both be calculated from dynamical models for the expansion of the SN ejecta. These models typically depend on the energy of the explosion, the mass and initial density profile of the ejecta, and on the density profile of the circumstellar medium the ejecta are expanding into.

Itoh (1985) adopts the self-similar solutions from Chevalier (1982) for ejecta-dominated (ED – see Sec. 2.1) supernova remnants having ejecta with a power-law density distribution (characterised by the index $n > 5$) expanding into a circumstellar medium which also has a power-law density distribution (with index $s < 3$).

Many of the works discussed in Sec. 5 are based on the analytical models of Truelove and McKee (1999) for the evolution of a young SNR transitioning be-

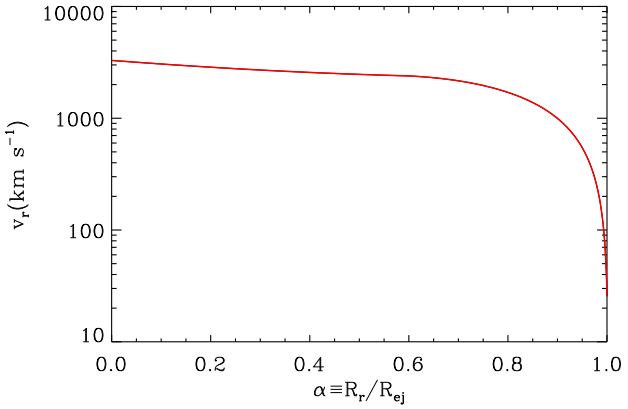

Fig. 11 Velocity of the reverse shock as a function of the parameter α for homogeneous SN ejecta expanding into a uniform medium. The value $\alpha = 1$ corresponds to the outermost ejecta layer, while $\alpha = 0$ to the innermost one. Figure reproduced from Dwek (2005).

tween the ED and Sedov-Taylor (ST – see Sec. 2.1) phases. Truelove and McKee (1999) highlight the fact that the ED stage is strongly dependent on the ejecta parameters, and provide analytical expressions that smoothly merge the blast-wave and reverse shock solutions between the ED and ST stages. These expressions are particularly suited to describe the dynamical evolution of young remnants like Cas A, which are currently in an intermediate step between the ED and ST phases.

In Dwek (2005), the evolution of the reverse shock is provided by the solutions from Truelove and McKee (1999) for the specific case of homogeneous ejecta expanding into a uniform medium. The ejecta are characterised using the parameter $\alpha \equiv R_r/R_{ej}$, where R_r is the radius of the reverse shock and R_{ej} is the outer radius of the ejecta. With this parametrisation, $\alpha = 1$ corresponds to the outermost ejecta layer, and $\alpha = 0$ to the innermost one. The velocity v_r of the reverse shock as a function of the parameter α is reproduced in Fig. 11.

Also Bianchi and Schneider (2007) and later on Bocchio et al (2016) describe the evolution of supernova remnants using the analytical solutions from Truelove and McKee (1999) for homogeneous ejecta expanding into a uniform medium. The ejecta are divided into spherical shells and those not yet visited by the reverse shock are considered to expand homologously. Three different values are adopted for the density of the interstellar medium where the remnants are expanding into. The strong adiabatic shocks under consideration are described using the classical Rankine-Hugoniot jump conditions. For these latter we think that the reader may find interesting to refer to the original publications (Rankine 1870, Hugoniot 1887, 1889). As Bianchi and Schneider (2007) emphasise, their approximation for the SNR evolution (density and temperature) is very crude, nevertheless it agrees with some 1D hydrodynamical models and simulations (van der Swaluw et al 2003, Del Zanna et al 2003).

To describe the evolution of the forward and reverse shocks in the supernova remnant, Nath et al (2008) adopt a slightly more sophisticated approach, using again the self-similar solutions from Truelove and McKee (1999) but for ejecta with a core-envelope density structure, where the power-law envelope is charac-

terised by the index n. The ejecta expand into a uniform ambient medium and different values of n are considered (which lead to different functional forms for the solutions – Truelove and McKee 1999): $n < 3$, $n = 4$ and $n > 5$. The ejecta are divided into a series of shells identified by the same parameter α as in Dwek (2005), but here called w. It is assumed that the ejecta in a given shell evolve adiabatically until they are hit by the reverse shock. At that point, density and temperature jump to their post-shock values before continuing to evolve adiabatically, i.e. $\rho \propto t^{-3}$ and $T \propto t^{-2}$ for a monoatomic gas.

Biscaro and Cherchneff (2014, 2016) consider simple homologous expansion of the ejecta into a homogeneous medium, and the same approach is adopted by Nozawa et al (2007) to study primordial type II supernovae (SNe II) and pair-instability supernovae (PI SNe), for which therefore the composition of the ambient medium is taken as primordial. Nozawa et al (2010) consider Type IIb SNe with application to the specific case of Cas A, and adopt for the circumstellar medium not only a uniform profile but also a power-law density profile with exponent $s = 2$, produced by a steady stellar wind during the evolution of the progenitor.

To describe the dynamical evolution of Cas A, Micelotta et al (2016) start from the seminal work of Truelove and McKee (1999) and its further development by Laming and Hwang (2003), but generalize their treatment to derive analytical expressions for the evolution of inhomogeneous ejecta (uniform core + power-law envelop with exponent $n = 9$) expanding into a non-uniform ambient medium (power-law with exponent $s = 2$ – pre-supernova steady stellar wind). This configuration represents indeed a closer match to the physical situation of Cas A and the adopted parametrisation allows to match the radii and velocities of the forward and reverse shocks and the pre-shock density of the smooth ejecta. The ejecta layers are characterised by the same parameter α as in Dwek (2005). Figure 12 shows the velocities of the forward and reverse shocks as a function of α, calculated with the equations derived by Micelotta et al (2016) for Cas A. The comparison with Fig. 11 reveals how a different density structure for the ejecta and the ambient medium modifies the behaviour of the reverse shock velocity. In the homogeneous ejecta – uniform ambient medium case (Fig. 11) the reverse shock starts at a very low velocity in the outermost ejecta layer ($\alpha = 1$) before rising steeply to its maximum value in the innermost layer ($\alpha = 0$). For inhomogeneous ejecta expanding into a power-law medium (Fig. 12) the situation is different: the velocity of the reverse shock is at maximum for $\alpha = 1$ and decreases to reach a constant value of $\sim$1600 km s^{-1}.

Finally, the results from the simulations in Silvia et al (2010, 2012) are not included into an evolutionary model of the reverse shock.

5.2 The physical properties of SN ejecta

There is a complex interplay between the physical properties of SN ejecta and the processing of dust grains within them. We already mentioned that the composition of the ejecta determines which species will bombard and erode dust grains. We have shown in Sec. 5.1 that different density profiles for the ejecta and the surrounding medium produce different temporal profiles for the reverse shock velocity. The proper evaluation of dust survival in SNRs requires a knowledge as

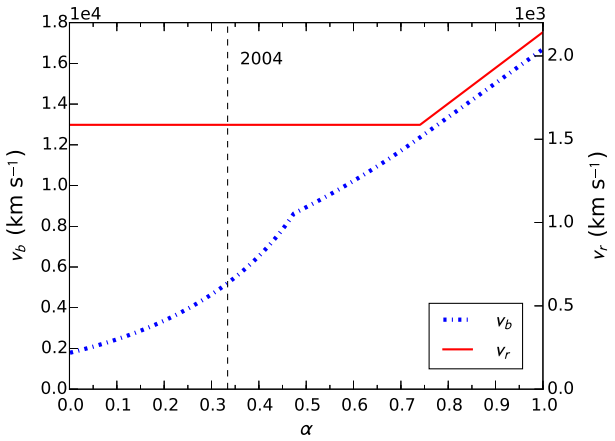

Fig. 12 Velocity of the blast-wave (v_b, left y-axis) and reverse shock (v_r, right y-axis) as a function of α, calculated for Cas A assuming inhomogeneous ejecta expanding into a non-uniform ambient medium. The curve for v_b gives the velocity of the blast-wave shock when the reverse shock hits a layer α of the ejecta. The reverse shock velocity is calculated in the frame of the unshocked ejecta ahead of it. The vertical line indicates the value $\alpha = 0.33$, which corresponds to the ejecta layer encountering the reverse shock in 2004. Figure reproduced from Micelotta et al (2016).

accurate as possible of the conditions where dust processing takes place. Some of the ejecta properties can be derived from observations, while SN models are necessary for some others, as shown below.

For the parameters of SN 1979c and SN 1980k, Itoh (1985) adopts estimates based on or consistent with the analysis of Dwek (1983). Bianchi and Schneider (2007) use the physical properties derived from the SN models of Woosley and Weaver (1995). These include the metallicity and mass of the progenitor star, which determine the initial composition of the ejecta, and the mass of the ejecta and the kinetic energy of the explosion, where these latter control the dynamics of the ejecta. The initial temperature and density of the ejecta are chosen to match those of SN 1987A. Dust grains collide with H, He and O in the ejecta, taken as the most abundant elements. However, this assumption does not fully apply to remnants like Cas A, whose hydrogen content is negligible (e.g. Nozawa et al 2007). For the specific case of Cas A, Bianchi and Schneider (2007) found that all the available observational constraints (at the time of publication) could be matched by a 15 – 25 $M_\odot$ progenitor which lost its hydrogen envelope. They apply their evolutionary model for the ejecta to a 12 $M_\odot$ progenitor star, but have to neglect the hydrogen mass. The adopted ejecta mass is ~3 $M_\odot$.

For primordial SNe II and PI SNe, Nozawa et al (2007) use the initial conditions for the density and velocity structure of the ejecta from the hydrodynamical models for Population III SNe by Umeda and Nomoto (2002). An important assumption is that SNe II and PI SNe have retained their thick hydrogen envelopes, because no mass loss seems possible in these massive metal-free stars. The best explosion model for each supernova studied by Bocchio et al (2016) is selected comparing the available physical properties derived from observations with the

output from the FRANEC stellar evolutionary code (Limongi and Chieffi 2006). For the shocked gas in all the considered remnants, Bocchio et al (2016) adopt a composition of H^+, He^{++} and O^+, taken as the most abundant elements. They do not provide a description of the ionisation state of the gas, under the hypothesis that the very high temperatures considered will imply full ionisation for the gas. These assumption might not be completely valid in all the remnants under examination. Oxygen is the most abundant element in the smooth ejecta of Cas A, but Ne, Mg, Si, S, Ar, and Fe are also present (Hwang and Laming 2012) while H and He are negligible. The results from the photo-ionization and shock modelling code Mappings III (Allen et al 2008) indicate that the dominant ionisation state for oxygen is +6 or higher, but full ionisation for the other elements is unlikely (Micelotta et al 2016). For all remnants, the temperature of the shocked gas is calculated assuming equilibration between ions and electrons. However, this is not the case for Tycho (Yamaguchi et al 2014) or Cas A (Micelotta et al 2016, see Sec. 5.4).

Biscaro and Cherchneff (2014, 2016) consider for Cas A a model with stratified ejecta, microscopic mixing in each layer and no leakage between zones. The elemental composition is given by the model of Rauscher et al (2002) for a 19 $M_\odot$ SN progenitor. Number density and temperature profiles are taken from the explosion models for type IIb SNe of Nozawa et al (2010) which assume homologous expansion for the ejecta gas. All the parameters adopted by Micelotta et al (2016) for Cas A or derived from their dynamical evolution model are in agreement with current estimates and/or observations and are explicitly reported in their Table 1. Both Biscaro and Cherchneff (2014, 2016) and Micelotta et al (2016) model the ejecta as overdense clouds embedded into a tenuous and smoother medium, in agreement with observations (e.g. Fesen et al 2001, Rho et al 2009a, 2012, Wallström et al 2013). It is assumed that the clouds have a composition of pure oxygen (Docenko and Sunyaev 2010, Chevalier and Kirshner 1979). For the smooth inter-clump medium Micelotta et al (2016) adopt the composition determined by Hwang and Laming (2012) from X-ray observations, which consists of O, Ne, Mg, Si, S, Ar, and Fe, while H and He are negligible. The inclusion of such heavier elements implies higher sputtering rates with respect to the case when much lighter projectiles are considered. The properties of the ejecta clouds and the importance of considering a clumpy medium are discussed in Sec. 5.3.

5.3 Clumpy ejecta

SN ejecta are not homogeneous but they show a variety of structures, ranging from dense clouds to filaments. As already mentioned, this is the case for Cas A, where dense clumps become optically visible due to heating by the reverse shock and fade out progressively. The dust residing inside the clumps is processed by the reverse shock. Biscaro and Cherchneff (2014) have shown that the presence of warm dust in Cas A detected in the IR seems to require high-density clumps in the ejecta as main sources of molecules and dust. Indeed, the low-density stratified ejecta resulting from explosion models of type IIb SNe which do not include overdense regions are incapable of synthesising large amounts of molecules and are almost dust-free.

The presence of clumpy ejecta has a strong impact on the survival of dust because it changes the physical conditions under which processing occurs. To study this problem, Silvia et al. focus on the specific idealised case of an individual ejecta clump encountering a planar reverse shock, performing three-dimensional (3D) cloud-crushing simulations. The analogue problem of ISM clouds hit by SN-driven shocks has been already treated using hydrodynamic simulations (Bedogni and Woodward 1990, Stone and Norman 1992, Klein et al 1994, Mac Low et al 1994, Orlando et al 2005, Patnaude and Fesen 2005, Nakamura et al 2006). Here, the parameter space is adjusted to the new physical conditions, although it should be noted that the simulations are not included into an evolutionary model of the reverse shock. The simulations are performed using the cosmological, Eulerian adaptive mesh refinement (AMR), hydrodynamics + N-body code, Enzo (Bryan and Norman 1997, Norman and Bryan 1999, O'Shea et al 2005). When the reverse shock with velocity $v_{\rm shock}$ encounters a cloud with constant overdensity χ, its propagation velocity inside the cloud is reduced by a factor of $\chi^{1/2}$. The simulations follow the dynamical fragmentation of the cloud due to the passage of the shock, whose timescale is given by the cloud-crushing time $t_{\rm cc} = \chi^{1/2}\, r_{\rm cloud}/v_{\rm shock}$, where $r_{\rm cloud}$ is the radius of the cloud (Klein et al 1994). In fact, $t_{\rm cc}$ is the time required by the reverse shock to cross half of the cloud diameter. The calculations are performed for different values of $\chi^{1/2}$ and $v_{\rm shock}$ and consider the effect of gas cooling as well (see Sec. 5.4). An example of the results is shown in Fig. 13, which compares the evolution of an ejecta clump with and without cooling in the case of $\chi = 1000$ and $v_{\rm shock} = 1000$ km s^{-1}. It can be noted that while the simulation progresses, more and more material gets shredded by the constant inflow. When cooling is turned on, cold and dense nodules form in the fragmenting cloud. These features appear to be amplifications of overdensities created in the clump.

Biscaro and Cherchneff (2014, 2016) consider dense ejecta clumps which are currently being processed in Cas A. For the velocity of the reverse shock inside the clump, they explore the range 35 – 200 km s^{-1} (consistent with the results of Docenko and Sunyaev 2010) which can be obtained adopting $\chi = 100 - 1000$ and velocities of the reverse shock between 1000 and 2000 km s^{-1} (compatible with the value of ∼2000 km s^{-1} from Morse et al 2004). The time variation of the gas parameters of the clumps shocked by the reverse shock is derived from the model of Borkowski and Shull (1990) and the results of Docenko and Sunyaev (2010), combined with the equation for homologous expansion of the ejecta from Nozawa et al (2010). The lifetime of the cloud against shock disruption is given by $3 \times \tau_{\rm cc}$ (Klein et al 1994, Silvia et al 2010), where Biscaro and Cherchneff (2016) adopt for $\tau_{\rm cc}$ a value of 100 years (given by a clump radius of 10^{16} cm, a density contrast of 1000 and a velocity of the reverse shock of 1000 km s^{-1}, Silvia et al 2010). It should be noted, however, that this cloud lifetime does not agree with the optical lifetime of ∼30 years deduced from optical observations for the Fast Moving Knots (FMKs) in Cas A (Kamper and van den Bergh 1976).

Biscaro and Cherchneff (2016) assume that dust is processed via inertial sputtering in the clumps and it is instantaneously released into the smooth ejecta after the cloud has been disrupted. However, this approach does not take into account the fact that the residence time of the dust in the clumps can be shortened by the thermal evaporation of the clouds (Cowie and McKee 1977) and by the capability of the grains to escape from the cloud due to their ballistic velocities. These

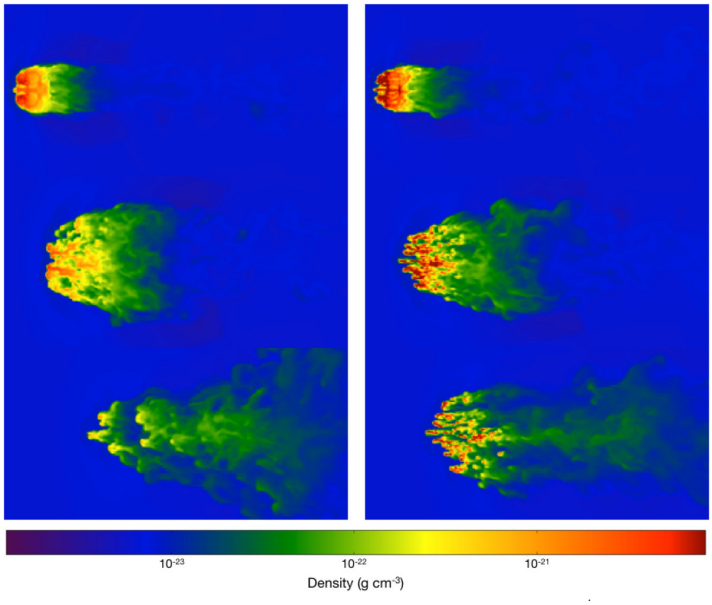

Fig. 13 Evolution of an ejecta clump with density contrast $\chi = 1000$ crushed by a shock with velocity $v_{\rm shock} = 1000$ km s^{-1}. The figure depicts the density projections ($x - z$ plane) for a simulation with cooling off (left panel) and cooling on. Time progresses from top to bottom and the three snapshots have been taken at $t = 1.8t_{\rm cc}$, $2.4t_{\rm cc}$, $3.0t_{\rm cc}$. Figure reproduced from Silvia et al (2010).

phenomena have been investigated by Micelotta et al (2016) and are discussed in Sec. 5.6.

For the properties of the ejecta clouds Micelotta et al (2016) adopt a fixed set of values capable of reproducing observations. The assumed pre-shock density for the clouds is $n_{\rm cloud} = 100$ cm^{-3} with a density contrast $\chi = 100$, which allow to reproduce the optical spectra of the fast moving knots (FMKs) in Cas A (Sutherland and Dopita 1995). The resulting pre-shock density of the smooth ejecta, $n_{\rm smooth} = n_{\rm cloud}/\chi = 1.0$ cm^{-3}, is consistent with the ambient density of 0.1 – 10 cm^{-3} estimated by Morse et al (2004). The diameter of a typical cloud is taken as $1.5{\times}10^{16}$ cm $\simeq 0.005$ pc, within the observed range of $(1 - 5){\times}10^{16}$ cm (Fesen et al 2011). The passage of the reverse shock inside the clouds heats them up so that they become optically visible before and/or while getting fragmented. This optical lifetime is defined as the time required by the reverse shock to cross the cloud and is therefore given by twice the cloud crushing time. With their calculated value of ~ 1600 km s^{-1} for the current velocity of the reverse shock in the smooth ejecta of Cas A, Micelotta et al (2016) obtain $2t_{\rm cc} = 30$ yr, in agreement with the determinations from Kamper and van den Bergh (1976).

5.4 Ejecta cooling

The type and level of processing of dust in SNRs depends on the temperature of the ejecta embedding the grains. The temperature of the immediate post-shock gas can be calculated using the classical expression derived from the Rankine-Hugoniot jump conditions:

$$T = \frac{3}{16}\,\frac{\mu}{k_{\rm B}}\,v_{\rm s}^2, \tag{12}$$

where μ is the mean molecular mass per particle and $v_{\rm s}$ is the velocity of the shock. The temperature depends therefore not only on the velocity of the shock but also on the mass and ionisation state of the gas particles (included in the term μ). Eq. 12 has been used (implicitly or explicitly) in all the papers discussed in Sec. 5. The equation assumes full electron-ion temperature equilibration, however the validity of this assumption depends on the velocity of the shocks considered. As pointed out by Micelotta et al (2016), for the reverse shock in Cas A ($v_{\rm s} \sim 1600$ km s^{-1}) the results of van Adelsberg et al (2008) would indicate that the hypothesis of temperature equilibration may not be fully justified.

The typical temperature of the post-shock X-ray emitting gas in the smooth ejecta of SNRs like Cas A is of the order of $10^7 - 10^8$ K. The value of the immediate post-shock temperature during the propagation of the reverse shock is determined by the model adopted for the evolution of the reverse shock itself coupled with Eq. 12. The ejecta at any given location of the remnant are assumed to evolve adiabatically until they are hit by the reverse shock. After the gas gets shocked, the temperature jumps to its post-shock values before continuing to evolve adiabatically. For the high temperatures under consideration, gas radiative cooling is generally negligible. This has been shown explicitly by Micelotta et al (2016) for Cas A. The temperature evolution of the shocked smooth ejecta is calculated using Mappings III under non-equilibrium ionization (NEI) conditions. The results show that the temperature remains constant at $\sim 10^8$ K for more than 10^4 years before dropping abruptly. This is longer than the time frame for dust evolution considered in their work, and it holds for the majority of the studies considered here. In addition to atomic and inverse Compton cooling, Nozawa et al (2007) include thermal cooling from the collisionally heated dust in the post-shock gas, showing that this has little effect on the dust destruction efficiency.

If the ejecta contain dense clumps, these latter will be shocked and heated up as well by the reverse shock propagating through them, but the post-shock temperature will be lower because of the reduced speed of the shock (the shock velocity inside the clumps is reduced by a factor of $\sqrt{\chi}$, where χ is the ratio between the density of the cloud and the density of the smooth medium outside). Silvia et al (2010) investigate the effects on dust survival of including radiative cooling in a gas with half-solar metallicity. Cooling is described using the analytical formula of Sarazin and White (1987), which approximates the cooling rate as a function of temperature for a gas with half-solar metallicity in ionisation equilibrium. Silvia et al (2012), considers the more realistic case of metal-enriched ejecta knots including the cooling of a gas with metallicity ranging from $Z = Z_\odot$ to $Z = 100 Z_\odot$. This is an important point to address because the ejecta are indeed expected to have a high metal content, which would change their cooling properties and also provide heavier particles which are more efficient in sputtering the dust. In this

case, cooling is calculated using the photoionisation code Cloudy (Ferland et al 1998) with the assumptions that *i*) the gas is in ionisation equilibrium, and *ii*) both ions and electrons have the same temperature. These assumptions may not be fully valid in some supernova remnants like Cas A (Micelotta et al 2016).

For the post-shock temperature of the oxygen-rich dense clumps in Cas A, Biscaro and Cherchneff (2014, 2016) adopt the values from Borkowski and Shull (1990) and Docenko and Sunyaev (2010). For the sputtering calculation, the specific value of 1500 K from Docenko and Sunyaev (2010) is used.

To calculate the immediate post-shock temperature in the ejecta clouds of Cas A, Micelotta et al (2016) as well use Eq. 12, assuming that the pre-shock ionisation state of oxygen is +2. The assumption of temperature equilibration between ions and electrons implicit in Eq. 12 is justified in the present case because the equilibration length scale is of the order of about $(2-4)\times10^{13}$ cm (Itoh 1981, J. Raymond, private communication) corresponding to less than 0.27% of the diameter of clumps. Such a quick temperature equilibration is in agreement with the findings from van Adelsberg et al (2008) and Ghavamian et al (2007). The resulting post-shock temperature is $T_{\rm cloud} \sim 3\times10^6$ K, consistent with Sutherland and Dopita (1995) and Borkowski and Shull (1990). Micelotta et al (2016) calculate explicitly the post-shock cosoling of the dense clumps, using the functions computed by Sutherland and Dopita (1995, see their Fig. 2) which differ from the equilibrium curves often used (e.g. by Silvia et al 2012). The work of Sutherland and Dopita (1995) appears indeed as the only available estimate of the cooling function of an oxygen-rich shocked gas. The calculations performed by Micelotta et al (2016) shows that the cooling is very rapid due to the extreme metallicity of the gas. On a timescale of six months the temperature drops from $\sim3\times10^6$ K to 300 K. The thickness of the layer beyond the shock front having a temperature sufficiently high for efficient thermal sputtering ($\sim10^5$ K) represents only 1.4% of the diameter of the clump. A very small amount of dust populates at each time such a thin layer, which allows to neglect thermal sputtering in the ejecta clumps.

5.5 The initial grain size distribution and composition of the newly formed dust

The initial composition and size distribution of the dust synthesised in SN ejecta are two of the key input parameters in any model of dust processing inside SNRs. Such knowledge relies heavily on theoretical models of dust formation, which can produce very different results even for similar initial conditions. The various scenarios for dust formation in SN ejecta are discussed in our companion paper (Sarangi et al 2018). We summarise here the choices made in the studies we are discussing, in the perspective of evaluating the impact of these parameters in the resulting dust survival rate.

Nozawa et al (2007) assume that dust condenses in the He core, where the metal-rich cooling gas provides the appropriate conditions for grain nucleation and grow according to classical nucleation theory (CNT – see e.g. Kalikmanov 2013, for a recent review). The resulting dust composition and size distributions depend on the elemental abundance inside the He core (Kozasa et al 1989). Dust formation is based on the Nozawa et al (2003) model, whose calculated distributions for dust synthesised in a CCSN with a progenitor mass of 20 $M_\odot$ are also those adopted by Silvia et al (2010, 2012). Nozawa et al (2003) consider two cases for the elemental

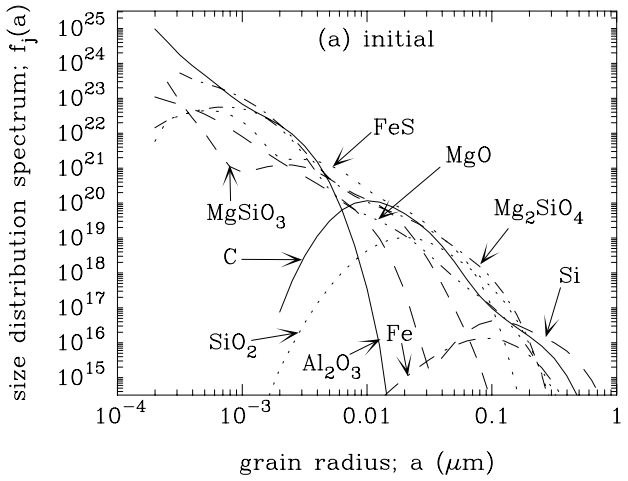

Fig. 14 Size distributions of the different dust species synthesised in SN ejecta (standard model). Figure reproduced from Nozawa et al (2007).

composition of the ejecta: i) Unmixed ejecta which retain their original onion-like structure, where different grains will be produced in the different layers: carbon grains in the C-rich He layer; Al_2O_3 (alumina), Mg_2SiO_4 (forsterite) and MgO grains in the O-Mg-Si layer; Al_2O_3, $MgSiO_3$ (enstatite) and SiO_2 (silica) grains in the O-Si-Mg layer; Si and FeS grains in the Si-S-Fe layer; and Fe grains in the innermost Fe-Ni core.; ii) Mixed ejecta where oxides (Al_2O_3 and Fe_3O_4 - magnetite) and silicates ($MgSiO_3$, Mg_2SiO_4 and SiO_2) form in uniformly mixed ejecta with C/O<1. As an example, we reproduce in Fig. 14 the size distribution of each dust species expected from the "standard model" in Nozawa et al (2007) i.e. the one with progenitor mass $M_{\rm pr}$ = 20 $M_\odot$, initial hydrogen ambient density $n_{\rm H,0}$ = 1 cm^{-3} and unmixed grain model inside the He core. The same approach is used by Nozawa et al (2010), who find that the average radius of the produced dust is smaller than 0.01 μm, much less than the size of grains produced by SNe II-P with massive hydrogen envelopes.

CNT is also used by Bianchi and Schneider (2007) to form amorphous carbon (AC), iron, Al_2O_3, Fe_3O_4, $MgSiO_3$, Mg_2SiO_4 and SiO_2 with the expected log-normal distribution. The same code used in Bianchi and Schneider (2007) but with an upgraded molecular network from Marassi et al (2015) is utilised by Bocchio et al (2016). For the size distribution of the dust grains condensed in the SN ejecta, Nath et al (2008) refer to the work of Todini and Ferrara (2001) and Nozawa et al (2003) and adopt two power-laws dn/d$a \propto a^\alpha$, where a is the radius of the grain and α = -2.5 for smaller grains and α = -3.5 for larger grains. A simplified composition of graphite and silicate grains is considered (as in the interstellar medium, see the review from Draine 2003, and the references therein) and the same size range 10^{-7} – 3×10^{-5} cm is assumed for all grains, although an upper limit of 10^{-6} cm is also considered.

Because of its relative simplicity, CNT has been widely used to model the formation of dust grains in astrophysical environments (starting from e.g. Yamamoto and Hasegawa 1977, Draine and Salpeter 1977) including SN ejecta (e.g. Kozasa et al 1989, Todini and Ferrara 2001, Nozawa et al 2003, Schneider et al 2004,

Nozawa et al 2007, Bianchi and Schneider 2007), however Biscaro and Cherchneff (2014, 2016) emphasise the fact that this formalism is likely inadequate for this purpose because the assumed gas equilibrium conditions do not apply to a shocked gas in an environnement controlled by radioactivity (Donn and Nuth 1985, Cherchneff and Dwek 2009). In addition, the CNT approach does not discriminate between possible dust chemical composition, likely leading to a variety of condensates which have not been identified in SN emission spectra or pre-solar grains. Instead of CNT, Biscaro and Cherchneff (2014) use a chemical kinetic approach under non-equilibrium conditions to determine the masses and types of molecules and dust clusters synthesised by the SNe, and feed the results into the model developed by Sarangi and Cherchneff (2015) for grain growth via coalescence and coagulation of these dust clusters. This procedure is used to calculate the grain size distributions and masses expected from the SN progenitor for four types of dust: silicates in the form of forsterite (Mg_2SiO_4), alumina (Al_2O_3), carbon, and silicon carbide (SiC). The preferred chemical kinetic treatment provides a more realistic description of the environmental conditions where dust forms and a more complete approach to dust formation which includes both the gas phase (molecules formation) and the solid phase (dust formation via condensation of dust clusters).

Due to the uncertainties in the initial grain size distribution of SN-condensed dust, Micelotta et al (2016) adopt as a test case the classical MRN power-law expression with exponent -3.5 typically found in the diffuse ISM (Mathis et al 1977), although this may not fully apply to SN dust. A simplified composition of silicates ($MgSiO_3$) and amorphous carbon (AC) is assumed. The MRN distribution has also been the choice of Itoh (1985).

5.6 Dust destruction in SNRs: thermal and inertial sputtering

Dust grains progressively embedded in the reverse-shocked gas are affected by a variety of destructive processes resulting from the collisions with gas particles and other dust grains. However, not all these processes have the same importance in modifying the initial size distribution of the dust under the conditions found in supernova remnants. The four main processes to consider are the following: *i*) sputtering, i.e. the ejection of atoms from the grain surface due to grain collisions with high-velocity atoms and ions, with consequent erosion of the target dust particles; *ii*) sublimation, i.e. the direct transition from the solid to the gas phase due to collisional heating in the high-temperature gas; *iii*) shattering, i.e. fragmentation of the dust particles into smaller fragments due to grain-grain collisions; *iv*) partial or complete vaporisation of the grains, i.e. rapid destruction with return of the dust constituents to the gas phase due to the intense heat generated in grain-grain collisions.

The relative contribution of these four processes has been evaluated by Bocchio et al (2016). Sublimation is treated in the same way and gives the same results as in Bianchi and Schneider (2007), i.e. a negligible contribution to dust destruction for all the SNRs considered in their work. Shattering and vaporisation are evaluated using the method from Tielens et al (1994) and Jones et al (1996) and lead as well to a minor contribution to dust processing with respect to sputtering, because of the low dust density which prevents frequent grain-grain collisions,

as also pointed out by Biscaro and Cherchneff (2016) and Bianchi and Schneider (2007). The main destruction agent for dust in SNRs is therefore sputtering, defined *kinetic* (or *inertial* or *non-thermal*) when the collision velocities are determined by the relative motion between the grains and the gas, and it is defined *thermal* when the collision velocities arise from the thermal motion of the gas. In this case, the erosion rate depends on the gas temperature.

The classical formalism for sputtering in solids (Matsunami et al 1981, Andersen and Bay 1981, Sigmund 1981, Bohdansky 1984) has been widely used to describe the sputtering of cosmic dust. Itoh (1985) considers thermal sputtering in the hot post-shock gas adopting a constant sputtering rate of 10^{-6} μm cm^3 yr^{-1} (Draine and Salpeter 1979a). This value represents a reasonable approximation (within 30%) of the sputtering rate of graphite, silicate, iron, and H_20 ice bombarded by hydrogen, helium and oxygen with relative abundances of 1, 0.1 and 0.001 respectively. All the other theoretical works discussed in Sec. 5 adopt the sputtering yields from Tielens et al (1994) and/or Nozawa et al (2006). The sputtering yield, Y, is defined as the number of atoms/molecules ejected from a grain per incident projectile of a given composition and depends on the energy of the projectiles. In particular, Bocchio et al (2016) use a revised version of such formalism (Bocchio et al 2014) where thermal and inertial velocities are not treated separately but their combined effect is estimated using a skewed Maxwellian distribution, as originally implemented by Shull (1978) and later on by Guillet (2008) and Bocchio et al (2014). The sputtering yields are corrected to take into account the fact that sputtering is size-dependent because the targets are not semi-infinite slabs of material but particles with a finite radius (Jurac et al 1998, Serra Díaz-Cano and Jones 2008, Bocchio et al 2014). The mass of (sub)nano-sized species like PAHs is estimated negligible, thus the specific dissociation of these particles (Micelotta et al 2010a,b) has not been implemented. However, this hypothesis still needs to be fully verified.

The dust erosion rate strongly depends on the dynamics of the dust. When passing through the reverse shock, grains of different sizes will have different velocities due to the effect of drag forces. These differential velocities are responsible for kinetic sputtering. Itoh (1985) estimates that the relative motion between dust and gas gets quickly and strongly reduced via direct collisions, dominating over Coulomb collisions. Magnetic forces, even if present, would not increase relative motions because of the reduction of the magnetic field due to the expansion of the remnant. Thermal sputtering is therefore the dominant dust erosion mechanism. Nozawa et al (2007, 2010), Bocchio et al (2016) and Biscaro and Cherchneff (2016) evaluate the contribution of both thermal and inerttial sputtering. They treat explicitly the dynamics of the dust using the classical expressions from Draine and Salpeter (1979a), McKee et al (1987). Betatron acceleration of the dust due to the effect of magnetic fields on charged grains is estimated to be unimportant (Bocchio et al 2016). Bianchi and Schneider (2007) also consider both thermal and inertial sputtering but without treating dust dynamics. Gas drag and grain charge are not included and all grains are kept at the same initial velocity. Nath et al (2008) do not include dust dynamics and consider only thermal sputtering in the hot post-shock gas. In the numerical simulations of Silvia et al (2010, 2012) the dust is assumed to be fully coupled with the flow of the gas in the cloud. This implies operating in the limit of purely thermal sputtering.

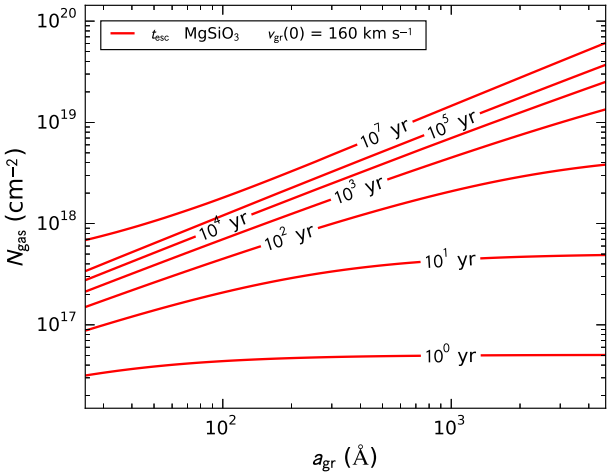

Fig. 15 Time t_{esc} required by a silicate dust grain with radius a_{gr} and initial velocity $v_{gr}(0) = 160$ km s^{-1} to traverse a column density of gas N_{gas}. Figure reproduced from Micelotta et al (2016).

The presence of overdense clumps strongly modifies the dynamics and processing time-scale of the dust grains residing in there. Micelotta et al (2016) study the dynamics of the dust grains located inside the cold ejecta clouds of Cas A using the formalism from Baines et al (1965), Draine and Salpeter (1979a) and McKee et al (1987). The grains acquire a relative velocity with respect to the gas due to the cloud shock propagating inside the cloud itself and generated by the interaction between the clump and the reverse shock. Gas-grain collisions reduce asymptotically to zero such relative velocity while eroding progressively the grains via kinetic sputtering. Figure. 15 shows the time t_{esc} required by a silicate grain of a given size to traverse a column density of gas N_{gas}. The contour plot depicts t_{esc} as a function of the column density of gas traversed and dust grains radius. Large grains sitting close to the edge of the clump may be able to escape before suffering substantial sputtering, while smaller grains located in the inner regions are likely eroded and/or stopped before getting close to the surface.

The level of destruction due to inertial sputtering depends on how much time the grains spend inside the clumps. As mentioned in Sec. 5.3, there are three main phenomena affecting the residence time of the grains in the clouds (Micelotta et al 2016). The first is the possibility for the grains to escape from the cloud due to their ballistic velocities, and the corresponding timescale is given by t_{esc}, discussed in the previous paragraph. The second is the dynamical fragmentation of the clouds due to the passage of the reverse shock. Following Klein et al (1994), the time required for dynamical fragmentation, t_{dest}, is taken as $t_{dest} = 3.5t_{cc}$ where t_{cc} is the cloud crushing time already discussed. With this choice of parameters, Micelotta et al (2016) calculate $t_{cc} = 15$ yr and $t_{dest} = 52.5$ yr. This is much shorter than the value of 300 years adopted by Biscaro and Cherchneff (2016). It is assumed that after the time t_{dest} the ejecta cloud is fragmented and dispersed, releasing into the smooth ejecta the fresh dust still residing in there. The third competing process is the thermal evaporation of the clouds (Cowie and McKee 1977). The evaporation

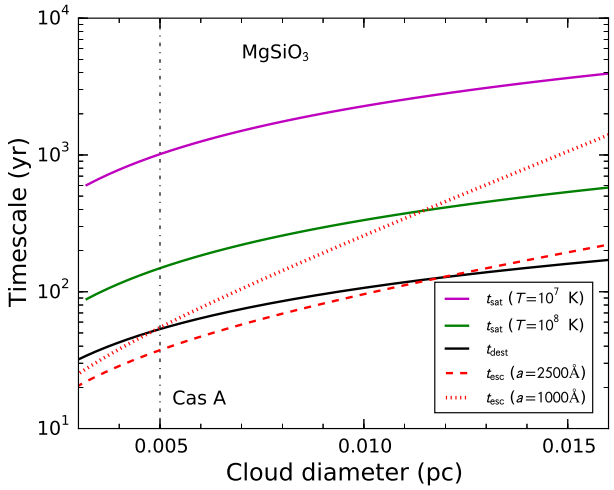

Fig. 16 Comparison between cloud destruction time t_{dest}, cloud evaporation time t_{sat} (calculated for two temperatures of the smooth ejecta) and dust escape time t_{esc} (calculated for two grain sizes) as a function of the diameter of the clump. For the calculation of both t_{esc} and t_{dest}, the initial velocity of the grains is $v_{gr}(0)$ = 160 km s^{-1}. The vertical line indicates the diameter adopted for the Cas A clumps. Figure reproduced from Micelotta et al (2016).

timescale, t_{sat}, is calculated using the results from Dalton and Balbus (1993) for the case of highly saturated conduction appropriate for the Cas A knots.

Fig. 16 shows the above timescales for silicate grains as a function of the diameter of the clouds. The evaporation time is calculated for two temperatures of the smooth ejecta surrounding the clouds: T=10^7 K (consistent with the electron temperature derived from X-ray observations Hwang and Laming 2009) and T=10^8 K (derived from Eq. 12). The two curves for the escape time t_{esc} are calculated for two grain sizes: 2500 Å (upper limit of the MRN grain size distribution) and 1000 Å (an intermediate value). Because the cloud diameter is the maximum distance that a dust grain would have to cross to escape, the plotted value of t_{esc} is the largest possible. Both t_{esc} and t_{dest} are calculated assuming for the grains an initial velocity of 160 km s^{-1}, which is the lowest velocity reached by the reverse shock inside the ejecta clumps of Cas A (see Fig. 12) It follows therefore that the plotted t_{dest} is also an upper limit. The inspection of the figure and the considerations above clearly show that in Cas A the trade is between the escape time and the destruction time. If the grains are sufficiently big, they will escape from the clouds before these latter get disrupted and will start experiencing thermal sputtering in the hot smooth ejecta.

The initial size of the grains and their position inside the cloud determine whether they will be injected into the smooth ejecta before the cloud gets fragmented and dispersed. Such fugitive grains will thus start to be eroded by thermal sputtering in the smooth ejecta while the remaining dust population is still trapped inside the cloud. Micelotta et al (2016) couple explicitly dust erosion and dust deceleration and implement their analytical expressions into a Monte Carlo simulation which allows to follow “on the fly” the journey of each particle through

kinetic sputtering (in the clumps) and thermal sputtering (in the smooth ejecta) and determine the resulting dust size and mass.

Another important factor influencing the dust erosion rate is the location of the grains inside the remnants (Nozawa et al 2007, Bianchi and Schneider 2007, Biscaro and Cherchneff 2014, 2016, Bocchio et al 2016, Micelotta et al 2016). The rate of deceleration and erosion depend on the dust chemical composition and size but also on the temperature and density of the shocked gas. All these may vary across the remnant and during its evolution. The composition of the dust and of the projectiles that will be impinging on it depend on the composition of the ejecta layer where the dust form and on the level of mixing of the ejecta (Nozawa et al 2007, Bianchi and Schneider 2007, Biscaro and Cherchneff 2014, 2016). As an example, Fe dust, which is formed in the innermost He core, will be crossing O-rich gas, experiencing efficient sputtering, while for C-dust in the outermost part of the He core, the possibility of a quick escape together with the smaller sputtering yield of carbon with respect to other species will result in a higher chance to survive (Nozawa et al 2007). In the external layers, erosion is mostly due to He^+ and will affect carbon and SiC which form in there, while silicates and allumina form in the oxygen-rich zone and are mostly eroded by heavier O^+ and Mg^+ projectiles (Biscaro and Cherchneff 2016). Because large grains can travel longer distances in the shocked gas before being stopped, if they are located at the edges of the remnants they can more easily escape and avoid further erosion. The presence of ejecta clouds where the dust initially resides introduces an additional level of complexity. Because of the expansion of the supernova remnant, the density of the smooth ejecta changes while inertial sputtering is occurring inside the clouds. Therefore, dust is progressively injected into a medium whose density changes continuously, which implies different erosion rates (Micelotta et al 2016).

5.7 Mass and size distribution of the surviving dust: theoretical results and comparison with observations

One of the main goals of all theoretical studies about dust processing in SNRs is to provide an estimate of the amount of surviving dust. Such estimate can be given as an *absolute value* or as a *fraction*. This latter option depends exclusively on dust processing, with all the assumptions made to compute it, of course. The former option requires in addition an estimate of the amount of dust initially produced by the SN, which is still one of the most uncertain parameters in this field. In Sec. 5.7.1 we summarise the theoretical results obtained by the different studies under consideration and in Sec. 5.7.2 we show how the theoretical results for specific SNRs compare with observations. We would like to emphasise the fact that the different approaches, models, parameters and parameters' values chosen by the different authors prevent a direct global comparison between the results.

5.7.1 Theoretical results for dust survival in SNRs

The calculations from Itoh (1985) already indicate that sputtering in the ejecta can heavily modify the amount of dust synthesised in SNe.

Dwek (2005) uses the ratio $\tau_{\rm sput}/t$ versus α to identify where in the remnant dust sputtering takes place efficiently. The quantity $\tau_{\rm sput}$ is the sputtering lifetime

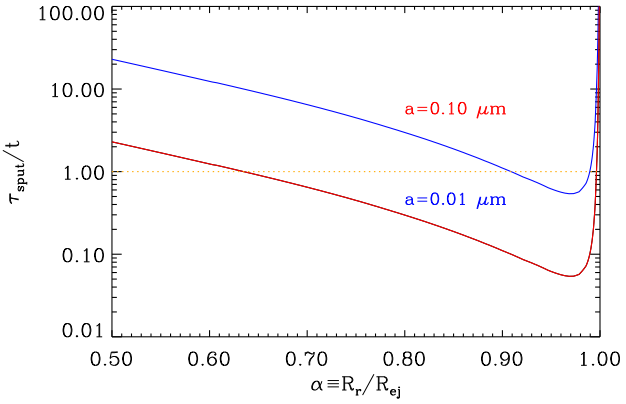

Fig. 17 Ratio τ_{sput}/t as a function of α calculated for grains with radius a = 0.1, 0.01 μm embedded in smooth oxygen-rich ejecta. Destruction occurs when $\tau_{sput}/t < 1$. Figure reproduced from Dwek (2005).

and t is the expansion age of the ejecta. As shown in Fig. 17, destruction occurs in the layers $0 < \alpha < 1$ where a combination of gas temperature (given by the reverse shock velocity) and ejecta density gives $\tau_{sput}/t < 1$. In the outer ejecta layer ($\alpha = 1$) the velocity of the reverse shock is zero, which implies a very low gas temperature and therefore projectiles which are not energetic enough to trigger the sputtering process. In the inner layer ($\alpha = 0$), the reverse shock velocity reaches its maximum value, but the corresponding high gas temperature does not compensate the very low density of projectiles. For smaller particles the condition $\tau_{sput}/t < 1$ is fulfilled over a wider range of α values than for the larger particles.

Similar conclusions about the location of efficient dust sputtering in SNRs are also reached by Bianchi and Schneider (2007) and Nath et al (2008), which is not surprising because they also refer to the fully homogenous case of the Truelove and McKee (1999) model for the evolution of the supernova remnant. However, this trend also appears for ejecta density profiles with $n = 2, 4$ (Nath et al 2008), even if in this case the velocity is a peaked function (Truelove and McKee 1999).

The calculated size distributions resulting from processing reveal that, for all the dust species considered, small grains (radius below a few 10^6 cm) are much more eroded that the bigger ones. These latter can survive sputtering but their distribution is shifted towards smaller sizes. The size distributions recovered by Nozawa et al (2007) show an abrupt cut at small radii (Figure 18), while those in Bianchi and Schneider (2007) flatten at the small-sizes end. According to Nozawa et al (2007), this difference has to be ascribed to the fact that Bianchi and Schneider (2007) do not consider the dynamics of the dust: the grains are trapped and confined at their initial location where they are sputtered until the density drop prevents further erosion. In the case considered by Nozawa et al (2007), even small grains with initial radius lower than 0.05 μm are able to penetrate into the hot plasma between the reverse and forward shocks, where they are completely eroded by thermal sputtering in the relatively high-density gas.

The amount of surviving dust depends in a complicated way on the approach used for the calculations and on the adopted initial conditions. It is strongly influenced by the composition and size distribution of the freshly formed dust (Bianchi and Schneider 2007, Nozawa et al 2007, 2010, Bocchio et al 2016, Biscaro and Cherchneff 2016). Because these latter differ from model to model, it is diffi-

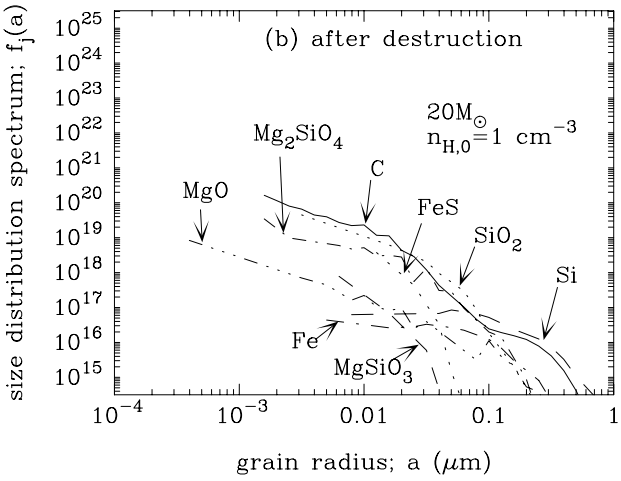

Fig. 18 Size distributions of the surviving dust resulting from processing in SNRs. Figure reproduced from Nozawa et al (2007).

cult to establish the relation between the destruction efficiency and the mass of the progenitor for each dust species (Nozawa et al 2007). SNe exploding in a denser medium produce a reverse shock which travels faster through the ejecta and encounters denser gas, producing more sputtering. As a result, the mass of surviving dust decreases with increasing ambient density (Bianchi and Schneider 2007, Nozawa et al 2007, Fig. 19 and Fig.20a respectively) while the shape of the size distributions is almost unaffected (Bianchi and Schneider 2007). The amount of surviving dust is not impacted substantially by the metallicity of the progenitor (Bianchi and Schneider 2007) but it is reduced for higher explosion energies (Nozawa et al 2007, Bocchio et al 2016), in mixed SN ejecta (Nozawa et al 2007) and when smaller sticking coefficients are considered for dust formation. This is because the resulting grains are smaller, therefore more prone to dissociation (Bianchi and Schneider 2007). Nath et al (2008) find that the *fractions* of surviving dust mass have an intricate dependency on the explosion energy and ejecta mass, but they do not depend on the density of the ambient medium.

An important point addressed by Nozawa et al (2007) and Nozawa et al (2010) is the effect of the thickness of the H envelope. In particular, the detailed study from Nozawa et al (2010) on Type IIb SNe shows that the much thinner hydrogen envelope and higher expansion velocity of the He core in Type IIb SNRs with respect to Type II-P SNRs implies that the reverse shock reaches the He core at earlier times. Sputtering occurs in a denser medium and the increased collision rate between dust particles and gas projectiles leads to a more efficient erosion of the grains. This fact, combined with the smaller sizes of the synthesised grains, results in a complete destruction for all grains (and no injection into the ISM) if the ambient gas density exceeds 0.1 cm^{-3} (see Fig. 20b). Nozawa et al (2010) conclude that, if the circumstellar medium is roughly spherical, low-mass envelope SNe cannot inject a significant amount of dust into the interstellar medium.

Bianchi and Schneider (2007) and Nozawa et al (2007) provide the *absolute mass* of surviving dust with respect to the initial values calculated from their SN

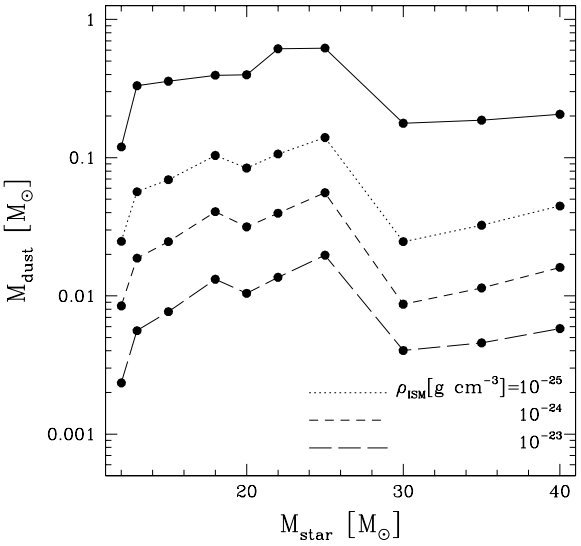

Fig. 19 Mass of dust surviving the processing by the reverse shock, as a function of the mass of the progenitor star, calculated for three densities of the ambient medium. The solid line represents the initial dust mass. Figure reproduced from Bianchi and Schneider (2007).

and dust coagulation models (Figs. 19 – 20b). Conversion to fractional values leads to various ranges, depending on the adopted parameters: between 2% and 20% of the initial value for Bianchi and Schneider (2007) and between 0 and 80% for Nozawa et al (2007). Nath et al (2008) calculate fractional values (Fig. 21) and with their power-law initial grain size distributions they find that between 80% and 99% of the mass of graphite and silicate grains is preserved if the ejecta have a shallow density profile ($n < 5$). If the profile is steeper, the inner shells may contain a large fraction of mass which will remain untouched. This suggests that a considerable fraction of the dust synthesised in SNe could reside in cold (still unshocked) ejecta. The fractions of surviving dust mass are larger than those reported by Bianchi and Schneider (2007) and Nozawa et al (2007). These latter in particular include in their calculation the significant sputtering occurring in the hot gas located between the reverse and forward shocks, which is not considered in the analytical treatment of Nath et al (2008). The density of such gas, and therefore the sputtering rate, strongly depends on the density of the ambient medium. Another point to consider is that the adopted rates for thermal sputtering from Tielens et al (1994) are valid for a gas with solar composition, while SN ejecta are expected to be rich in metals, whose sputtering yields are much higher than those of hydrogen and helium. The power-laws adopted by Nath et al (2008) extend over a wider range of sizes than the peaked distributions from Bianchi and Schneider (2007) which include smaller grains more prone to dissociation ($\leq 0.01\,\mu$m for silicates and $\leq 0.05\,\mu$m for graphite). These two factors would increase the fraction of mass sputtered away.

The simulations of Silvia et al (2010) show that the relative velocity between the clumps and the reverse shock combined with the density of the clumps has a strong impact on the survival rate of the dust residing in the clouds, resulting in a ~50% additional mass loss (with respect to the low-velocity case) for high-density clumps ($\chi = 1000$) crossed by the highest velocity shock considered (5000 km s^{-1}). The total amount of surviving dust varies with the grain species and the

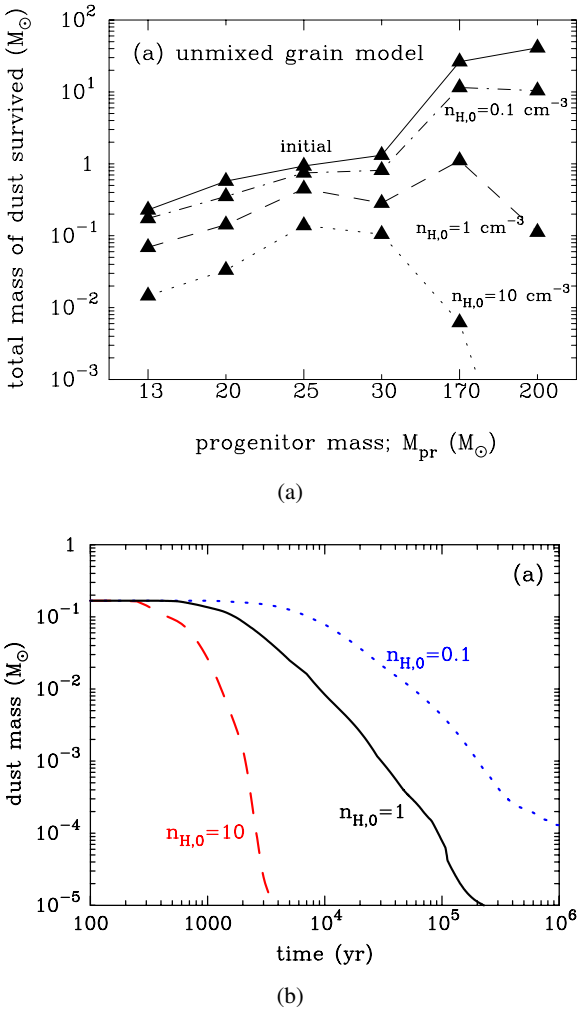

Fig. 20 (a) – Total mass of surviving dust as a function of the mass of the progenitor star, calculated for different densities of the ambient medium, $n_{H,0}$, for the unmixed grain model. The solid line represents the initial total mass of the formed dust. Figure reproduced from Nozawa et al (2007). (b) – Temporal evolution of the total mass of dust inside a Type IIb SNR expanding into a homogeneous circumstellar medium having different densities. Figure reproduced from Nozawa et al (2010).

adopted values of the parameters. As an example, Fig. 22 reproduces the *fractional* dust mass as a function of time for the case $\chi = 1000$ when the sputtering rates from Nozawa et al (2006) are used. For high-velocity shocks impacting a high-density cloud, the percentage of surviving dust mass of some key species is the following: C – 62%, SiO_2 – 20%, Fe – 80%. Switching on cooling in the gas with half-solar metallicity considered in the study has little effect on the final amount of surviving dust.

In the higher metallicity gas investigated by Silvia et al (2012) the abundances of hydrogen and helium are kept at their solar values, while for the other metals the abundances are increased by a factor of 10 and 100 with respect to solar. The results are shown in Fig. 23. The degree of destruction spans the entire parameter space, ranging from almost negligible destruction (Fe and Si, high-metallicity gas, low-velocity shock) to almost complete destruction (Al_2O_3, FeS, and $MgSiO_3$,

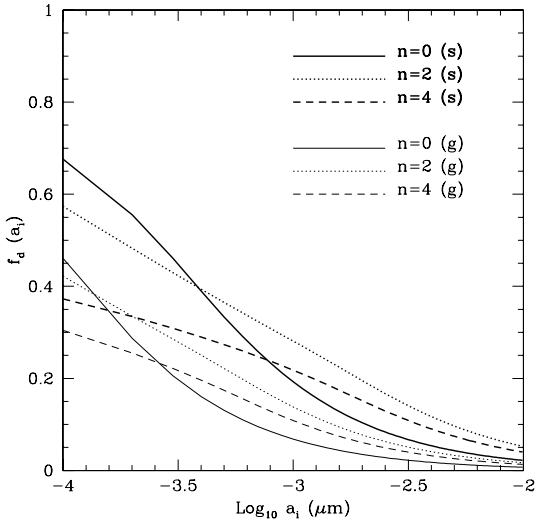

Fig. 21 Resulting fraction of dust mass sputtered by the reverse shock as a function of the initial radius of the grain, for graphite (thin lines - g) and silicate (thick lines - s) dust. The calculations have been performed for three ejecta mass profiles: n = 0, 2, 4 and the resulting fractions have been weighted by the mass of the shell where the grains are formed. Figure reproduced from Nath et al (2008).

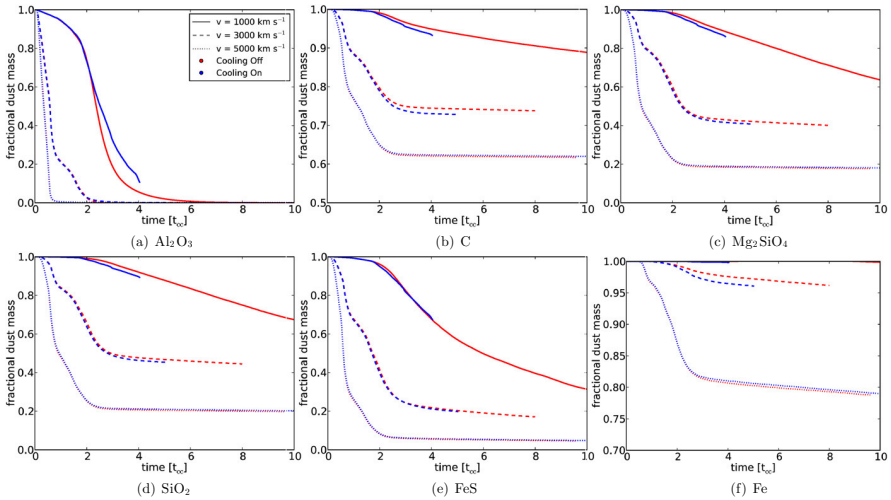

Fig. 22 Dust mass evolution (fractional dust mass as a function of time) calculated for a clump with χ = 1000 adopting the sputtering rates from Nozawa et al (2006, solar metallicity). Figure reproduced from Silvia et al (2010).

high-metallicity gas, high-velocity shock). There is a clear correlation between shock velocity and amount of destroyed dust mass, and this latter increases sharply at early times when the shock velocity transitions from 1000 to 3000 km s^{-1}. For the key species C, SiO_2 and Fe, the simulations for a high-metallicity gas result in a wide range of surviving dust mass: 44% – 96%, 7% – 95%, and 24% – 99% respectively. The modifications introduced by Silvia et al (2012), i.e. cooling functions and erosion rates more appropriate for high metallicities, a higher shock velocity considered, suppressed cooling in the medium surrounding the cloud, do not invalidate the results from Silvia et al (2010). Indeed, the differences do not

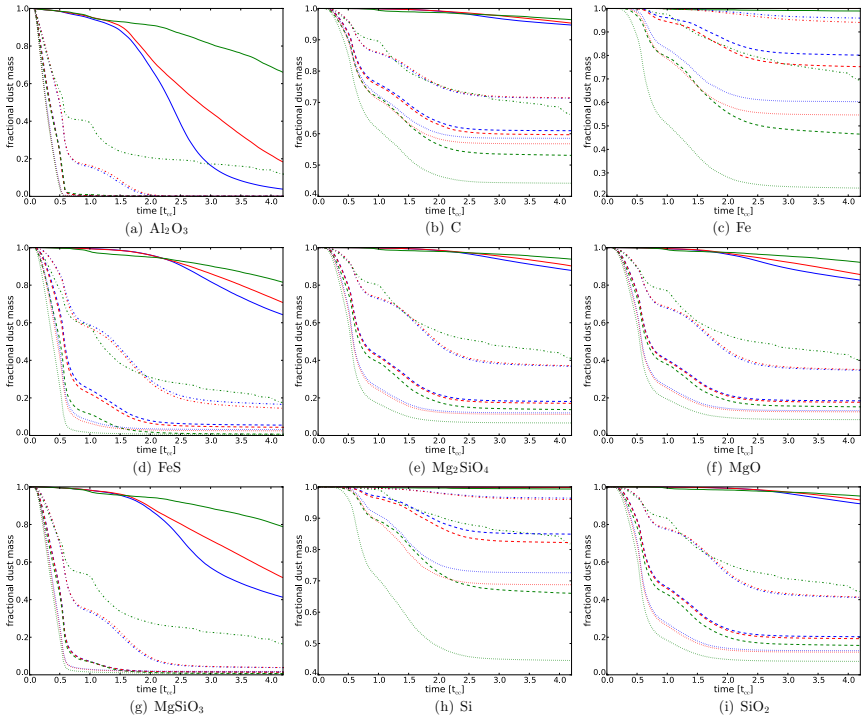

Fig. 23 Dust mass evolution (fractional dust mass as a function of time) calculated in the high-metallicity case. For each dust species, the curves show the results for four shock velocities: 10^3 km s^{-1} – solid, 3×10^3 km s^{-1} – dot-dashed, 5×10^3 km s^{-1} – dashed, and 10^4 km s^{-1} – dotted. Each colour corresponds to a different metallicity: $Z = 1\,Z_\odot$ (blue), $10\,Z_\odot$ (red), $100 Z_\odot$ (green). Figure reproduced from Silvia et al (2012).

become significant until the abundances of metals are taken as 100 times their solar values.

Marassi et al (2015) use the same code as in Bianchi and Schneider (2007) but with an upgraded molecular network to evaluate dust survival in the remnants from *standard* and *faint* Population III (Pop III) CCSNe, finding that 3–50% and 10–80% of the initially formed amount of dust survives, respectively.

Bocchio et al (2016) study the evolution of dust mass in four supernova remnants: SN 1987A, Cas A, the Crab Nebula and N49. The results, given in terms of *absolute* masses of surviving dust, are compared with those from Bianchi and Schneider (2007), where the dynamics of the gas and the effect of the forward shock were not included, and with the observed dust masses (Fig. 24). Except for N49, the results from the models appear to be consistent with the observations, but this should take into account the very large error bars of the datapoints. Between 10^3 and 10^4 years after explosion, Bocchio et al (2016) predicts a larger mass of surviving dust than Bianchi and Schneider (2007), because in this time interval the dust decouples from the gas and travels in the region between the forward and reverse shocks, where the physical conditions are milder. For $t \gtrsim 10^4$ the situation is reversed because most of the grains have travelled beyond the forward shock,

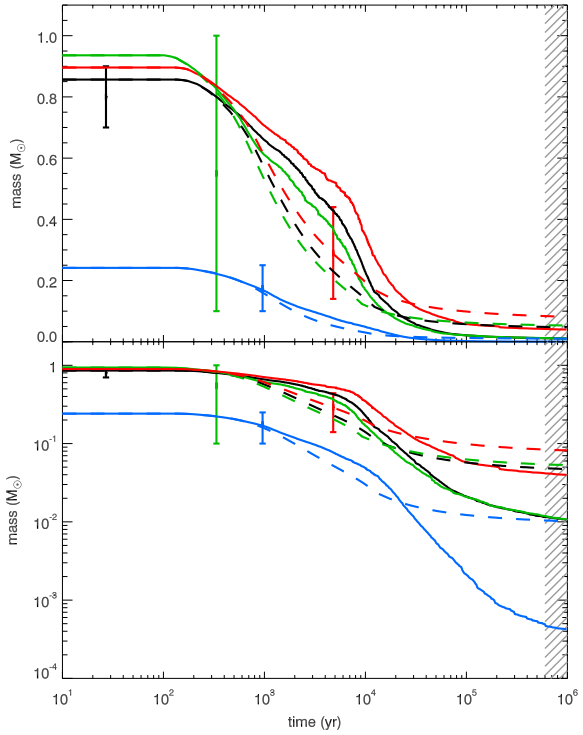

Fig. 24 Temporal evolution of dust mass in SN 1987A (black), Cas A (green), the Crab Nebula (blue) and N49 (red). The results obtained from the GRASH_Rev code (solid lines) are compared with the output from the Bianchi and Schneider (2007) model calculated using the same set of initial conditions. The theoretical curves are overlaid with the observed datapoints. The dust mass is shown on a linear scale in the top panel and on a logarithmic scale in the bottom one. The hatched area shows the time interval when the processing of dust becomes negligible. Figure reproduced from Bocchio et al (2016).

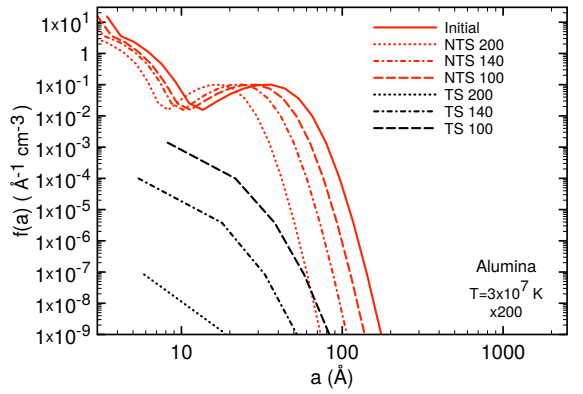

Fig. 25 Calculated grain size distributions for Cas A (χ = 200) for alumina (red) processed by non-thermal sputtering (NTS) in the oxygen-rich clump and by thermal sputtering (TS) in the inter-clump medium (with temperature $T = 3 \times 10^7$ K). Three shock velocities in the clump have been considered: 200, 140 and 100 km s^{-1}. The solid line represents the initial distribution. Figure reproduced from Biscaro and Cherchneff (2016).

where dust erosion proceeds efficiently. Globally, the final masses estimated by Bocchio et al (2016) are ∼5 – 50% of those derived by Bianchi and Schneider (2007).

Biscaro and Cherchneff (2016) study the processing of dust grains by the reverse shock first inside the clumps and after in the inter-clump medium. They consider two over-density factors: 200, appropriate for Cas A, and 2000, typical of the homogeneous ejecta of Type II-P SNe (Sarangi and Cherchneff 2013, 2015). For Cas A, Biscaro and Cherchneff (2016) assume that thermal sputtering starts

at $t_{\rm thermal} = 340 + 3 \times \tau_{\rm cc}$ (yr), where 340 years is the age of the remnant and $3 \times \tau_{\rm cc}$ is the lifetime of a clump against shock disruption (Klein et al 1994, Silvia et al 2010). As already mentioned, a value of 100 years is taken for $\tau_{\rm cc}$, which implies that the lifetime of the cloud is comparable to the age of the remnant and that thermal sputtering should not be currently happening. This is in contrast with Micelotta et al (2016), which recover for the cloud a much shorter lifetime, in agreement with optical observations and which implies that thermal sputtering already started and is currently ongoing in Cas A. Dust is eroded in the clumps by non-thermal sputtering for $\sim 3\tau_{\rm cc} = 300$ yr, after which the resulting grain size distribution is injected into the hot inter-clump medium where it is further processed via thermal sputtering for ∼4000 years, until the sputtering rate becomes negligible. During this time, it is assumed that the temperature of the gas remains in the initial range $10^6 - 10^8$ K. As an example, Fig. 25 shows the resulting size distributions for Cas A for allumina processed by the heavy O^+ and Mg^+ ions in the oxygen-rich core.

Micelotta et al (2016) calculate dust processing in Cas A over the entire remnant and during its evolution, using the appropriate profiles derived for quantities like the reverse shock velocity and the ejecta density. The results of the Monte Carlo simulation in terms of the total *fraction* of surviving dust (processed + still unprocessed) as a function of α are reported in Fig. 26 for both carbon and silicate dust. The curves show the effect of kinetic sputtering alone and in combination with thermal sputtering. The reduced fraction of surviving silicate grains is due to the combined effect of their slightly higher sputtering yield, the higher average mass of the sputtered particles (23 amu versus 12 amu for AC), and the longer exposure to thermal sputtering due to the fact that a larger fraction of silicate grains tends to escape the ejecta cloud before disruption. The impact of a higher temperature for the smooth ejecta becomes noticeable in the inner layers of Cas A ($\alpha \lesssim 0.55$). When the reverse shock reaches the centre of the remnant, the surviving fraction is reduced to 15.9% for Am C and 11.8% for $MgSiO_3$ ($T = 10^7$ K), 12.3% for Am C and 8.7% for $MgSiO_3$ ($T = 10^8$ K). Kinetic sputtering alone is able to destroy 20% of the carbon and 40% of the silicate grains.

5.7.2 Comparison with observations

The theoretical results from Itoh (1985) applied to SN 1979c and SN 1980k indicate that dust sputtering in the ejecta of these remnants may be important, although the lack of observations did not allow to validate such findings.

For the specific case of Cas A, the model adopted by Bianchi and Schneider (2007) predicts the formation of ∼0.1 $M_\odot$ of dust, reduced to ≈ 0.05 $M_\odot$ after ∼ 325 yr (current age of Cas A) and to ∼7% of this initial value when the reverse shock reaches the centre of the remnant. These results have been updated in the follow-up paper from Bocchio et al (2016), where the initial amount of dust is set to ∼0.9 $M_\odot$ and little dust destruction is currently predicted for Cas A, with only 0.06 $M_\odot$ of dust heated in the post-shock gas and 0.77 $M_\odot$ unshocked and therefore cold. These values have to be compared with the results from fitting observations from polarimetry (∼1 $M_\odot$ – cold dust, Dunne et al 2009) and Spitzer (0.02 – 0.054 $M_\odot$, Rho et al 2008, Arendt et al 2014) and with the recent estimates of (0.3 – 0.5) $M_\odot$ and ∼1.1 $M_\odot$ from De Looze et al (2017) and Bevan et al (2017) respectively.

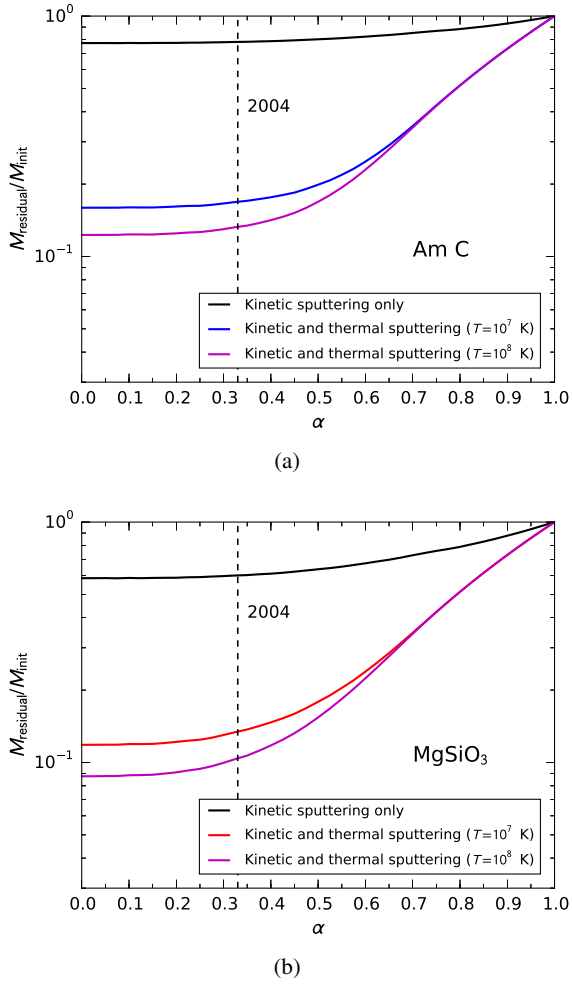

Fig. 26 Total mass fraction of surviving dust in Cas A as a function of α. The top black curve gives the effect of kinetic sputtering alone, the other two show the combined effect of kinetic plus thermal sputtering, this latter evaluated for smooth ejecta having T =10^7 K and T =10^8 K. Figure reproduced from Micelotta et al (2016).

Nozawa et al (2010) use the output from their dust evolution simulations to recover the spectral energy distributions (SEDs) expected from the shock-heated dust inside the SNRs. The calculated SEDs are compared with the synchrotron-subtracted IR flux densities of Cas A in the window 8-100 μm taken from the photometric observations tabulated in Hines et al (2004). The datapoints are reasonably fitted considering 0.008 $M_\odot$ of shocked dust and 0.072 $M_\odot$ of unshocked dust, where the newly formed grains are eroded and heated in a SNR expanding into a power-law medium with an initial hydrogen density of 120 cm^{-3}. The recovered dust masses have to be compared with more recent estimates of ~1.1 $M_\odot$ and (0.3 – 0.5) $M_\odot$ (at ~30 K) by Bevan et al (2017) and De Looze et al (2017) respectively (see Sec. 3.2). The sputtering calculations from Nozawa et al (2010) indicate that all the dust produced in Cas A should be destroyed before reaching the ISM. However, their treatment does not consider the formation of an aspherical circumstellar medium (Nomoto et al 1995, 1996) nor the clumpiness and asym-

metry of the ejecta of Cas A (Willingale et al 2002, Ennis et al 2006, Smith et al 2009). These factors may increase the chances of the grains to survive processing and being injected into the ISM.

The results from both Silvia et al (2010) and Silvia et al (2012) are qualitatively in agreement with the observation of Si dust in Cas A (Rho et al 2008), and with the lack of Al_2O_3 and the presence of large amorphous carbon grains in SNR 1E0102-7219 (Sandstrom et al 2009).

In terms of the amount of dust which should have formed in SN 1987A, Matsuura et al (2015) report 0.8 $M_\odot$ of dust in the ejecta (0.5 $M_\odot$ of silicates and 0.3 $M_\odot$of amorphous carbon). If the current limit of ∼0.25 $M_\odot$ of carbon predicted by nucleosynthesis models is ignored, then the observed SED can be fitted with 0.5 $M_\odot$ of amorphous carbon. Bocchio et al (2016) predict the formation of ∼0.85 $M_\odot$ of dust in SN 1987A and estimate that this represents, and matches, current observations, because the reverse shock did not have time to process the ejecta yet.

For the Crab Nebula, the simulations from Bocchio et al (2016) predict a current total dust mass of 0.17 $M_\odot$, almost equally distributed between carbon grains and silicates. These values have to be compared with the estimates deduced from observations. The Herschel data on the Crab Nebula (51 – 670 μm, Gomez et al 2012) have been fitted with two-temperature blackbodies using carbonaceous and silicate grains having either high or low temperature (55-63 K and 28-33 K respectively). The total inferred masses are 0.12 $M_\odot$ of carbonaceous dust and 0.25 $M_\odot$ of silicates. Using the same data, Temim and Dwek (2013) model the heating of dust grains by the pulsar wind nebula adopting a continuous distribution of grain sizes which leads to a continuous temperature gradient. The resulting total dust masses are 0.019 $M_\odot$ and 0.13 $M_\odot$, assuming a composition of pure amorphous carbon and pure silicate grains respectively. These values are lower than previous estimates and result from the continuous temperature distribution but also from the use of different dust emissivities. This is indeed the case for carbon dust, whose mass is not significantly modified by adopting a distribution of temperatures. Owen and Barlow (2015) constructed radiative transfer models used to fit the SEDs defined by Spitzer and Herschel observations of the Crab Nebula. The results from the fits favour a clumpy mass distribution with (0.18 – 0.27) $M_\odot$ of amorphous carbon dust. If mixed dust chemistry models are considered, the resulting dust masses are (0.11 – 0.13) $M_\odot$ for amorphous carbon and (0.39 – 0.47) $M_\odot$ for silicates.

Observations of N49 indicate masses of warm dust of the order of 0.1 $M_\odot$ (carbonaceous) and 0.4 $M_\odot$ (silicates), taking these two species as the main constituents (Otsuka et al 2010). The cold dust is difficult to detect because of contamination from the parent cloud. The fit has been done using a single dust temperature, which could lead to large uncertainties (Mattsson et al 2015). The simulations predict a mass of warm (shocked) dust of ∼0.48 $M_\odot$ dominated by silicates, ∼15% higher than the dust mass deduced from observations.

Bocchio et al (2016) conclude that between 10 and 40% of the synthesised dust has been destroyed up to now by the passage of the reverse shock but they do not provide the fraction of destroyed dust for each single SNR they consider (except for SN 1987A for which this fraction is zero). From Fig. 24 we derive that the fraction of destroyed dust is ∼10% for Cas A, ∼30% for the Crab Nebula and

~40% for N49. For this latter remnant, the high fraction is consistent with its older age (~4800 years). The very low destroyed dust fraction in Cas A (~335 years old) has to be compared with the 40% - 70% range estimated by Biscaro and Cherchneff (2016) and with the 83% - 90% range (depending on dust composition and gas temperature) found by Micelotta et al (2016). The significant destruction fraction calculated for the Crab Nebula (960 years old) is in contrast with the fact that there is no currently visible reverse shock in the remnant (Hester 2008, review). Indeed, the formation of the reverse shock in remnants like the Crab Nebula is expected to occur on a timescale of $\sim 10^4$ years (Blondin et al 2001). At the end of the simulations (after 10^6 years) Bocchio et al (2016) find that only 1 – 8% of the dust mass currently observed is expected to contribute to the ISM enrichment.

Biscaro and Cherchneff (2016) find that the gas and shock conditions characterising Cas A result in the complete destruction of silicates and the survival of a small fraction of allumina, SiC and carbon grains. For the total initial dust mass before sputtering, Biscaro and Cherchneff (2016) assume a value of 2.7×10^{-2} $M_\odot$. This should correspond to the dust mass synthesised by the SN and is much lower than the currently observed dust in Cas A estimated by Arendt et al (2014), Bevan et al (2017) and De Looze et al (2017) and which includes the cold component. Biscaro and Cherchneff (2016) estimate that between 30% and 60% of their initial dust mass should have survived non-thermal sputtering and be present today in the remnant. This is globally consistent with the values derived from mid-infrared observations for the warm dust (see Fig. 27). After ~4000 years of processing, the surviving fraction is reduced to 6% – 11% of the initial value.

For χ=2000, the fraction of surviving dust mass is larger, between 14% and 45%. Non-thermal sputtering is important and reduces the dust mass to 20-47% of its initial value before thermal sputtering starts. Biscaro and Cherchneff (2016) also study a specific sub-case where a Type II-P SN with a progenitor mass of 19 $M_\odot$ is taken as a surrogate for SN 1987A (with the caveat that SN 1987A is a Peculiar Type II-P supernova). Their results indicate that non-thermal sputtering in the clumps is unimportant and that even after ~4000 years of thermal sputtering in the inter-clump medium, erosion is negligible.

Biscaro and Cherchneff (2016) point out that kinetic models produce smaller amounts of dust with different size distributions and chemical compositions than those based on CNT. This has to be taken into account, because sputtering is indeed very sensitive to dust size and composition. The formation and survival of dust in SNe is also strongly influenced by the clumpiness of the ejecta. Biscaro & Cherchneff conclude that Type II-b SNe may not be significant dust contributors, while SNe with dense and clumpy ejecta and their remnants could enrich the ISM with a significant amount of dust.

To compare their results with observations, Micelotta et al (2016) adopt a different approach. The calculated current fractions of surviving dust in Cas A (α = 0.33) are 16.9% and 13.3% for Am C, and of 13.4% and 10.4% for $MgSiO_3$ (for a gas temperature of 10^7 K and 10^8 K respectively). If the total amount of dust (warm + cold) currently observed in Cas A is ~0.1 $M_\odot$ (Arendt et al 2014) and represents the surviving fraction, the corresponding amount of SN produced dust is about 0.8–1 $M_\odot$, consistent with theoretical predictions from CNT-based dust coagulation models in CCSNe ejecta (0.1–1 $M_\odot$). If the estimate of ~0.5 $M_\odot$ from De Looze et al (2017) is adopted, the corresponding amount of fresh dust would

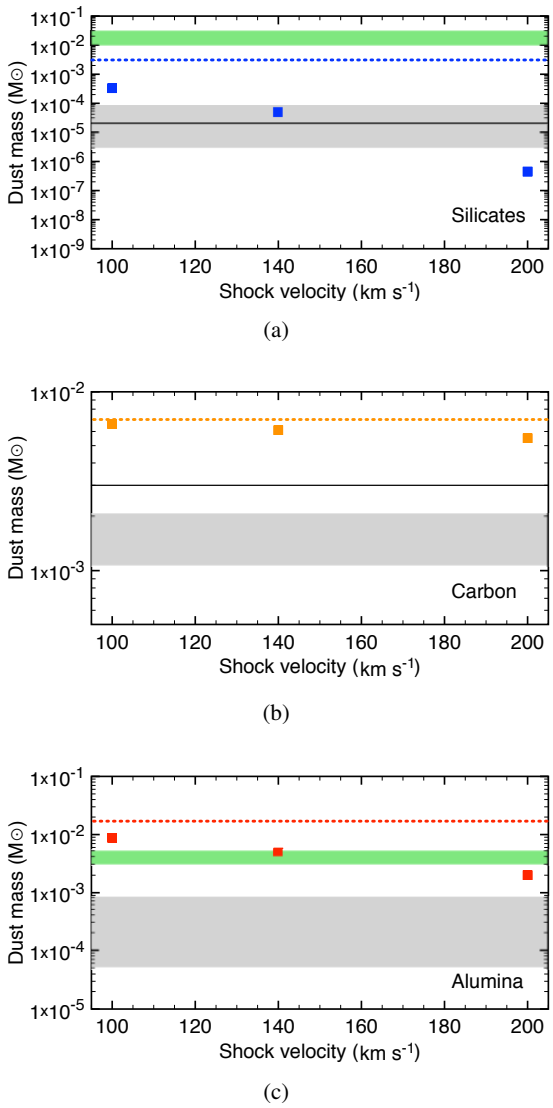

(a)

(b)

(c)

Fig. 27 Calculated masses of carbon, silicates and alumina (solid squares) compared with the masses derived from Spitzer observations (Rho et al 2008, Arendt et al 2014, grey shaded area and green shaded area respectively). The mass of dust of each species initially synthesised by the supernova is represented by the dotted lines. The solid black line indicates the dust masses derived for SNR 1E 0102.2-7219 in the Small Magellanic Cloud (Spitzer data, Sandstrom et al 2009). Figure reproduced from Biscaro and Cherchneff (2016).

be around 5 $M_{\odot}$. However, the survival rates from Micelotta et al (2016) should be considered as a lower limit, because they do not include phenomena that could favor the survival of the dust, as the possibility for the grains to escape the shell of shocked ejecta thanks to their residual ballistic velocities.

6 The role of SNRs as a dust source and sink

The impact between the blast wave (or forward shock) generated by the explosion of a high-mass star as a SN, and the circumstellar material results in the formation of a reverse shock which processes and destroy the dust newly formed in the ejecta. At the same time, the forward shock propagating into the ISM processes and destroys the preexisting ambient dust. While this review focuses on the processing and survival of dust in SNRs, in this section we briefly discuss some implications of such processing (Sec. 6.1) and the role of forward shock processing in determining the lifetime of dust in the ISM (Sec. 6.2).

6.1 Dust destruction by the reverse shock

As shown in Sec. 5.7.1, the calculated fraction of surviving dust ranges from almost 0 to 100%. Determining the dust survival rate is crucial to establish whether the dust produced in SN ejecta will be eventually integrated into the ISM, and thus whether SNe can be an important dust source in the ISM. The results from the theoretical models that we have discussed are summarised in Table 2. We would like to stress again that, while a direct comparison between them is not really feasible, such a summary table allows to appreciate the variety of such results and how they evolved with time.

Explaining the amount of dust detected in high-redshift galaxies with SN sources would require the release of about 0.1 $M_\odot$ per SN (Nozawa et al 2006, Dwek and Cherchneff 2011). If dust destruction is close to 100%, SNe could not be sufficient to provide the required 0.1 $M_\odot$ each. However, if each SN could form 0.2–0.5 $M_\odot$ of dust (Gall et al 2011, Matsuura 2017, Sarangi et al 2018) and nearly half of it can survive, SNe could be an important dust supplier in the ISM.

6.2 The lifetime of dust in the ISM: destruction by expanding SNRs

Dust residing in the ISM is heavily processed and destroyed by the expanding blast waves generated by SN explosions. The dust destruction rate increases with increasing shock velocities. Table 2 summarises some relevant estimations of the fraction of surviving dust resulting from SN shock processing in the ISM.

These results have been used to estimate the lifetime of dust in the ISM, $t_{\rm ISM}$, as described in e.g McKee and Ostriker (1977), McKee et al (1987), McKee (1989), Draine (2009):

$$t_{\rm ISM} = \frac{M_{\rm ISM} t_{\rm SN}}{\epsilon M_{\rm s}}, \tag{13}$$

where $M_{\rm ISM}$ is the total mass of dust and gas residing in the ISM of a single galaxy, $t_{\rm SN}$ is the effective interval between SNe in a galaxy, $M_{\rm s}$ is the mass of gas shocked by a SNR in the Sedov-Taylor stage to at least 100 km s^{-1} and ϵ is the dust destruction efficiency. In the Sedov-Taylor phase, the shock speed drops continuously. Assuming that the initial explosion energy, E_0, of a SN is converted into kinetic energy (Salpeter 1977, Draine 2009), and that the final shock velocity for which dust can be destroyed is 100–200 km s^{-1}, we have that M_s would be around

Table 2 Theoretically calculated fractions of surviving dust mass, $F_{\rm srv}$ resulting from processing by the reverse shock (in the SNR cavity) and by the forward shock (in the ISM).

Work	$F_{\rm srv}$ %	Remarks
Reverse shock		
Bianchi and Schneider (2007)	2–20	
Nozawa et al (2007)	0–80	Primordial SNRs
Nath et al (2008)	80–99	Graphite & silicates, shallow ejecta profile ($n < 5$)
Silvia et al (2010)	62	C, high-velocity shocks, high-density clouds
	20	SiO_2
	80	Fe
Silvia et al (2012)	44–96	C
	7–95	SiO_2
	24–99	Fe
Marassi et al (2015)	3–50	*Standard* Population III CCSNe
	10–80	*Faint* Population III CCSNe
Bocchio et al (2016)	90	Cas A, current
	70	Crab Nebula, but no reverse shock detected yet
	60	N49
	1–8	Global, end of processing (after 10^6 yr)
Biscaro and Cherchneff (2016)	30–60	Cas A (χ=200), current
	6–11	Cas A, end of processing (after 4000 yr)
	14–45	Dense clumps (χ=2000)
Micelotta et al (2016)	13–17	Amorphous carbon, Cas A, current
	10–13	$MgSiO_3$
	12–16	Amorphous carbon, Cas A, after 8000 yr
	9–12	$MgSiO_3$
Forward shock		
Draine and Salpeter (1979b)	70–85	Graphite, $v_{\rm s}$=100 km s^{-1}, $a_{\rm gr}$=0.1 μm
	40–60	Silicates
Seab and Shull (1983)	85	Graphite, B=1 μm, $v_{\rm s}$=100 km s^{-1}, n_0=10 cm^{-3}
	50	Silicates
McKee et al (1987)	62–75	Silicates, B=1 μG, $v_{\rm s}$=100 km s^{-1}, n_0=0.25 cm^{-3}
	84–90	B = 3 μG
Jones et al (1994)	81	Graphite, B=1 μG, $v_{\rm s}$=100 km s^{-1}, n_0=0.25 cm^{-3}
	89	Graphite, B=3 μG
	62	Silicates, B=1 μG
	78	Silicates, B=3 μG
Jones et al (1996)	93	Graphite, B=3 μG, $v_{\rm s}$=100 km s^{-1}, n_0=0.25 cm^{-3}
	82	Silicates
Serra Díaz-Cano and Jones (2008)	69	a-C:H, B=3 μG, $v_{\rm s}$=100 km s^{-1}, n_0=0.25 cm^{-3}
Bocchio et al (2014)	9	a-C:H, B=3 μG, $v_{\rm s}$=100 km s^{-1}, n_0=0.25 cm^{-3}
	71	Silicates

Notes – χ: density contrast between the ejecta clumps and the smooth ejecta, $v_{\rm s}$: shock velocity, $a_{\rm gr}$: initial dust grain radius, B: pre-shock magnetic field intensity, n_0: pre-shock ambient density, a-C:H: hydrogenated amorphous carbon.

Table 3 Estimated dust lifetime against processing by supernova shocks in the ISM.

Work	Dust lifetime (yrs)	Note
Salpeter (1977)	$\sim 7 \times 10^8$	Silicates
Barlow (1978)	2×10^8	Ice grains
	5×10^8	$MgSiO_3$
	2×10^9	Graphite
Jones et al (1994)	4×10^8	Graphite
	2.2×10^8	Silicates
Jones et al (1996)	6×10^8	Graphite
	4×10^8	Silicates
Serra Díaz-Cano and Jones (2008)	2×10^8	a-C:H
Micelotta et al (2010a)	$(1.4–4)\times 10^8$	PAHs
Jones and Nuth (2011)	$(0.3–10)\times 10^8$	Silicates
	$(0.2–5.1)\times 10^8$	a-C:H
Bocchio et al (2014)	$(6.2\pm 5.7)\times 10^7$	a-C:H
	$(3.1\pm 2.7)\times 10^8$	Silicates
Temim et al (2015)	$(2.2\pm 1.3)\times 10^7$	Silicates, LMC
	$(2.0\pm 1.7)\times 10^7$	Carbon dust, LMC
	$(5.4\pm 3.2)\times 10^7$	Silicates, SMC
	$(7.2\pm 4.3)\times 10^7$	Carbon dust, SMC
Slavin et al (2015)	3.2×10^9	Carbon dust
	2.0×10^9	Silicates

1000–3000 $M_\odot$. The explosion energy of a SN is typically around 10^{51} ergs. It is not well determined yet how much of its energy will be converted into kinetic energy, and how much will be carried away by neutrinos. Nevertheless, 10^{51} ergs provides the correct order of magnitude.

The typical time scale for dust formation and injection from asymptotic giant branch (AGB) stars is $\sim 2 \times 10^9$ years, much longer than the calculated dust lifetimes in the ISM (except for Slavin et al 2015, see Table 3) thus, dust should not be detectable, unless there is an additional dust source. These estimates are based upon the assumption that SNe form little dust. Recent theoretical models have shown that a reasonable fraction of the ejecta dust could survive the processing by the reverse shock. This could potentially speed up the dust injection time scale from SNe. In the past few years there has been more evidence that core-collapse SNe can form a substantial amount of dust (from 10^{-2} to nearly 1 $M_\odot$; Matsuura 2017, Sarangi et al 2018). Even if 20 % of this dust survives the passage of the reverse shock, it will not be sufficient to compensate for the high destruction rate in the ISM. Jones and Nuth (2011) and Bocchio et al (2014) have carefully examined the uncertainties involved in dust destruction calculations, finding that they can get to 90 %. This implies that the estimates of dust destruction will substantially improve when better models and more refined parameters' values will be available.

7 Summary & Conclusions

This paper is the second of a series of two aiming to review the topic of dust in supernovae and supernova remnants. In Paper I (Sarangi et al 2018) we have summarised the scenarios for dust formation in supernova ejecta and the observations of dust formation in core-collapse supernovae. Here in Paper II, we have focused on the theoretical models aiming to describe the processing of dust *inside* supernova remnants and to quantify the amount of surviving grains. We have also discussed the observational evidence of dust processing and destruction in supernova remnants and summarised some of the methods adopted to quantify dust destruction from observations.

In young SN 1987A the reverse shock did not reach the ejecta yet, but there is evidence of interaction between the blast wave shock and the circumstellar material, arranged in series of rings, where dust grains should undergo shock processing and heating. In Cas A (age ∼335 years), dust has been detected in both the shocked and unshocked regions inside the cavity of the remnant. The temperature of the dust in these two regions is different, which would indicate that dust is collisionally heated and potentially destroyed by sputtering in the shocked gas. In the 10,000 years old Sagittarius A East SNR, where the reverse shock should have reached the centre of the remnant, dust emission has been detected in the central region, coincident with shocked gas. The excess far-infrared emission suggests the presence of large grains which could have survived shock processing.

Different methods can be used to derive the amount of emitting dust and to make estimates of the fraction which will eventually survive processing. These include fitting measured flux data points at infrared wavelengths, and modelling the infrared emission from dust whose size distribution has been modified by sputtering and shattering in a hot shocked gas, and which has been collisionally heated by the same gas. Both methods have their own advantages and limitations and they should always carefully take into account the properties of every specific SNR under examination.

From a theoretical point of view, the different studies presented in this review clearly show that modelling the processing of dust in SNRs is challenging. The ideal model should be based on a realistic description of the remnant under consideration and include an accurate description of the dust and of all processes potentially capable of affecting it. In reality, our knowledge of these fundamental ingredients is affected by large uncertainties. SNRs are complex objects, often inhomogenous and exhibiting a variety of physical conditions. Dust composition and size distribution are subject of debate while dust processing depends on the environmental conditions, which vary within the remnant.

Many of the works presented here are built on a common ground: take an evolutionary model for the SNRs (typically young ones) and combine it with a description of dust and dust processing. However, it is revealing and instructing to compare the different implementations of this basic recipe and the specific aspects of the problem which have been investigated.

For the dynamics of the remnant, in particular the evolution of the reverse shock velocity, which directly affects the processing of dust via sputtering, Itoh (1985) adopts the self-similar solutions from Chevalier (1982) for ejecta-dominated supernova remnants having ejecta with a power-law density distribution (charac-

terised by the index $n > 5$) expanding into a circumstellar medium which also has a power-law density distribution (with index $s < 3$). Dwek (2005) uses the analytical expressions of Truelove and McKee (1999) but for the simplest case: homogeneous ejecta expanding into a uniform medium. The solutions from Truelove and McKee (1999) are particularly suited for young SNRs (like Cas A) which are transitioning between the ejecta-dominated and Sedov-Taylor phases, because they allow a smooth merging of the solutions corresponding to the two stages. The same kind of solutions has been used by Bianchi and Schneider (2007), Marassi et al (2015) and Bocchio et al (2016), while Nath et al (2008) include the core-envelope density structure of the ejecta from Truelove and McKee (1999), considering power-law envelopes with $n < 3$, $n = 4$ and $n > 5$. Nozawa et al (2007) and Biscaro and Cherchneff (2014, 2016) consider simple homologous expansion of homogeneous ejecta expanding into a uniform medium, while Nozawa et al (2010) consider the case of a power-law ambient medium (exponent $s = 2$). Following the work of Truelove and McKee (1999) and Laming and Hwang (2003), Micelotta et al (2016) develop for Cas A the solutions corresponding to core-envelope ejecta expanding into a power-law medium, while Silvia et al (2010, 2012) do not include their results into an evolutionary model for the reverse shock. Dwek (2005) also pointed out that SN ejecta are clumpy and that this will affect dust processing. The hydrodynamics + N-body simulations of Silvia et al (2010, 2012) focus on the behaviour of a single dust-containing over-dense clump impacted by a planar shock, in terms of cloud fragmentation and dust sputtering. Biscaro and Cherchneff (2014, 2016) and Micelotta et al (2016) include the treatment of dusty ejecta clumps into a supernova model.

The adopted or calculated initial grain size distributions of the newly formed dust are based of the CNT formalism (Bianchi and Schneider 2007, Nozawa et al 2007, Nath et al 2008, Nozawa et al 2010, Silvia et al 2010, 2012, Marassi et al 2015, Bocchio et al 2016) or on a chemical kinetic approach (Biscaro and Cherchneff 2014, 2016). Itoh (1985) and Micelotta et al (2016) adopt as a test case the MRN interstellar grain size distribution. Dust composition includes silicates and carbon grains, but it can be more or less sophisticated depending on the model used. Sputtering, both thermal and inertial, is the main destructive process for dust inside supernova remnants. It is treated using the classical formalism for sputtering in solids (Matsunami et al 1981, Andersen and Bay 1981, Sigmund 1981, Bohdansky 1984) adopting the sputtering yields from Draine and Salpeter (1979a), Tielens et al (1994) and/or Nozawa et al (2006). In addition, Bocchio et al (2016) estimate the combined effect of thermal and inertial sputtering and introduce a correction to the sputtering yields to take into account the finite size of the grains. Dust dynamics is included in the work of Itoh (1985), Nozawa et al (2007), Nozawa et al (2010), Bocchio et al (2016), Biscaro and Cherchneff (2016) and Micelotta et al (2016). This latter couples explicitly dust erosion and dust slowing-down in the ejecta clouds, to calculate the time required by a grain to escape from the cloud depending on its size and position. These analytical expressions implemented into a Monte Carlo simulations allow to follow dust sputtering "on-the-fly". Cooling of the ejecta has been taken into account by Nozawa et al (2007), by Silvia et al (2010, 2012) who compared dust sputtering in a dense cloud with cooling both off and on, and by Micelotta et al (2016) who calculated explicitly for Cas A the cooling of both the smooth ejecta and the over-dense clumps,

using for these latter the cooling function for an oxygen-rich shocked gas from Sutherland and Dopita (1995).

The results of these different works in terms of the fraction of surviving dust mass span a wide range of values. Bianchi and Schneider (2007) find that after $(4 - 8) \times 10^4$ years of processing, the fraction of surviving dust mass is between 2% and 20% (depending on the adopted parameters). These values are reduced to 1–8% using the updated model presented by Bocchio et al (2016), which extend the simulations up to 10^6 years after explosion (into the radiative phase of supernova remnant evolution). Using an updated version of the code from Bianchi and Schneider (2007), Marassi et al (2015) find that 3–50% and 10–80% of the dust initially formed in standard and faint Pop III CCSNe, respectively, survives the passage of the reverse shock. Nozawa et al (2007) as well extend their calculations to the radiative stage, finding that 0-80% of the dust mass survives processing, while Nath et al (2008) recover a surviving fraction larger than 80% considering the ED and ST phases only. The numerical simulations of Silvia et al (2010, 2012) predict that between 7 and 99% of the initial dust mass will survive, these results however are not included into a supernova remnant evolutionary model and cannot be directly compared with other works. Biscaro and Cherchneff (2016) find that after 4000 years of processing, the fraction of surviving dust will be 6% to 11% in Cas A and between 14 and 45% in Type II-P supernovae. For Cas A, the results of Micelotta et al (2016) indicate that ∼8000 years after explosion (when the reverse shock reaches the centre of the remnant) the survival fractions range from 9% to 16%, depending on dust composition and temperature of the smooth ejecta.

This variety of results reflects the different approaches used (analytical or numerical) and the different physical descriptions and conditions adopted for the supernova remnants, the ambient medium and the dust grains. Apart from the N49 remnant investigated by Bocchio et al (2016), the theoretical amounts of surviving dust are consistent with the dust masses derived from observations, and/or with theoretical predictions about the amount of dust which should be initially synthesised by supernovae. This with the caveat that the dust mass estimate from photometric and spectroscopic data and the theoretical evaluation of dust formation and processing are affected by major uncertainties. In the specific case of the Crab Nebula, Bocchio et al (2016) find that the amount of observed dust is consistent with their model which predicts that ∼30% of the dust has been already destroyed by the reverse shock. However, no reverse shock has been detected so far in the Crab Nebula (960 years old) and it is not expected to form before $\sim 10^4$ years. This illustrates the importance of developing realistic models for each specific remnant under examination.

Determining the net amount of SN-condensed dust that is ultimately able to reach the ISM is crucial to determine whether SNe can indeed supply the large dust masses detected in high-redshift galaxies, especially if alternative routes like dust reformation and growth in the ISM are not viable (e.g. Ferrara et al 2016). While this goal has not been reached yet, the increasing interest in facing the problem in its whole complexity puts us on the right track.

Acknowledgements We would like to thank the referee for the careful reading and the many useful suggestions. We also deeply acknowledge the support from the International Space Science Institute in Bern, Switzerland and their successful endeavour to organise the Supernovae workshop. We are grateful to Isabelle Cherchneff for her help at the beginning of this project.

E. R. M. wishes to acknowledge the support of Academy of Finland grant 1285769 and M. M. acknowledges support from an STFC Ernest Rutherford fellowship (ST/L003597/1).

References

Allen MG, Groves BA, Dopita MA, Sutherland RS, Kewley LJ (2008) The MAPPINGS III Library of Fast Radiative Shock Models. ApJS 178:20–55, DOI 10.1086/589652, 0805.0204

Andersen HH, Bay HL (1981) Sputtering yield measurements, p 145. DOI 10.1007/3540105212“¨9

Arendt RG, Dwek E, Moseley SH (1999) Newly Synthesized Elements and Pristine Dust in the Cassiopeia A Supernova Remnant. ApJ 521:234–245, DOI 10.1086/307545, astro-ph/9901042

Arendt RG, Dwek E, Blair WP, Ghavamian P, Hwang U, Long KS, Petre R, Rho J, Winkler PF (2010) SPITZEROBSERVATIONS OF DUST DESTRUCTION IN THE PUPPIS A SUPERNOVA REMNANT. ApJ 725(1):585–597

Arendt RG, Dwek E, Kober G, Rho J, Hwang U (2014) Interstellar and Ejecta Dust in the Cas A Supernova Remnant. ApJ 786:55, DOI 10.1088/0004-637X/786/1/55, 1403.3008

Arendt RG, Dwek E, Bouchet P, Danziger IJ, Frank KA, Gehrz RD, Park S, Woodward CE (2016) INFRARED CONTINUUM AND LINE EVOLUTION OF THE EQUATORIAL RING AROUND SN 1987A. AJ 151(3):62

Arnett WD, Bahcall JN, Kirshner RP, Woosley SE (1989) Supernova 1987A. IN: Annual review of astronomy and astrophysics Volume 27 (A90-29983 12-90) Palo Alto 27:629

Baines MJ, Williams IP, Asebiomo AS (1965) Resistance to the motion of a small sphere moving through a gas. MNRAS 130:63

Barlow MJ (1978) The destruction and growth of dust grains in interstellar space. I - Destruction by sputtering. MNRAS 183(3):367–395

Barlow MJ, Krause O, Swinbank BM, Sibthorpe B, Besel MA, Wesson R, Ivison RJ, Dunne L, Gear WK, Gomez née Morgan HL, Hargrave PC, Henning T, Leeks SJ, Lim TL, Olofsson G, Polehampton ET (2010) A Herschel PACS and SPIRE study of the dust content of the Cassiopeia A supernova remnant. A&A 518:L138

Barlow MJ, Krause O, Swinyard BM, Sibthorpe B, Besel MA, Wesson R, Ivison RJ, Dunne L, Gear WK, Gomez HL, Hargrave PC, Henning T, Leeks SJ, Lim TL, Olofsson G, Polehampton ET (2010) A Herschel PACS and SPIRE study of the dust content of the Cassiopeia A supernova remnant. A&A 518:L138, DOI 10.1051/0004-6361/201014585, 1005.2688

Bedogni R, Woodward PR (1990) Shock wave interactions with interstellar clouds. A&A 231:481–498

Bertoldi F, Carilli CL, Cox P, Fan X, Strauss MA, Beelen A, Omont A, Zylka R (2003) Dust emission from the most distant quasars. A&A 406:L55–L58, DOI 10.1051/0004-6361:20030710, astro-ph/0305116

Bevan A, Barlow MJ (2016) Modelling supernova line profile asymmetries to determine ejecta dust masses: SN 1987A from days 714 to 3604. MNRAS 456(2):1269–1293

Bevan A, Barlow MJ, Milisavljevic D (2017) Dust masses for SN 1980K, SN1993J and Cassiopeia A from red-blue emission line asymmetries. MNRAS 465:4044–4056, DOI 10.1093/mnras/stw2985, 1611.05006

Bianchi S, Schneider R (2007) Dust formation and survival in supernova ejecta. MNRAS 378:973–982, DOI 10.1111/j.1365-2966.2007.11829.x, 0704.0586

Biscaro C, Cherchneff I (2014) Molecules and dust in Cassiopeia A. I. Synthesis in the supernova phase and processing by the reverse shock in the clumpy remnant. A&A 564:A25, DOI 10.1051/0004-6361/201322932, 1401.5594

Biscaro C, Cherchneff I (2016) Molecules and dust in Cassiopeia A. II. Dust sputtering and diagnosis of supernova dust survival in remnants. A&A 589:A132, DOI 10.1051/0004-6361/201527769, 1511.05487

Blair WP, Ghavamian P, Long KS, Williams BJ, Borkowski KJ, Reynolds SP, Sankrit R (2007) Spitzer Space TelescopeObservations of Kepler's Supernova Remnant: A Detailed Look at the Circumstellar Dust Component. The Astrophysical Journal 662(2):998–1013

Blondin JM, Chevalier RA, Frierson DM (2001) Pulsar Wind Nebulae in Evolved Supernova Remnants. ApJ 563:806–815, DOI 10.1086/324042, astro-ph/0107076

Bocchio M, Jones AP, Slavin JD (2014) A re-evaluation of dust processing in supernova shock waves. A&A 570:A32, DOI 10.1051/0004-6361/201424368
Bocchio M, Marassi S, Schneider R, Bianchi S, Limongi M, Chieffi A (2016) Dust grains from the heart of supernovae. A&A 587:A157, DOI 10.1051/0004-6361/201527432, 1601.06770
Bohdansky J (1984) A universal relation for the sputtering yield of monatomic solids at normal ion incidence. Nucl. Instrum. Methods B 2:587–591, DOI 10.1016/0168-583X(84)90271-4
Borkowski KJ, Shull JM (1990) Pure-oxygen radiative shocks with electron thermal conduction. ApJ 348:169–185, DOI 10.1086/168225
Borkowski KJ, Lyerly WJ, Reynolds SP (2001) Supernova Remnants in the Sedov Expansion Phase: Thermal X-Ray Emission. ApJ 548:820–835, DOI 10.1086/319011, astro-ph/0008066
Borkowski KJ, Williams BJ, Reynolds SP, Blair WP, Ghavamian P, Sankrit R, Hendrick SP, Long KS, Raymond JC, Smith RC, Points S, Winkler PF (2006) Dust Destruction in Type Ia Supernova Remnants in the Large Magellanic Cloud. ApJl 642:L141–L144, DOI 10.1086/504472, astro-ph/0602313
Borkowski KJ, Williams BJ, Reynolds SP, Blair WP, Ghavamian P, Sankrit R, Hendrick SP, Long KS, Raymond JC, Smith RC, Points S, Winkler PF (2006) Dust Destruction in Type Ia Supernova Remnants in the Large Magellanic Cloud. Astrophysical Journal 642(2):L141–L144
Bouchet P, De Buizer JM, Suntzeff NB, Danziger IJ, Hayward TL, Telesco CM, Packham C (2004) High-Resolution Mid-infrared Imaging of SN 1987A. ApJ 611:394–398, DOI 10.1086/421936, astro-ph/0312240
Bouchet P, Dwek E, Danziger J, Arendt RG, De Buizer IJM, Park S, Suntzeff NB, Kirshner RP, Challis P (2006) SN 1987A after 18 Years: Mid-Infrared Gemini and Spitzer Observations of the Remnant. ApJ 650:212
Bryan GL, Norman ML (1997) Simulating X-Ray Clusters with Adaptive Mesh Refinement. In: Clarke DA, West MJ (eds) Computational Astrophysics; 12th Kingston Meeting on Theoretical Astrophysics, Astronomical Society of the Pacific Conference Series, vol 123, p 363, astro-ph/9710186
Cherchneff I, Dwek E (2009) The Chemistry of Population III Supernova Ejecta. I. Formation of Molecules in the Early Universe. ApJ 703:642–661, DOI 10.1088/0004-637X/703/1/642, 0907.3621
Chevalier RA (1982) Self-similar solutions for the interaction of stellar ejecta with an external medium. ApJ 258:790–797, DOI 10.1086/160126
Chevalier RA, Kirshner RP (1979) Abundance inhomogeneities in the Cassiopeia A supernova remnant. ApJ 233:154–162, DOI 10.1086/157377
Clayton DD, Nittler LR (2004) Astrophysics with Presolar Stardust. ARA&A 42:39–78, DOI 10.1146/annurev.astro.42.053102.134022
Cowie LL, McKee CF (1977) The evaporation of spherical clouds in a hot gas. I - Classical and saturated mass loss rates. ApJ 211:135–146, DOI 10.1086/154911
Cropper M, Bailey J, McCowage J, Cannon RD, Couch WJ (1988) Spectropolarimetry of SN 1987A - Observations up to 1987 July 8. MNRAS 231:695
Dalton WW, Balbus SA (1993) A flux-limited treatment for the conductive evaporation of spherical interstellar gas clouds. ApJ 404:625–635, DOI 10.1086/172316
Danziger IJ, Gouiffes C, Bouchet P, Lucy LB (1989) Supernova 1987A in the Large Magellanic Cloud. IAU Circ 4746
De Looze I, Barlow MJ, Swinyard BM, Rho J, Gomez HL, Matsuura M, Wesson R (2017) The dust mass in Cassiopeia A from a spatially resolved Herschel analysis. MNRAS 465(3):3309–3342
Del Zanna L, Bucciantini N, Londrillo P (2003) An efficient shock-capturing central-type scheme for multidimensional relativistic flows. II. Magnetohydrodynamics. A&A 400:397–413, DOI 10.1051/0004-6361:20021641, astro-ph/0210618
Docenko D, Sunyaev RA (2010) Fine-structure infrared lines from the Cassiopeia A knots. A&A 509:A59, DOI 10.1051/0004-6361/200810366, 0806.1801
Donn B, Nuth JA (1985) Does nucleation theory apply to the formation of refractory circumstellar grains? ApJ 288:187–190, DOI 10.1086/162779
Draine BT (1981) Infrared emission from dust in shocked gas. Astrophysical Journal 245:880
Draine BT (2003) Interstellar Dust Grains. ARA&A 41:241–289, DOI 10.1146/annurev.astro.41.011802.094840, astro-ph/0304489

Draine BT (2009) Interstellar Dust Models and Evolutionary Implications. Cosmic Dust - Near and Far ASP Conference Series 414:453
Draine BT (2011) Physics of the Interstellar and Intergalactic Medium. Princeton University Press
Draine BT, Salpeter EE (1977) Time-dependent nucleation theory. JCP 67:2230–2235, DOI 10.1063/1.435116
Draine BT, Salpeter EE (1979a) Destruction mechanisms for interstellar dust. ApJ 231:77–94, DOI 10.1086/157165
Draine BT, Salpeter EE (1979b) On the physics of dust grains in hot gas. ApJ 231:438–455, DOI 10.1086/157206
Dunne L, Maddox SJ, Ivison RJ, Rudnick L, Delaney TA, Matthews BC, Crowe CM, Gomez HL, Eales SA, Dye S (2009) Cassiopeia A: dust factory revealed via submillimetre polarimetry. MNRAS 394:1307–1316, DOI 10.1111/j.1365-2966.2009.14453.x, 0809.0887
Dwek E (1983) The infrared echo of a type II supernova with a circumstellar dust shell - Applications to SN 1979c and SN 1980k. ApJ 274:175–183, DOI 10.1086/161435
Dwek E (1986) Temperature fluctuations and infrared emission from dust particles in a hot gas. Astrophysical Journal 302:363–370
Dwek E (1987) The infrared diagnostic of a dusty plasma with applications to supernova remnants. Astrophysical Journal 322:812
Dwek E (2005) Interstellar dust: what is it, how does it evolve, and what are its observational consequences? In: Popescu CC, Tuffs RJ (eds) The Spectral Energy Distributions of Gas-Rich Galaxies: Confronting Models with Data, American Institute of Physics Conference Series, vol 761, pp 103–122, DOI 10.1063/1.1913921, astro-ph/0412344
Dwek E, Arendt RG (1992) Dust-gas interactions and the infrared emission from hot astrophysical plasmas. ARA&A 30:11–50, DOI 10.1146/annurev.aa.30.090192.000303
Dwek E, Arendt RG (2015) The Evolution of Dust Mass in the Ejecta of SN1987A. ApJ 810(1):75
Dwek E, Cherchneff I (2011) The Origin of Dust in the Early Universe: Probing the Star Formation History of Galaxies by Their Dust Content. ApJ 727:63, DOI 10.1088/0004-637X/727/2/63, 1011.1303
Dwek E, Petre R, Szymkowiak A, Rice WL (1987) IRAS observations of supernova remnants - A comparison between their infrared and X-ray cooling rates. ApJl 320:L27–L33, DOI 10.1086/184971
Dwek E, Moseley SH, Glaccum W, Graham JR, Loewenstein RF, Silverberg RF, Smith RK (1992) Dust and gas contributions to the energy output of SN 1987A on day 1153. ApJl 389:L21–L24, DOI 10.1086/186339
Dwek E, Arendt RG, Bouchet P, Burrows DN, Challis P, Danziger IJ, De Buizer JM, Gehrz RD, Kirshner RP, McCray RA, Park S, Polomski EF, Woodward CE (2008) Infrared and X-Ray Evidence for Circumstellar Grain Destruction by the Blast Wave of Supernova 1987A. ApJ 676:1029
Dwek E, Arendt RG, Bouchet P, Burrows DN, Challis P, Danziger IJ, De Buizer JM, Gehrz RD, Park S, Polomski EF, Slavin JD, Woodward CE (2010) FIVE YEARS OF MID-INFRARED EVOLUTION OF THE REMNANT OF SN 1987A: THE ENCOUNTER BETWEEN THE BLAST WAVE AND THE DUSTY EQUATORIAL RING. ApJ 722(1):425–434
Ennis JA, Rudnick L, Reach WT, Smith JD, Rho J, DeLaney T, Gomez H, Kozasa T (2006) Spitzer IRAC Images and Sample Spectra of Cassiopeia A's Explosion. ApJ 652:376–386, DOI 10.1086/508142, astro-ph/0610838
Ferland GJ, Korista KT, Verner DA, Ferguson JW, Kingdon JB, Verner EM (1998) CLOUDY 90: Numerical Simulation of Plasmas and Their Spectra. PASP 110:761–778, DOI 10.1086/316190
Ferrara A, Viti S, Ceccarelli C (2016) The problematic growth of dust in high-redshift galaxies. MNRAS 463:L112–L116, DOI 10.1093/mnrasl/slw165, 1606.07214
Fesen RA, Morse JA, Chevalier RA, Borkowski KJ, Gerardy CL, Lawrence SS, van den Bergh S (2001) Hubble Space Telescope WFPC2 Imaging of Cassiopeia A. AJ 122:2644–2661, DOI 10.1086/323539, astro-ph/0108193
Fesen RA, Hammell MC, Morse J, Chevalier RA, Borkowski KJ, Dopita MA, Gerardy CL, Lawrence SS, Raymond JC, van den Bergh S (2006) Discovery of Outlying High-Velocity Oxygen-Rich Ejecta in Cassiopeia A. ApJ 636:859–872, DOI 10.1086/498092, astro-ph/0509067

Fesen RA, Zastrow JA, Hammell MC, Shull JM, Silvia DW (2011) Ejecta Knot Flickering, Mass Ablation, and Fragmentation in Cassiopeia A. ApJ 736:109, DOI 10.1088/0004-637X/736/2/109, 1105.3970

France K, McCray RA, Heng K, Kirshner RP, Challis P, Bouchet P, Crotts A, Dwek E, Fransson C, Garnavich PM, Larsson J, Lawrence SS, Lundqvist P, Panagia N, Pun CSJ, Smith N, Sollerman J, Sonneborn G, Stocke JT, Wang L, Wheeler JC (2010) Observing Supernova 1987A with the Refurbished Hubble Space Telescope. Science 329:1624

Frank KA, Zhekov SA, Park S, McCray RA, Dwek E, Burrows DN (2016) Chandra Observes the End of an Era in SN 1987A. ApJ 829(1):40

Fransson C, Larsson J, Migotto K, Pesce D, Challis P, Chevalier RA, France K, Kirshner RP, Leibundgut B, Lundqvist P, McCray RA, Spyromilio J, Taddia F, Jerkstrand A, Mattila S, Smith N, Sollerman J, Wheeler JC, Crotts A, Garnavich P, Heng K, Lawrence SS, Panagia N, Pun CSJ, Sonneborn G, Sugerman BEK (2015) THE DESTRUCTION OF THE CIRCUMSTELLAR RING OF SN 1987A. ApJ 806(1):L19

Gaensler BM, Slane PO (2006) The Evolution and Structure of Pulsar Wind Nebulae. ARA&A 44:17–47, DOI 10.1146/annurev.astro.44.051905.092528, astro-ph/0601081

Gall C, Hjorth J, Andersen AC (2011) Production of dust by massive stars at high redshift. A&Ar 19:43, DOI 10.1007/s00159-011-0043-7, 1108.0403

Ghavamian P, Laming JM, Rakowski CE (2007) A Physical Relationship between Electron-Proton Temperature Equilibration and Mach Number in Fast Collisionless Shocks. ApJl 654:L69–L72, DOI 10.1086/510740, astro-ph/0611306

Ghavamian P, Raymond JC, Blair WP, Long KS, Tappe A, Park S, Winkler PF (2009) Spitzer Spectroscopy of the Galactic Supernova Remnant G292.0+1.8: Structure and Composition of the Oxygen-Rich Ejecta. ApJ 696:1307–1318, DOI 10.1088/0004-637X/696/2/1307, 0902.2804

Gomez HL, Krause O, Barlow MJ, Swinyard BM, Owen PJ, Clark CJR, Matsuura M, Gomez EL, Rho J, Besel MA, Bouwman J, Gear WK, Henning T, Ivison RJ, Polehampton ET, Sibthorpe B (2012) A Cool Dust Factory in the Crab Nebula: A Herschel Study of the Filaments. ApJ 760:96, DOI 10.1088/0004-637X/760/1/96, 1209.5677

Gordon KD, Roman-Duval J, Bot C, Meixner M, Babler B, Bernard JP, Bolatto A, Boyer ML, Clayton GC, Engelbracht C, Fukui Y, Galametz M, Galliano F, Hony S, Hughes A, Indebetouw R, Israel FP, Jameson K, Kawamura A, Lebouteiller V, Li A, Madden SC, Matsuura M, Misselt K, Montiel E, Okumura K, Onishi T, Panuzzo P, Paradis D, Rubio M, Sandstrom KM, Sauvage M, Seale J, Sewiło M, Tchernyshyov K, Skibba R (2014) DUST AND GAS IN THE MAGELLANIC CLOUDS FROM THE HERITAGE HERSCHELKEY PROJECT. I. DUST PROPERTIES AND INSIGHTS INTO THE ORIGIN OF THE SUBMILLIMETER EXCESS EMISSION. The Astrophysical Journal 797(2):85

Gotthelf EV, Koralesky B, Rudnick L, Jones TW, Hwang U, Petre R (2001) [ITAL]Chandra[/ITAL] Detection of the Forward and Reverse Shocks in Cassiopeia A. ApJ 552(1):L39–L43

Grefenstette BW, Harrison FA, Boggs SE, Reynolds SP, Fryer CL, Madsen KK, Wik DR, Zoglauer A, Ellinger CI, Alexander DM, An H, Barret D, Christensen FE, Craig WW, Forster K, Giommi P, Hailey CJ, Hornstrup A, Kaspi VM, Kitaguchi T, Koglin JE, Mao PH, Miyasaka H, Mori K, Perri M, Pivovaroff MJ, Puccetti S, Rana V, Stern D, Westergaard NJ, Zhang WW (2014) Asymmetries in core-collapse supernovae from maps of radioactive 44Ti in CassiopeiaA. Nature 506(7488):339–342

Guillet V (2008) Dust evolution in interstellar shocks. Theses, Université Paris Sud - Paris XI, URL https://tel.archives-ouvertes.fr/tel-00332738

Hammell MC, Fesen RA (2008) A Catalog of Outer Ejecta Knots in the Cassiopeia A Supernova Remnant. ApJS 179:195, DOI 10.1086/591528

Hester JJ (2008) The Crab Nebula: An Astrophysical Chimera. ARA&A 46:127–155, DOI 10.1146/annurev.astro.45.051806.110608

Hildebrand RH (1983) The Determination of Cloud Masses and Dust Characteristics from Submillimetre Thermal Emission. QJRAS 24:267

Hines DC, Rieke GH, Gordon KD, Rho J, Misselt KA, Woodward CE, Werner MW, Krause O, Latter WB, Engelbracht CW, Egami E, Kelly DM, Muzerolle J, Stansberry JA, Su KYL, Morrison JE, Young ET, Noriega-Crespo A, Padgett DL, Gehrz RD, Polomski E, Beeman JW, Haller EE (2004) Imaging of the Supernova Remnant Cassiopeia A with the Multiband Imaging Photometer for Spitzer (MIPS). ApJS 154:290–295, DOI 10.1086/422583

Hugoniot H (1887) Mémoire sur la propagation des mouvements dans les corps et spécialement dans les gaz parfaits (première partie). Journal de l'École Polytechnique 57:3–97
Hugoniot H (1889) Mémoire sur la propagation des mouvements dans les corps et spécialement dans les gaz parfaits (deuxième partie). Journal de l'École Polytechnique 58:1–125
Hwang U, Laming JM (2009) The Circumstellar Medium of Cassiopeia a Inferred from the Outer Ejecta Knot Properties. ApJ 703:883–893, DOI 10.1088/0004-637X/703/1/883, 0907.5177
Hwang U, Laming JM (2012) A Chandra X-Ray Survey of Ejecta in the Cassiopeia A Supernova Remnant. ApJ 746:130, DOI 10.1088/0004-637X/746/2/130, 1111.7316
Hwang U, Laming JM, Badenes C, Berendse F, Blondin JM, Cioffi D, DeLaney TA, Dewey D, Fesen R, Flanagan KA, Fryer CL, Ghavamian P, Hughes JP, Morse JA, Plucinsky PP, Petre R, Pohl M, Rudnick L, Sankrit R, Slane PO, Smith RK, Vink J, Warren JS (2004) A Million Second ChandraView of Cassiopeia A. ApJ 615(2):L117–L120
Indebetouw R, Matsuura M, Dwek E, Zanardo G, Barlow MJ, Baes M, Bouchet P, Burrows DN, Chevalier R, Clayton GC, Fransson C, Gaensler B, Kirshner R, Lakićević M, Long KS, Lundqvist P, Martí-Vidal I, Marcaide J, McCray R, Meixner M, Ng CY, Park S, Sonneborn G, Staveley-Smith L, Vlahakis C, van Loon J (2014) Dust Production and Particle Acceleration in Supernova 1987A Revealed with ALMA. ApJl 782:L2, DOI 10.1088/2041-8205/782/1/L2, 1312.4086
Isensee K, Olmschenk G, Rudnick L, DeLaney TA, Rho J, Smith JD, Reach WT, Kozasa T, Gomez HL (2012) NUCLEOSYNTHETIC LAYERS IN THE SHOCKED EJECTA OF CASSIOPEIA A. ApJ 757(2):126
Itoh H (1981) Shockwave Model for the Optical Emission from Oxygen-Rich Supernova Ejecta - Part Two - Precursor Region. PASJ 33:521
Itoh H (1985) The destruction of dust grains in collisions of a supernova with a circumstellar medium. MNRAS 212:309–323, DOI 10.1093/mnras/212.2.309
Jakobsen P, Albrecht R, Barbieri C, Blades JC, Boksenberg A, Crane P, Deharveng JM, Disney MJ, Kamperman TM, King IR, Macchetto F, Mackay CD, Paresce F, Weigelt G, Baxter D, Greenfield P, Jedrzejewski R, Nota A, Sparks WB, Kirshner RP, Panagia N (1991) First results from the Faint Object Camera - SN 1987A. ApJ 369:L63
Jones AP, Nuth JA (2011) Dust destruction in the ISM: a re-evaluation of dust lifetimes. A&A 530:A44, DOI 10.1051/0004-6361/201014440
Jones AP, Nuth JA III (2011) Dust destruction in the ISM: a re-evaluation of dust lifetimes. Astronomy and Astrophysics 530:A44
Jones AP, Tielens AGGM, Hollenbach DJ, McKee CF (1994) Grain destruction in shocks in the interstellar medium. ApJ 433:797–810, DOI 10.1086/174689
Jones AP, Tielens AGGM, Hollenbach DJ (1996) Grain Shattering in Shocks: The Interstellar Grain Size Distribution. ApJ 469:740, DOI 10.1086/177823
Jones AP, Fanciullo L, Köhler M, Verstraete L, Guillet V, Bocchio M, Ysard N (2013) The evolution of amorphous hydrocarbons in the ISM: dust modelling from a new vantage point. Astronomy and Astrophysics 558:A62
Jones AP, Köhler M, Ysard N, Bocchio M, Verstraete L (2017) The global dust modelling framework THEMIS. Astronomy and Astrophysics 602:A46
Jurac S, Johnson RE, Donn B (1998) Monte Carlo Calculations of the Sputtering of Grains: Enhanced Sputtering of Small Grains. ApJ 503:247–252, DOI 10.1086/305994
Kalikmanov VI (ed) (2013) Nucleation Theory, Lecture Notes in Physics, Berlin Springer Verlag, vol 860, DOI 10.1007/978-90-481-3643-8
Kamper K, van den Bergh S (1976) Optical studies of Cassiopeia A. V - A definitive study of proper motions. ApJS 32:351–366, DOI 10.1086/190400
Klein RI, McKee CF, Colella P (1994) On the hydrodynamic interaction of shock waves with interstellar clouds. 1: Nonradiative shocks in small clouds. ApJ 420:213–236, DOI 10.1086/173554
Koo BCC, Lee JJ, Jeong IG, Seok JY, Kim HJ (2016) Infrared Supernova Remnants and their Infrared-to-X-ray Flux Ratios. ApJ 821(1):20
Kozasa T, Hasegawa H, Nomoto K (1989) Formation of dust grains in the ejecta of SN 1987A. ApJ 344:325–331, DOI 10.1086/167801
Krause O, Birkmann SM, Usuda T, Hattori T, Goto M, Rieke GH, Misselt KA (2008) The Cassiopeia A Supernova Was of Type IIb. Science 320(5880):1195–1197

Lagage PO, Claret A, Ballet J, Boulanger F, Cesarsky CJ, Cesarsky D, Fransson C, Pollock A (1996) Dust formation in the Cassiopeia A supernova. A&A 315:L273–L276

Lakicevic M, van Loon JT, Meixner M, Gordon KD, Bot C, Roman-Duval J, Babler B, Bolatto A, Engelbracht C, Filipović M, Hony S, Indebetouw R, Misselt K, Montiel E, Okumura K, Panuzzo P, Patat F, Sauvage M, Seale J, Sonneborn G, temim t, Urošević D, Zanardo G (2015) THE INFLUENCE OF SUPERNOVA REMNANTS ON THE INTERSTELLAR MEDIUM IN THE LARGE MAGELLANIC CLOUD SEEN AT 20-600 μm WAVELENGTHS. ApJ 799(1):50

Laming JM, Hwang U (2003) On the Determination of Ejecta Structure and Explosion Asymmetry from the X-Ray Knots of Cassiopeia A. ApJ 597:347–361, DOI 10.1086/378268, arXiv:astro-ph/0306119

Larsson J, Fransson C, Östlin G, Groningsson P, Jerkstrand A, Kozma C, Sollerman J, Challis P, Kirshner RP, Chevalier RA, Heng K, McCray RA, Suntzeff NB, Bouchet P, Crotts A, Danziger IJ, Dwek E, France K, Garnavich PM, Lawrence SS, Leibundgut B, Lundqvist P, Panagia N, Pun CSJ, Smith N, Sonneborn G, Wang L, Wheeler JC (2011) X-ray illumination of the ejecta of supernova 1987A. Nature 474(7352):484–486

Lau RM, Herter TL, Morris MR, Li Z, Adams JD (2015) Old supernova dust factory revealed at the Galactic center. Science 348(6233):413–418

Limongi M, Chieffi A (2006) The Nucleosynthesis of ^{26}Al and ^{60}Fe in Solar Metallicity Stars Extending in Mass from 11 to 120 M_{solar}: The Hydrostatic and Explosive Contributions. ApJ 647:483–500, DOI 10.1086/505164, astro-ph/0604297

Lucy LB, Danziger IJ, Gouiffes C, Bouchet P (1989) Dust Condensation in the Ejecta of SN 1987 A. Structure and Dynamics of the Interstellar Medium 350:164

Mac Low MM, McKee CF, Klein RI, Stone JM, Norman ML (1994) Shock interactions with magnetized interstellar clouds. 1: Steady shocks hitting nonradiative clouds. ApJ 433:757–777, DOI 10.1086/174685

Marassi S, Schneider R, Limongi M, Chieffi A, Bocchio M, Bianchi S (2015) The metal and dust yields of the first massive stars. MNRAS 454:4250–4266, DOI 10.1093/mnras/stv2267, 1509.08923

Mathis JS, Rumpl W, Nordsieck KH (1977) The size distribution of interstellar grains. ApJ 217:425–433, DOI 10.1086/155591

Matsunami N, Yamamura Y, Itikawa Y, Itoh N, Kazumata Y, Miyagawa S, Morita K, Shimizu R (1981) A semiempirical formula for the energy dependence of the sputtering yield. Radiation Effects 57(1-2):15–21, DOI 10.1080/01422448008218676, URL http://dx.doi.org/10.1080/01422448008218676, http://dx.doi.org/10.1080/01422448008218676

Matsuura M (2017) Dust and molecular formation in supernovae. In: Athem WA, Paul M (eds) "Handbook of Supernovae",, Springer International Publishing

Matsuura M, Dwek E, Meixner M, Otsuka M, Babler B, Barlow MJ, Roman-Duval J, Engelbracht C, Sandstrom KM, Lakicevic M, van Loon JT, Sonneborn G, Clayton GC, Long KS, Lundqvist P, Nozawa T, Gordon KD, Hony S, Panuzzo P, Okumura K, Misselt KA, Montiel E, Sauvage M (2011) Herschel Detects a Massive Dust Reservoir in Supernova 1987A. Science 333(6047):1258–1261

Matsuura M, Dwek E, Barlow MJ, Babler B, Baes M, Meixner M, Cernicharo J, Clayton GC, Dunne L, Fransson C, Fritz J, Gear W, Gomez HL, Groenewegen MAT, Indebetouw R, Ivison RJ, Jerkstrand A, Lebouteiller V, Lim TL, Lundqvist P, Pearson CP, Roman-Duval J, Royer P, Staveley-Smith L, Swinyard BM, van Hoof PAM, van Loon JT, Verstappen J, Wesson R, Zanardo G, Blommaert JADL, Decin L, Reach WT, Sonneborn G, Van de Steene GC, Yates JA (2015) A Stubbornly Large Mass of Cold Dust in the Ejecta of Supernova 1987A. ApJ 800:50, DOI 10.1088/0004-637X/800/1/50, 1411.7381

Mattsson L, Gomez HL, Andersen AC, Matsuura M (2015) From flux to dust mass: Does the grain-temperature distribution matter for estimates of cold dust masses in supernova remnants? MNRAS 449:4079–4090, DOI 10.1093/mnras/stv487, 1504.02664

McCray R (1993) Supernova 1987A revisited. ARA&A 31:175–216, DOI 10.1146/annurev.aa.31.090193.001135

McCray RA (1993) Supernova 1987A revisited. ARA&A 31:175

McCray RA, Fransson C (2016) The Remnant of Supernova 1987A. ARA&A 54(1):19–52

McKee C (1989) Dust Destruction in the Interstellar Medium. Proceedings of the International Astronomical Union 135:431

McKee CF, Ostriker JP (1977) A theory of the interstellar medium - Three components regulated by supernova explosions in an inhomogeneous substrate. ApJ 218:148
McKee CF, Hollenbach DJ, Seab GC, Tielens AGGM (1987) The structure of the time-dependent interstellar shocks and grain destruction in the interstellar medium. ApJ 318:674–701, DOI 10.1086/165403
Mennella V, Brucato JR, Colangeli L, Palumbo P, Rotundi A, Bussoletti E (1998) Temperature Dependence of the Absorption Coefficient of Cosmic Analog Grains in the Wavelength Range 20 Microns to 2 Millimeters. ApJ 496(2):1058–1066
Micelotta ER, Jones AP, Tielens AGGM (2010a) Polycyclic aromatic hydrocarbon processing in a hot gas. A&A 510:A37, DOI 10.1051/0004-6361/200911683, 0912.1595
Micelotta ER, Jones AP, Tielens AGGM (2010b) Polycyclic aromatic hydrocarbon processing in interstellar shocks. A&A 510:A36, DOI 10.1051/0004-6361/200911682, 0910.2461
Micelotta ER, Dwek E, Slavin JD (2016) Dust destruction by the reverse shock in the Cassiopeia A supernova remnant. A&A 590:A65, DOI 10.1051/0004-6361/201527350, 1602.02754
Milisavljevic D, Fesen RA (2013) A Detailed Kinematic Map of Cassiopeia A's Optical Main Shell and Outer High-velocity Ejecta. ApJ 772:134, DOI 10.1088/0004-637X/772/2/134, 1306.2310
Milisavljevic D, Fesen RA (2015) The bubble-like interior of the core-collapse supernova remnant Cassiopeia A. Science 347(6221):526–530
Morse JA, Fesen RA, Chevalier RA, Borkowski KJ, Gerardy CL, Lawrence SS, van den Bergh S (2004) Location of the Optical Reverse Shock in the Cassiopeia A Supernova Remnant. ApJ 614:727–736, DOI 10.1086/423709
Moseley SH, Dwek E, Glaccum W, Graham JR, Loewenstein RF (1989) Far-infrared observations of thermal dust emission from supernova 1987A. Nature 340:697–699, DOI 10.1038/340697a0
Nakamura F, McKee CF, Klein RI, Fisher RT (2006) On the Hydrodynamic Interaction of Shock Waves with Interstellar Clouds. II. The Effect of Smooth Cloud Boundaries on Cloud Destruction and Cloud Turbulence. ApJS 164:477–505, DOI 10.1086/501530, astro-ph/0511016
Nath BB, Laskar T, Shull JM (2008) Dust Sputtering by Reverse Shocks in Supernova Remnants. ApJ 682:1055–1064, DOI 10.1086/589224, 0804.3472
Nomoto K, Iwamoto K, Suzuki T, Pols OR, Yamaoka H, Hashimoto M, Hoflich P, van den Heuvel EPJ (1996) The Origin of Type Ib-Ic-IIb-IIL Supernovae and Binary Star Evolution. In: van Paradijs J, van den Heuvel EPJ, Kuulkers E (eds) Compact Stars in Binaries, IAU Symposium, vol 165, p 119
Nomoto KI, Iwamoto K, Suzuki T (1995) The evolution and explosion of massive binary stars and Type Ib-Ic-IIb-IIL supernovae. PR 256:173–191, DOI 10.1016/0370-1573(94)00107-E
Norman ML, Bryan GL (1999) Cosmological Adaptive Mesh Refinement^{CD}. In: Miyama SM, Tomisaka K, Hanawa T (eds) Numerical Astrophysics, Astrophysics and Space Science Library, vol 240, p 19, DOI 10.1007/978-94-011-4780-4˙3, astro-ph/9807121
Nozawa T, Kozasa T, Umeda H, Maeda K, Nomoto K (2003) Dust in the Early Universe: Dust Formation in the Ejecta of Population III Supernovae. ApJ 598:785–803, DOI 10.1086/379011, astro-ph/0307108
Nozawa T, Kozasa T, Habe A (2006) Dust Destruction in the High-Velocity Shocks Driven by Supernovae in the Early Universe. ApJ 648:435–451, DOI 10.1086/505639, astro-ph/0605193
Nozawa T, Kozasa T, Habe A, Dwek E, Umeda H, Tominaga N, Maeda K, Nomoto K (2007) Evolution of Dust in Primordial Supernova Remnants: Can Dust Grains Formed in the Ejecta Survive and Be Injected into the Early Interstellar Medium? ApJ 666:955–966, DOI 10.1086/520621, 0706.0383
Nozawa T, Kozasa T, Tominaga N, Maeda K, Umeda H, Nomoto K, Krause O (2010) Formation and Evolution of Dust in Type IIb Supernovae with Application to the Cassiopeia A Supernova Remnant. ApJ 713:356–373, DOI 10.1088/0004-637X/713/1/356, 0909.4145
Orlando S, Peres G, Reale F, Bocchino F, Rosner R, Plewa T, Siegel A (2005) Crushing of interstellar gas clouds in supernova remnants. I. The role of thermal conduction and radiative losses. A&A 444:505–519, DOI 10.1051/0004-6361:20052896, astro-ph/0508638
O'Shea BW, Bryan GL, Bordner J, Norman ML, Abel T, Harkness R, Kritsuk A (2005) Introducing Enzo, an AMR Cosmology Application in: Adaptive Mesh Refinement - Theory and Applications. Lecture Notes in Computational Science and Engineering, vol 41. Springer,

Berlin
Ossenkopf V, Henning T, Mathis JS (1992) Constraints on cosmic silicates. A&A 261:567
Otsuka M, van Loon JT, Long KS, Meixner M, Matsuura M, Reach WT, Roman-Duval J, Gordon K, Sauvage M, Hony S, Misselt K, Engelbracht C, Panuzzo P, Okumura K, Woods PM, Kemper F, Sloan GC (2010) Dust in the bright supernova remnant N49 in the LMC. A&A 518:L139, DOI 10.1051/0004-6361/201014642, 1005.2787
Owen PJ, Barlow MJ (2015) The Dust and Gas Content of the Crab Nebula. ApJ 801:141, DOI 10.1088/0004-637X/801/2/141, 1501.01510
Padmanabhan T (2001) Theoretical Astrophysics - Volume 2, Stars and Stellar Systems. DOI 10.2277/0521562414
Panagia N, Gilmozzi R, Macchetto F, Adorf HM, Kirshner RP (1991) Properties of the SN 1987A circumstellar ring and the distance to the Large Magellanic Cloud. ApJ 380:L23–L26
Patnaude DJ, Fesen RA (2005) Model Simulations of a Shock-Cloud Interaction in the Cygnus Loop. ApJ 633:240–247, DOI 10.1086/452627, astro-ph/0507330
Rankine WJM (1870) On the thermodynamic theory of waves of finite longitudinal disturbance. Philosophical Transactions of the Royal Society of London 160:277–288, DOI 10.1098/rstl.1870.0015, URL http://rstl.royalsocietypublishing.org/content/160/277.short, http://rstl.royalsocietypublishing.org/content/160/277.full.pdf+html
Rauscher T, Heger A, Hoffman RD, Woosley SE (2002) Nucleosynthesis in Massive Stars with Improved Nuclear and Stellar Physics. ApJ 576:323–348, DOI 10.1086/341728, astro-ph/0112478
Raymond JC, Ghavamian P, Williams BJ, Blair WP, Borkowski KJ, Gaetz TJ, Sankrit R (2013) GRAIN DESTRUCTION IN A SUPERNOVA REMNANT SHOCK WAVE. ApJ 778(2):161
Reynolds SP (2008) Supernova Remnants at High Energy. ARA&A 46:89–126, DOI 10.1146/annurev.astro.46.060407.145237
Rho J, Kozasa T, Reach WT, Smith JD, Rudnick L, DeLaney T, Ennis JA, Gomez H, Tappe A (2008) Freshly Formed Dust in the Cassiopeia A Supernova Remnant as Revealed by the Spitzer Space Telescope. ApJ 673:271–282, DOI 10.1086/523835, 0709.2880
Rho J, Jarrett TH, Reach WT, Gomez H, Andersen M (2009a) Carbon Monoxide in the Cassiopeia a Supernova Remnant. ApJl 693:L39–L43, DOI 10.1088/0004-637X/693/1/L39, 0901.2308
Rho J, Reach WT, Tappe A, Hwang U, Slavin JD, Kozasa T, Dunne L (2009b) Spitzer Observations of the Young Core-Collapse Supernova Remnant 1E0102-72.3: Infrared Ejecta Emission and Dust Formation. ApJ 700:579–596, DOI 10.1088/0004-637X/700/1/579
Rho J, Reach WT, Tappe A, Rudnick L, Kozasa T, Hwang U, Andersen M, Gomez H, Delaney T, Dunne L, Slavin J (2009c) Dust Formation Observed in Young Supernova Remnants with Spitzer. In: Henning T, Grün E, Steinacker J (eds) Cosmic Dust - Near and Far, Astronomical Society of the Pacific Conference Series, vol 414, p 22, 0901.1699
Rho J, Onaka T, Cami J, Reach WT (2012) Spectroscopic Detection of Carbon Monoxide in the Young Supernova Remnant Cassiopeia A. ApJl 747:L6, DOI 10.1088/2041-8205/747/1/L6, 1202.4540
Salpeter EE (1977) Formation and destruction of dust grains. Annual Review of Astronomy and Astrophysics 15(1):267–293
Sandstrom KM, Bolatto AD, Stanimirović S, van Loon JT, Smith JDT (2009) Measuring Dust Production in the Small Magellanic Cloud Core-Collapse Supernova Remnant 1E 0102.2-7219. ApJ 696:2138–2154, DOI 10.1088/0004-637X/696/2/2138, 0810.2803
Sankrit R, Williams BJ, Borkowski KJ, Gaetz TJ, Raymond JC, Blair WP, Ghavamian P, Long KS, Reynolds SP (2010) DUST DESTRUCTION IN A NON-RADIATIVE SHOCK IN THE CYGNUS LOOP SUPERNOVA REMNANT. ApJ 712(2):1092–1099
Sarangi A, Cherchneff I (2013) The Chemically Controlled Synthesis of Dust in Type II-P Supernovae. ApJ 776:107, DOI 10.1088/0004-637X/776/2/107, 1309.5887
Sarangi A, Cherchneff I (2015) Condensation of dust in the ejecta of Type II-P supernovae. A&A 575:A95, DOI 10.1051/0004-6361/201424969, 1412.5522
Sarangi A, Matsuura M, Micelotta E (2018) Dust in supernovae and supernova remnants i : the scenario of dust formation. SSRv
Sarazin CL, White RE III (1987) Steady state cooling flow models for normal elliptical galaxies. ApJ 320:32–48, DOI 10.1086/165522

Savage BD, Sembach KR (1996) INTERSTELLAR ABUNDANCES FROM ABSORPTION-LINE OBSERVATIONS WITH THE HUBBLE SPACE TELESCOPE. ARA&A 34(1):279–329

Schneider R, Ferrara A, Salvaterra R (2004) Dust formation in very massive primordial supernovae. MNRAS 351:1379–1386, DOI 10.1111/j.1365-2966.2004.07876.x, astro-ph/0307087

Seab CG, Shull JM (1983) Shock processing of interstellar grains. ApJ 275:652–660, DOI 10.1086/161563

Sedov LI (1959) Similarity and Dimensional Methods in Mechanics

Seok JY, Koo BCC, Onaka T (2013) A SURVEY OF INFRARED SUPERNOVA REMNANTS IN THE LARGE MAGELLANIC CLOUD. ApJ 779(2):134

Seok JY, Koo BC, Hirashita H (2015) Dust Cooling in Supernova Remnants in the Large Magellanic Cloud. ApJ 807:100, DOI 10.1088/0004-637X/807/1/100, 1506.07926

Serra Díaz-Cano L, Jones AP (2008) Carbonaceous dust in interstellar shock waves: hydrogenated amorphous carbon (a-C:H) vs. graphite. A&A 492:127–133, DOI 10.1051/0004-6361:200810622

Shull JM (1978) Disruption and sputtering of grains in intermediate-velocity interstellar clouds. ApJ 226:858–862, DOI 10.1086/156666

Sigmund P (1981) Sputtering by Particle Bombardment Vol.1. in Topics in Applied Physics, Vol. 47, Springer - Verlag

Silvia DW, Smith BD, Shull JM (2010) Numerical Simulations of Supernova Dust Destruction. I. Cloud-crushing and Post-processed Grain Sputtering. ApJ 715:1575–1590, DOI 10.1088/0004-637X/715/2/1575, 1001.4793

Silvia DW, Smith BD, Shull JM (2012) Numerical Simulations of Supernova Dust Destruction. II. Metal-enriched Ejecta Knots. ApJ 748:12, DOI 10.1088/0004-637X/748/1/12, 1111.0302

Slavin JD, Dwek E, Jones AP (2015) Destruction of Interstellar Dust in Evolving Supernova Remnant Shock Waves. ApJ 803:7, DOI 10.1088/0004-637X/803/1/7, 1502.00929

Smith JDT, Rudnick L, Delaney T, Rho J, Gomez H, Kozasa T, Reach W, Isensee K (2009) Spitzer Spectral Mapping of Supernova Remnant Cassiopeia a. ApJ 693:713–721, DOI 10.1088/0004-637X/693/1/713, 0810.3014

Stone JM, Norman ML (1992) The three-dimensional interaction of a supernova remnant with an interstellar cloud. ApJl 390:L17–L19, DOI 10.1086/186361

Sutherland RS, Dopita MA (1995) Young oxygen-rich supernova remnants. 2: an oxygen-rich emission mechanism. ApJ 439:381–398, DOI 10.1086/175181

Taylor G (1950) The Formation of a Blast Wave by a Very Intense Explosion. I. Theoretical Discussion. Proceedings of the Royal Society of London Series A 201:159–174, DOI 10.1098/rspa.1950.0049

Temim T, Dwek E (2013) The Importance of Physical Models for Deriving Dust Masses and Grain Size Distributions in Supernova Ejecta. I. Radiatively Heated Dust in the Crab Nebula. ApJ 774:8, DOI 10.1088/0004-637X/774/1/8, 1302.5452

Temim T, Slane P, Reynolds SP, Raymond JC, Borkowski KJ (2010) Deep Chandra Observations of the Crab-like Pulsar Wind Nebula G54.1+0.3 and Spitzer Spectroscopy of the Associated Infrared Shell. ApJ 710:309–324, DOI 10.1088/0004-637X/710/1/309, 0912.4538

Temim T, Dwek E, Tchernyshyov K, Boyer ML, Meixner M, Gall C, Roman-Duval J (2015) Dust Destruction Rates and Lifetimes in the Magellanic Clouds. ApJ 799:158, DOI 10.1088/0004-637X/799/2/158, 1411.4574

Temim T, Dwek E, Arendt RG, Borkowski KJ, Reynolds SP, Slane P, Gelfand JD, Raymond JC (2017) A Massive Shell of Supernova-formed Dust in SNR G54.1+0.3. ApJ 836:129, DOI 10.3847/1538-4357/836/1/129, 1701.01117

Tielens AGGM (2010) The Physics and Chemistry of the Interstellar Medium. Cambridge University Press

Tielens AGGM, McKee CF, Seab CG, Hollenbach DJ (1994) The physics of grain-grain collisions and gas-grain sputtering in interstellar shocks. ApJ 431:321–340, DOI 10.1086/174488

Todini P, Ferrara A (2001) Dust formation in primordial Type II supernovae. MNRAS 325:726–736, DOI 10.1046/j.1365-8711.2001.04486.x, astro-ph/0009176

Truelove JK, McKee CF (1999) Evolution of Nonradiative Supernova Remnants. ApJS 120:299–326, DOI 10.1086/313176

Umeda H, Nomoto K (2002) Nucleosynthesis of Zinc and Iron Peak Elements in Population III Type II Supernovae: Comparison with Abundances of Very Metal Poor Halo Stars. ApJ 565:385–404, DOI 10.1086/323946, astro-ph/0103241

van Adelsberg M, Heng K, McCray R, Raymond JC (2008) Spatial Structure and Collisionless Electron Heating in Balmer-dominated Shocks. ApJ 689:1089–1104, DOI 10.1086/592680, 0803.2521

van der Swaluw E, Achterberg A, Gallant YA, Downes TP, Keppens R (2003) Interaction of high-velocity pulsars with supernova remnant shells. A&A 397:913–920, DOI 10.1051/0004-6361:20021488, astro-ph/0202232

Vancura O, Raymond JC, Dwek E, Blair WP, Long KS, Foster S (1994) A study of X-ray and infrared emissions from dusty nonradiative shock waves. ApJ 431:188–200, DOI 10.1086/174477

Vink J, Kaastra JS, Bleeker JAM (1996) A new mass estimate and puzzling abundances of SNR Cassiopeia A. A&A 307:L41–L44

Wallström SHJ, Biscaro C, Salgado F, Black JH, Cherchneff I, Muller S, Berné O, Rho J, Tielens AGGM (2013) CO rotational line emission from a dense knot in Cassiopeia A. Evidence for active post-reverse-shock chemistry. A&A 558:L2, DOI 10.1051/0004-6361/201322576, 1309.4229

Watson D, Christensen L, Knudsen KK, Richard J, Gallazzi A, Michałowski MJ (2015) A dusty, normal galaxy in the epoch of reionization. Nature 519:327–330, DOI 10.1038/nature14164, 1503.00002

Weiler KW, Sramek RA (1988) Supernovae and supernova remnants. ARA&A 26:295–341, DOI 10.1146/annurev.aa.26.090188.001455

Weingartner JC, Draine BT (2001) Dust Grain-Size Distributions and Extinction in the Milky Way, Large Magellanic Cloud, and Small Magellanic Cloud. The Astrophysical Journal 548:296

Wesson R, Barlow MJ, Matsuura M, Ercolano B (2014) The timing and location of dust formation in the remnant of SN 1987A. MNRAS 446(2):2089–2101

Whitelock PA, Catchpole RM, Menzies JW, Feast MW, Woosley SE, Allen D, van Wyk F, Marang F, Laney CD, Winkler H, Sekiguchi K, Balona LA, Carter BS, Spencer Jones JH, Laing JD, Evans TL, Fairall AP, Buckley DAH, Glass IS, Penston MV, da Costa LN, Bell SA, Hellier C, Shara M, Moffat AFJ (1989) Spectroscopic and photometric observations of SN1987A. VI - Days 617 to 792. MNRAS 240:7P

Williams BJ, Temim T (2016) Infrared Emission from Supernova Remnants: Formation and Destruction of Dust. DOI 10.1007/978-3-319-20794-0$ˆ-$94-1

Williams BJ, Borkowski KJ, Reynolds SP, Blair WP, Ghavamian P, Hendrick SP, Long KS, Points S, Raymond JC, Sankrit R, Smith RC, Winkler PF (2006) Dust Destruction in Fast Shocks of Core-Collapse Supernova Remnants in the Large Magellanic Cloud. ApJ 652(1):L33–L36

Williams BJ, Borkowski KJ, Reynolds SP, Ghavamian P, Blair WP, Long KS, Sankrit R (2012) DUST IN A TYPE Ia SUPERNOVA PROGENITOR: SPITZERSPECTROSCOPY OF KEPLER'S SUPERNOVA REMNANT. ApJ 755(1):3

Willingale R, Bleeker JAM, van der Heyden KJ, Kaastra JS, Vink J (2002) X-ray spectral imaging and Doppler mapping of Cassiopeia A. A&A 381:1039–1048, DOI 10.1051/0004-6361:20011614, astro-ph/0107270

Wilms J (2012) Supernova Remnants. X-ray Astronomy II, University of Erlangen-Nuremberg 4, http://pulsar.sternwarte.uni-erlangen.de/wilms/teach/xray2_0809/xray2chap4toc.html

Wongwathanarat A, Müller E, Janka HT (2015) Three-dimensional simulations of core-collapse supernovae: from shock revival to shock breakout. A&A 577:A48, DOI 10.1051/0004-6361/201425025, 1409.5431

Wooden DH (1997) Observational evidence for mixing and dust condensation in core-collapse supernovae. In: Zinner EK, Bernatowicz TJ (eds) American Institute of Physics Conference Series, American Institute of Physics Conference Series, vol 402, pp 317–376, DOI 10.1063/1.53315

Wooden DH, Rank DM, Bregman JD, Witteborn FC, Tielens AGGM, Cohen M, Pinto PA, Axelrod TS (1993) Airborne spectrophotometry of SN 1987A from 1.7 to 12.6 microns - Time history of the dust continuum and line emission. Astrophysical Journal Supplement Series (ISSN 0067-0049) 88:477

Woosley SE, Weaver TA (1995) The Evolution and Explosion of Massive Stars. II. Explosive Hydrodynamics and Nucleosynthesis. ApJS 101:181, DOI 10.1086/192237

Yamaguchi H, Eriksen KA, Badenes C, Hughes JP, Brickhouse NS, Foster AR, Patnaude DJ, Petre R, Slane PO, Smith RK (2014) New Evidence for Efficient Collisionless Heating of Electrons at the Reverse Shock of a Young Supernova Remnant. ApJ 780:136, DOI 10.1088/0004-637X/780/2/136, 1310.8355

Yamamoto T, Hasegawa H (1977) Grain Formation through Nucleation Process in Astrophysical Environment. Progress of Theoretical Physics 58:816–828, DOI 10.1143/PTP.58.816

Zanardo G, Staveley-Smith L, Ball L, Gaensler BM, Kesteven MJ, Manchester RN, Ng CY, Tzioumis AK, Potter TM (2010) Multifrequency Radio Measurements of Supernova 1987A Over 22 Years. ApJ 710(2):1515–1529

Zanardo G, Staveley-Smith L, Ng CY, Gaensler BM, Potter TM, Manchester RN, Tzioumis AK (2013) HIGH-RESOLUTION RADIO OBSERVATIONS OF THE REMNANT OF SN 1987A AT HIGH FREQUENCIES. ApJ 767(2):98

Zanardo G, Staveley-Smith L, Indebetouw R, Chevalier RA, Matsuura M, Gaensler BM, Barlow MJ, Fransson C, Manchester RN, Baes M, Kamenetzky JR, Lakićević M, Lundqvist P, Marcaide JM, Marti-Vidal I, Meixner M, Ng CY, Park S, Sonneborn G, Spyromilio J, van Loon JT (2014) SPECTRAL AND MORPHOLOGICAL ANALYSIS OF THE REMNANT OF SUPERNOVA 1987A WITH ALMA AND ATCA. ApJ 796(2):82

Zinner E (2008) Stardust in the Laboratory. PASA 25:7–17, DOI 10.1071/AS07039